

# POLITECNICO DI TORINO

Corso di Laurea Magistrale  
in NANOTECHNOLOGIES FOR ICTs

Tesi di Laurea Magistrale  
Study of the Effect of Carbon Nanofibers Electrodes  
Morphology on Sodium-ion Cells Electrochemical Performances



Supervisor: Prof. Claudio Gerbaldi  
Advisor: Prof. Jürgen Brugger  
Second Advisor: Prof. Carlo Ricciardi

Candidate  
Jacopo Cele'

Anno Accademico 2018/2019

# Contents

<b>ACKNOWLEDGMENTS</b>	<b>iv</b>
<b>PREFACE</b>	<b>v</b>
<b>1 Framework and Opportunities of Battery Energy Storage</b>	<b>1</b>
1.1 Thesis and Purpose of this work . . . . .	1
1.1.1 System Perspective . . . . .	1
1.1.2 Experimental Deliveries . . . . .	3
1.2 Stationary Energy Storage Systems . . . . .	3
1.2.1 Energy Storage Devices: a System Perspective . . . . .	4
1.2.2 Storage Technologies and Applications . . . . .	6
1.2.3 Market and Resources Analysis (2030) . . . . .	11
1.3 Electrochemical Energy Storage Devices . . . . .	14
1.3.1 Secondary Batteries . . . . .	14
1.3.2 Model and Parameters . . . . .	16
1.3.3 Comparison of Performances . . . . .	22
1.4 Sodium-ion Batteries Technology . . . . .	24
1.4.1 Cathode Materials . . . . .	26
1.4.2 Nanostructured Electrodes . . . . .	27
<b>2 Tools and Theoretical Background</b>	<b>34</b>
2.1 Ion-Based Cells: Physics and Production . . . . .	34
2.1.1 Electrochemical Cells . . . . .	35
2.1.2 Thermodynamics of Cells . . . . .	37
2.1.3 Slurry Electrodes . . . . .	44
2.1.4 Porous Electrodes Theory . . . . .	46
2.2 CNFs Production and Characterization . . . . .	48
2.2.1 CNFs and their Application . . . . .	48

## CONTENTS

2.2.2	CNFs Characterization . . . . .	52
2.3	Active Material . . . . .	55
2.3.1	NVP . . . . .	55
2.3.2	Loading of CNFs . . . . .	56
2.3.3	NVP Characterization . . . . .	57
2.4	Electrochemical Cells Testing . . . . .	58
2.4.1	Typical Cell Setup . . . . .	59
2.4.2	Cyclic Voltammetry (CV) . . . . .	61
2.4.3	Electrochemical Impedance Spectroscopy (EIS) . . . . .	65
2.4.4	Galvanostatic Cycling (GC) . . . . .	68
2.4.5	Reference Electrode and Half-Cell . . . . .	69
2.5	Summary . . . . .	71
<b>3</b>	<b>Experiments and Results</b>	<b>81</b>
3.1	CNFs Production . . . . .	82
3.1.1	E-spin setup and parameters control . . . . .	82
3.1.2	Stabilization and FTIR . . . . .	83
3.1.3	Carbonization SEM and Optical . . . . .	85
3.2	NVP Synthesis and Loading . . . . .	86
3.2.1	NVP Synthesis . . . . .	87
3.2.2	CNFs Loading (I): Dip-coating . . . . .	89
3.2.3	CNFs Loading (II): Buchner Filtration . . . . .	91
3.3	Electrochemical Cell Assembly and Testing . . . . .	93
3.3.1	Setups . . . . .	93
3.3.2	Batch 1 . . . . .	95
3.3.3	Batch 2 . . . . .	101
3.3.4	Batch 3 . . . . .	102
3.4	Future Experimental Perspective . . . . .	105
3.4.1	Study on CNFs . . . . .	106
3.4.2	Study on Loading . . . . .	106
3.4.3	Study on Cathode . . . . .	106
3.4.4	Study on Anode . . . . .	107
3.5	Summary . . . . .	107
<b>4</b>	<b>CONCLUSIONS</b>	<b>111</b>

CONTENTS

<b>APPENDIX A: Additional Images</b>	<b>113</b>
4.1 NVP . . . . .	113

# ACKNOWLEDGMENTS

I would like to acknowledge prof. Jürgen Brugger for its trust in two unknown students; for the time dedicated to our project and the valuable hints.

Prof. Claudio Gerbaldi for supervising our project and the writing of the present document.

Prof. Giovanni Boero for the suggestions and his teachings; for the help with EPR experiments.

Lorenzo Lucherini for being my project mate and for the invaluable support.

Prof. Carlo Ricciardi for the ability in cope with our mess and for being the coordinator of this master program.

Debora Conti and Matteo Lugli for the infinite discussions we made and for the inspiration for this project.

Prof. Doretta Capsoni and Irene Quinzeni for their help and support in the very first stage of our work.

Meligrana Giuseppina and Francesca Colò for their help from POLITO with electrochemical characterization and testing.

Prof. Jan Van Herle and Prof. Peter Hugh Middleton for their enthusiasm.

Prof. Mario Paolone for a clarifying talk on stationary storage systems.

The Mustache man from architecture atelier for its help with prototyping.

Christopher Chi Wai Tse for Postdoc Thursday.

The LMIS1 Family for its friendship and help.

Lorenz Hagelüken for its patience.

Séverine Eggli for the cakes.

Gloria for the beach-volley matches.

Giulia for the car.

Marco for the spirit of Milan.

Costantino, and Alessio for the pizza Sunday.

And my family for its support.

# PREFACE

## Personal Motivations

I have spent the last year and an half, before this thesis project begun, studying lots of different things, in different places, and with different methodologies. Despite the title of this travelling master course sounds like "Micro and nano-technologies" the most important teaching has been to always keep an eye on the big picture; not an easy task but worth to be pursued.

It takes me 1 year, after the first time me and my friend M. L. discussed about energy storage, to be brave enough to propose a project on sodium-ion battery to a micro-technique professor. "Fortune favours the bold" and I landed in the electrochemistry world: thanks to my project mate L.L. and the help of professor C.G. it has been a soft landing . This is not to say that I went in blind, actually I have always been fascinated by the possibility which can be unleashed by enough power in a small enough place. Of course the recent general excitement about renewable resources and electrical vehicles contributes pushing me in this direction.

## Abstract

Energy storage systems are wide spread in our life, from mobile phones to car batteries.

Electrochemical energy storages are the natural evolution of stationary storage systems, linked to energy production and distribution. With the mass production of lithium-ion battery due to future expansion of the electrical vehicles market and the consequently price fall, the possibility of introducing this technology in the stationary storage starts to be profitable.

Such an increase of lithium exploitation raises concerns about its sustainability, both environmental and economical. Different alternatives to lithium have been explored in the last decades and sodium is one of the most promising. Carbon nano-structured electrodes are particularly suited to enhance the strengths of sodium and shortens the gap between sodium and lithium with respect to total capacity. To reach the requirements of the target application the device needs good capacity and efficiency at high C-rate.

Electro-spun CNFs are an optimal solution in terms of cost, scalability, and maturity of the production process. They work as a sponge for the electrolyte and a scaffold for the active material. In the present work the full production line has been studied, with particular attention to the effects of fibres morphology and loading profile on the electrochemical performances. Cyclic voltammetry, impedance spectroscopy, and galvanostatic cycling are the main techniques employed.

# Chapter 1

# Framework and Opportunities of Battery Energy Storage

## 1.1 Thesis and Purpose of this work

The problem addressed in this work is the one of the energy storage devices linked with renewable energy production. The peculiarity of this field is an attention to the cost, efficiency and sustainability of the whole device and less constrains on the choice of material compared to the portable batteries market [16, 17, 8]. Focusing on energy storage systems for stationary application implies the necessity to linger on different aspects of storage devices from a system perspective.

The deliveries and the purpose of this work, from both the system point of view and the experimental point of view are summarized below.

### 1.1.1 System Perspective

#### **The Problem**

After the spreading of renewable energy in the last decades, the problem of intermittent power generation is a major concerns to the endemic exploitation of those kind of technologies. Because the energy production of solar and wind power may oscillate, while the demand is constant, periods of intense production must be exploited to cope with low production periods and optimize the plant performances. The variations take place on time scale of the order of seconds to minutes, hence storage systems to be embedded with renewables must have a quick response, instead of a very large energy capacity: among the main usages, the device is asked to store energy for just few seconds before it is asked back, and rarely to shift energy from day to night.

## 1.1. THESIS AND PURPOSE OF THIS WORK

One of the most important requirement is the ability of the system to release high power for few seconds with very high efficiency<sup>1</sup>, but the possibility to store small quantity of energy, at low cost, is still an appealing feature for energy self consumption: home photovoltaic systems may be used for both self consumption and for grid support; the requirements would be a trade off between the two characteristics.[2, 16, 8, 31, 6].

### The Solution

In order to address the above depicted scenario, all main choices have been explored, among the energy storage systems commercially available, altogether with the recent advancements in the research panorama. Electrochemical batteries seems to be the best choice from the point of view of price, safety, and performances, while there are some degree on the choice of the technology to be used.

Today, lithium-ion batteries are the mainstream choice for the few commercial device but the perspective of a lithium-based technology on a larger scale raises issues about its sustainability. It seems a dangerous option for both environmental safety, linked with lithium ion battery materials, and for the possible shortage of those materials in the next decades[16, 24]. The attention of researchers on the sodium-ion battery raised altogether with the awareness of possible problems, in the future, with lithium-ion; a sharp increase in publications testify this trend (figure 1.1).

The similarities among the two technologies permit a smooth shift of paradigm, but some

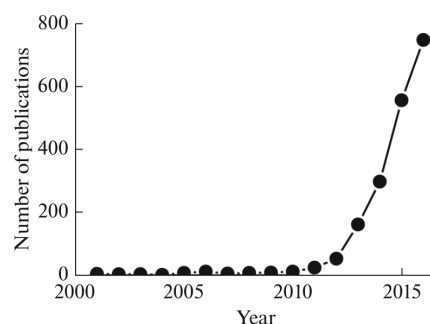


Figure 1.1: Growth in the number of publications about sodium-ion batteries between 2001 and 2016. Taken from [36]

drawbacks linked with sodium ions, require more advance designs to keep the pace with lithium-ion, in this early phase of development and keep high the interest in the technology. The usage of different nanostructures has been investigated and it seems the right path to pursue to reduce the gap[39, 32]. The proposal of this thesis is then to develop a process flow to investigate the production and the performances of carbon nanostructures (Carbon-Nano-Fibres or CNFs). To

---

<sup>1</sup>From this requirement one can argue that super-capacitor are the best choice

## 1.2. STATIONARY ENERGY STORAGE SYSTEMS

test the structure, sodium-vanadium-phosphate nanoparticles, one of the possible choices for sodium-ion battery, have been synthesized.

The focus of the work is then the controllability of the production process, in order to obtain reproducible devices and to clearly link the electrochemical performances with the nanostructure properties. In a second phase, the nanostructures are tested with different materials to study the performances variation, compared to standard process, and to assess the average effect of the structure on electrochemical cells.

### 1.1.2 Experimental Deliveries

During those six months a workflow has been designed in order to get all the results needed to support the thesis. The first work-block concerns the design of a lean and scalable production line for the samples. In particular, electro-spinning technique has been chosen: this technique is employed in the textile market and it is an extremely simple and effective one. During the production, different microscopy and spectroscopy techniques are used for material characterization and to assess the effect of variation of the process on the samples properties: SEM, XRD, FTIR. Optimization of the different process phases is a fundamental step, which allows both to take over control of the process and to verify the effectiveness of the chosen characterization techniques.

The second block is about the nanostructure itself and the effects on the electrochemical performances. The characterization is still the main tool, during the production process, to link the electrochemical performances with physical and morphological characteristics of the nanostructure. The effects resulting from the nanostructure have to be separated from the ones linked with the active material. The validation of the literature results, with electrochemical testing, is the first step for which cyclic voltammetry, impedance spectroscopy, and galvanostatic cycling are the most important techniques to be used.

## 1.2 Stationary Energy Storage Systems

Energy storage systems are widespread in our everyday life: each time we switch on our mobile phone or we use a remote controller we rely on them; every car is equipped with a battery and the major part of technological gadgets, our life is full of, exist thanks to small energy storage devices (the batteries). All these examples are taken from the portable energy storage devices world, where the electrochemical batteries are the major player. Less obvious and more differentiated is the stationary storage, where the hydro-pumped systems (dams) are the mainstream option but

## 1.2. STATIONARY ENERGY STORAGE SYSTEMS

a dozen of different technologies are exploited. While the former examples of energy storage have a clear application, the latter, because devoted to more technical aspects of energy distribution, have more obscure ones. An example is the energy accumulated in water as potential energy in a dam; this process is quite slow and the best application is shifting a certain amount of energy from the time span it is produced to the time span it is needed: for example the energy produced during the day but needed to light the houses after fall. Here the energy storage device acts as a buffer, to better exploit the existing energy production. Mechanical systems (spinning wheels) and battery have much faster response and are used for high frequency applications linked to local variation of production/demand during short time spans. Also the optimization of the load, to increase energy transport efficiency, requires the usage of capacitors or batteries.

In the last decades, with the introduction of renewable energy, stationary storage systems are growing in importance, and in particular the ones which can cope with the fast variations of wind and solar power implants. Different solutions are available: flow batteries, electrochemical batteries; hydrogen cells. The most critical point is the profitability of those systems, which are usually very expensive and it takes decades to pay off the investment[24]. In this framework, the ion batteries price is expected to lower, due to mass production of lithium ion batteries for automotive application, and may become the best option to be integrated in a renewable energy production site.

The remainder of this section is devoted to clarify the main concepts behind stationary storage, with a top down approach, starting with storage systems down to choice of materials.

### 1.2.1 Energy Storage Devices: a System Perspective

The macro area of this work is the energy production and distribution on power grids. Those

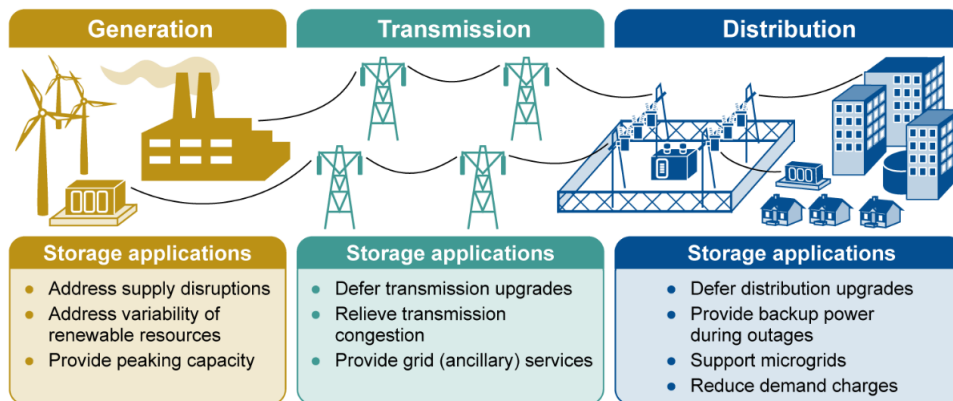


Figure 1.2: Examples of Potential Storage Applications on the Electricity Grid from [11]

huge infrastructures are used to distribute, optimize and control the electrical energy all around countries. In figure 1.2 a schematic representation of a power grid, with a list of the possible

## 1.2. STATIONARY ENERGY STORAGE SYSTEMS

applications of energy storage, is reported.

As capacitors are essential for power lines in circuits, storage elements have the very same role for the power lines of a country. They are used to increase control and reliability of line. The right sizing and adequate control leads to huge improvements of the line efficiency (line matching) which results in an economic return for energy producers. In the past years, stationary energy storage was a matter of big companies only, while today, with the spread among privates of energy production (wind and solar power), the demand of smaller, cheaper and more flexible storage devices is rising.

Before focusing on the different storage technology, it is important to explore in more details the storage devices present in the grid. Those systems are far more complex than batteries in mobile phones or cars, because to big implants is related an high risk<sup>2</sup> which must be carefully managed. The very same connections to the main grid require robust power electronics components and adequate control systems, while to connect a phone battery to the grid a small charger is enough. In figure 1.3 an example of a stationary storage system with all its components is reported.

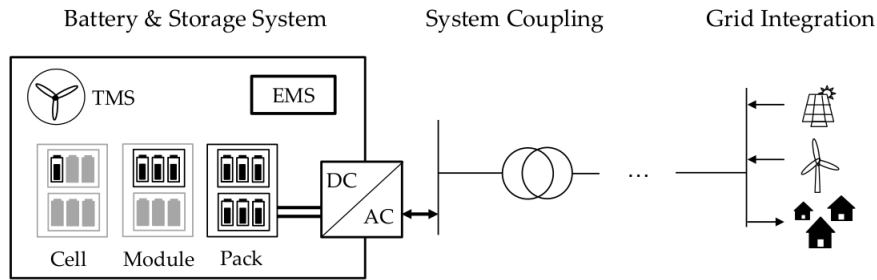


Figure 1.3: Schematic of stationary energy storage device, Taken from [13].

### Storage Element

The storage element determines under which form the electrical energy is stored before being used. Usually this element interfaces with the system through a transduction mechanism, which converts the energy back into current and voltage. In hydro-pumped systems, water is stored as potential energy in water and turbines are used to convert potential energy back and forth to electrical energy; In flywheels the energy is stored as kinetic energy, while in gas storage as pressure of the stored gas; molten salt systems store energy in form of heat.

<sup>2</sup>Explosion or dysfunction of mobile phone batteries is relatively harmless compared to implants failure

## 1.2. STATIONARY ENERGY STORAGE SYSTEMS

### **Energy Management System (EMS)**

The storage element status and interaction with the systems are controlled by means of automatic control systems. By monitoring the status of the storage, the performance can be optimized: increase the lifetime of the device and its efficiency. In order to accomplish those tasks the EMS need a reliable mathematical model, from which the status of the device can be assessed, by measuring simple quantities<sup>3</sup>. Batteries, which are rather complex systems and are particularly sensitive, need complex and expensive EMS to ensure proper working conditions.

### **Thermal Management Systems (TMS)**

While routine controls and optimization are carried on by the EMS, a dedicated system is designed to cope with the safety of the storage element. In particular, chemical and electrochemical storage systems performances are critically influenced by temperature: wrong working temperature results in poor performances or even in the system breakdown. Hence the TMS is a key element in any device and may account for a large part of the weight and cost.

### **Power electronics**

The major part of the power electronics is used to connect the storage element to the grid: AC/DC conversion, grid connector, transformer. Those components are usually bulky because large currents pass through them during grid-storage interactions. An accurate design and sizing is required not to waste power. A good battery with bad power electronics is the same as a bad battery.

### **1.2.2 Storage Technologies and Applications**

The center of the present work is the storage element while the other parts will not be discussed in more details. Notwithstanding the control part, the case and the interface with the external world have to remain as ghosts in our minds. Their existence and impact on the overall device must be kept in mind, and consideration about their size and complexity should be done as soon as in the early stage of development of a device.

The possible choices for stationary energy storage are presented below. It has to be noticed that all those technologies imply the storage element to be somehow rechargeable, while in the portable energy storage both rechargeable and not-rechargeable elements are encountered. The main reason is the necessity to payback large investments, resulting in long term life of the device as an initial constrain. A second reason can be found in the typical applications, which

---

<sup>3</sup>Velocity of the wheel, water in the dam, voltage of the battery.

## 1.2. STATIONARY ENERGY STORAGE SYSTEMS

usually use the storage element as buffer, which, implicitly, must be able to both store and provide energy.

### **Pumped Hydroelectric Storage (PHS)**

PHS is by far the most mature and exploited of all storage technologies: 96% (176 GW h in 2017) of the total storage capacity[16]. The principle is the management of a large quantity of energy under the form of gravitational energy in the water of dams. The energy is stored by pumping the water from a lower reservoir to an higher reservoir, using energy from the grid. The stored energy is proportional to the volume of water and to the height between the high and the lower reservoir. PHSs are characterized by very low self discharge rate (i.e. the energy stored is available after hours of idle operation without losses). The cost of storage is also relatively cheap compared with other systems, hence the best application is energy shifting: energy is stored during peak production and released during peak consumption. The main drawback of this technology is the necessity of particular topographic sites[16, 10].

### **Compressed Air Energy Storage (CAES)**

With this technology energy is stored as compressed air in underground caverns or tanks; to store and release energy, turbines are used as in PHS. The dimension of the cavern and the pressure of the air, altogether with its temperature, determine the amount of stored energy. As for PHS the main advantage is a good retention over several hours and are therefore used for energy shifting. Once again the availability of caverns is a constrain to realize big and cheap systems[16, 10].

### **Flywheel Energy Storage**

The rotation of a big mass is used to store energy in form of rotational inertia. By accelerating or breaking it with and electric engine, energy can be added or drained from the storage. The available energy depends on the weight and the speed of the mass, while retention is critically influenced by friction. Flywheels have fast charge/discharge capability, good life cycle and fast response. Those characteristics make this technology particularly suited for short-term, fast response applications like frequency regulation and power buffering. Their critical point is safety: insufficient protection and poor design may lead to damage to the surrounding environment[16, 10].

## 1.2. STATIONARY ENERGY STORAGE SYSTEMS

### Electrochemical Energy Storage (ECS)

ECS is based on reduction and oxidation reactions taking place in an electrochemical cell. The

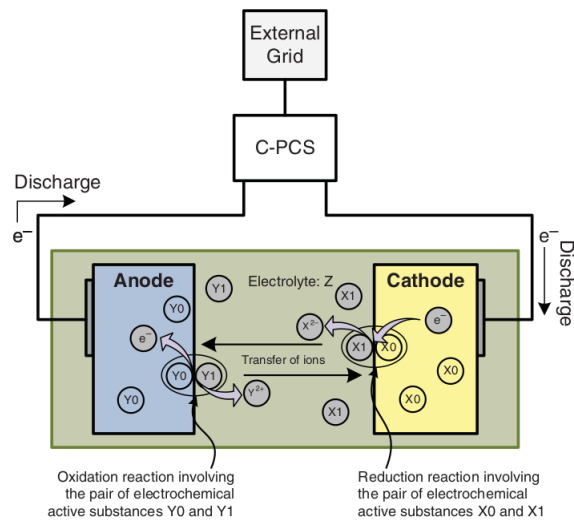


Figure 1.4: Schematic of an electrochemical cell. Taken from [10]

cell is composed of two electrodes (anode and cathode) where the two chemical reactions occur (figure 1.4), usually requiring some chemical species to travel between the two electrodes (e.g. ions). At the same time a conductive path must be established to allow electrons to be provided at one electrode and drained from the other.

The energy is stored in chemical form: change in the chemical bonds, phase transition, and alloying during reaction. Batteries and flow batteries are the two main families and both exploit

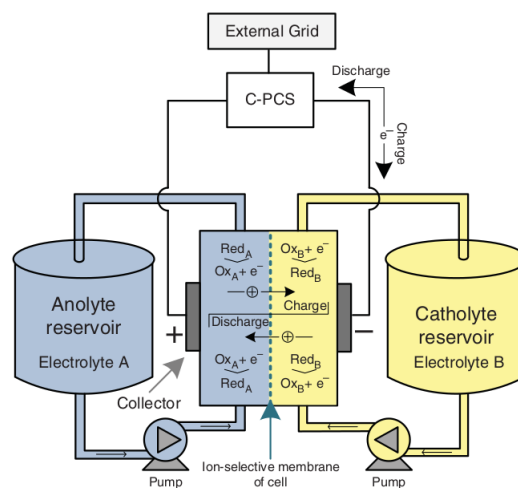


Figure 1.5: Schematic of a flow battery. Taken from [10]

redox reactions. The main difference is the storage mechanism of the active material: in batteries, it is stored in the very same electrode where the reaction takes place; in flow batteries, dedicated tanks store the active material in form of a solution, as shown in figure 1.5. Flow bat-

## 1.2. STATIONARY ENERGY STORAGE SYSTEMS

teries have more complex architectures and hence higher costs but, at the same time, they are safer and have better life cycle compared to batteries[16, 10]. Another interesting advantage of flow batteries is the possibility to tailor, independently, power (dimension of the reaction zone) and energy (dimension of the tanks) performances. Self consumption is an exclusive field of battery, thanks to small dimension and cost[16, 6, 24]. Peaks shaving and power quality can be addressed using electrochemical storage but is the frequency regulation application where the major part of batteries are exploited: 50% (0.95 GW h in 2017) of the total ECS storage capacity is used for frequency regulation and the dominant technology is lithium-ion (59 %)[16].

### Chemical Energy Storage

Chemical Energy Storage is represented by super-capacitors, which are, from the structure point of view, extremely close to batteries, except for the fact that no reaction takes place at the electrodes (figure 1.6). The energy is stored in the electrical double layer (EDL) which builds

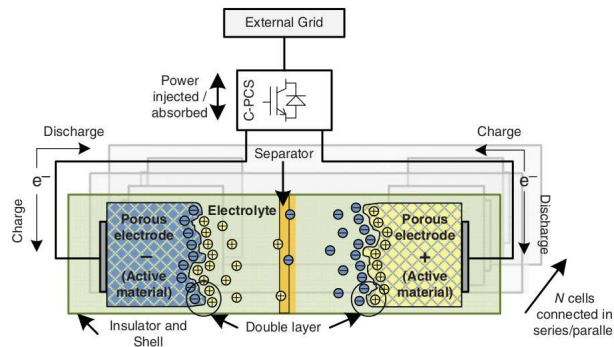


Figure 1.6: Schematic of a Supercapacitor. Taken from [10]

up at the interface between the electrode and the electrolyte<sup>4</sup>. When the electrode is positively charged negative ions accumulate near the interface (inner Helmholtz plane) and may interact with the metal. A second layer (outer Helmholtz plane), of non interacting ions, is formed near the inner plane. A diffusion layer connects the two layers with the bulk electrolyte[41]. In figure 1.7 the double layer is schematically depicted under different electrode polarization conditions. This structure results in a capacity which is proportional to the surface area of the electrodes. Super-capacitors show long cycle life and high power capability but lack of energy content and cannot store energy for more then some hours (high self discharge)[16, 10].

<sup>4</sup>Similar to the diffusion capacitance which forms at a metal-semiconductor junction.

## 1.2. STATIONARY ENERGY STORAGE SYSTEMS

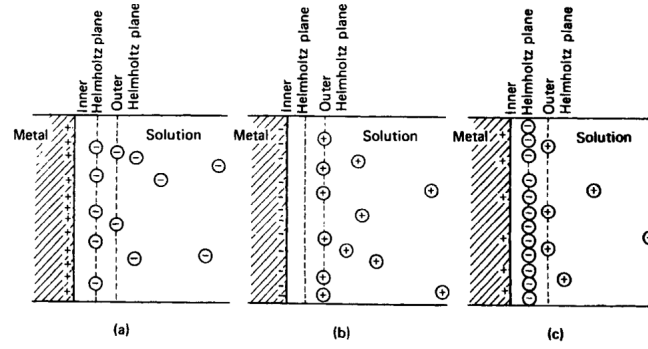


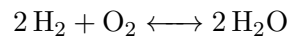
Figure 1.7: Formation of the electrical double layer: a) positive polarized electrode with anions interacting with the metal. Because the adsorbed ions are not enough to compensate for the charge on the metal, the outer plane and the diffusion layer are made of anions too. b) positive polarized electrode but no possible interaction between cations and metal: empty inner plane. c) positive polarized electrode with charge compensation due to high anions adsorption at the metal surface. The outer plane and the diffusion layer are made of cations. Taken from [41]

### Thermal Energy Storage (TES)

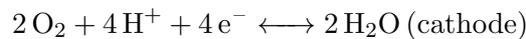
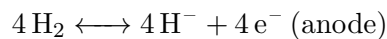
The energy is stored in form of heat of a medium; three different storage medium can be defined: sensitive heat media, latent heat media, and chemical heat media. In sensitive heat media the heat is stored as a difference of temperature between two media and it is the most used technology for TES. For example in solar field, where steam is produced, a sensitive heat medium is used to guarantee a certain inertia to the steam turbine and to prevent sudden power drop due to weather variations. Latent heat media exploit the phase transitions (solid-liquid-gas) of a material to provide/absorb heat at constant temperature. In chemical heat storage the heat is produced as by-product of an exothermic reversible reaction. which can absorb back the heat, as an endothermic one. Among thermal storage, molten salt technology is the dominant one in commercial applications, followed by water-based ones (ice, hot water). Those systems are characterized by a simple working principle but the cost is quite high and the self discharge dependent on the isolation of the medium with respect to the external environment[16, 10].

### Hydrogen-Based Energy Storage

Hydrogen storage relies on the reaction of water hydrolysis:



The reaction can be split into two components, one at anode and the other at cathode:



The device is composed by a chemical cell and a tank for hydrogen or water. If the cell is used to produce hydrogen from water it is called electrolyzer, while for the reverse reaction it is called

## 1.2. STATIONARY ENERGY STORAGE SYSTEMS

fuel cell. The hydrogen, once it is produced, can be easily stored for long period of time but the efficiency at room temperature of the device is about 65%. Because the process is a two steps one, the overall efficiency of electrolyzer and fuel cell is about 42%, which is the major limitation for this technology. Safety is of course an important issue with hydrogen, which is highly flammable[16, 10].

### 1.2.3 Market and Resources Analysis (2030)

As a conclusion of this section the market analysis for stationary storage till 2030 is presented. The Market analysis forecasts an expansion of the BES total installed power linked to the diffusion of private photovoltaic (PV) systems for self consumption. The diffusion of this systems will be boosted by both single country policy for decarbonization and falling price of the PV systems and associated storage systems<sup>5</sup>. The demand for private systems can be targeted only with small and cheap devices, hence the only possible choice is ECS. All the other systems require too large installation costs, safety measurements and space, to be appealing for a single family.

In this framework, the choice of lithium-ion batteries, which today dominate the market, seems the obvious one, both to exploit the already mature technology and the existing industrial plants. It is to justify of choice of a shift of paradigm, from lithium-ion to sodium-ion, that an analysis of the available resources and the quantity needed to cope with the forecast demand is proposed. The possible problems linked with the shortage of precursors and a price rising for lithium technology are the main stimuli to research a viable alternative.[16, 6, 24]

### Growth Rate for Demand

The energy storage capacity in the planet is estimate to grow from 4.68 TW h in 2017 to 6.62-7.82 TW h. If a doubling of the share of renewables is hypothesize, <sup>6</sup> the increase will be up to 11.89-15.27TW h. The leadership of PHS will not be jeopardize but may fall from 96% to only 88%-83%<sup>7</sup> by 2030. BES will experience an expansion from 11 GW h in 2017 to 100-167 GW h in 2030. The doubling case is particularly favourable for BES, which may grow up to 181-421GW h. The private sector will lead the expansion, with 78 to 197 GW h of capacity increase in the doubling case. Utility scale increase is estimate to be about 35-65 GW h in the standard scenario and up to 71-177GW h in the doubling case[16]. Summing up (figure 1.8), BES will

---

<sup>5</sup>Tesla Power Wall is an example of this tendency of selling both PVs and storage systems

<sup>6</sup>The hypothesis assumes the renewable energy production to double its contribution compared to 2017. This technology intrinsically requires more storage capacity with respect to fossil fuels.

<sup>7</sup>In the doubling case, due to the nature of renewable, which requires other types of storage, the share of PHS will fall to only 51%-45%

## 1.2. STATIONARY ENERGY STORAGE SYSTEMS

experience an expansion between 89 to 411GWh in worst and best case scenario. With those data it is possible to analyse lithium-ion and its precursors with a critical approach.

### Lithium and Precursors

In order to analyze the precursors of lithium-ion batteries, focus has been shrinked to the top three technologies available, today: Lithium Cobalt Oxide (LiCoO<sub>2</sub>), Lithium Manganese Oxide (LiMn<sub>2</sub>O<sub>4</sub>), and Lithium Nickel Manganese Cobalt Oxide (LiNiMnCoO<sub>2</sub>)[40]. All three refer to Cathode materials, while the anode is graphite for all of them. In table 1.1 a summary for each material is provided: the energy per kilo (Wh kg<sup>-1</sup>Wh/Kg), the precursors and the kgs of precursors to obtain 1 kg of active material. Among the three, LCO is the most used in

Active Material	Wh kg <sup>-1</sup> (commercial)	Precursor	kg
<i>LiCoO<sub>2</sub></i>	240	<i>LiCO<sub>2</sub></i>	0.88
		<i>Co</i>	0.6
<i>LiMn<sub>2</sub>O<sub>4</sub></i>	150	<i>LiCO<sub>2</sub></i>	0.5
		<i>MnO</i>	0.95
<i>LiNiMnCoO<sub>2</sub></i>	220	<i>LiCO<sub>2</sub></i>	0.3
		<i>Co</i>	0.2
		<i>MnO</i>	0.3
		<i>NiO</i>	0.25

Table 1.1: Materials for lithium ion batteries

commercial devices<sup>8</sup> but also the worst one, from the point of view of precursors sustainability. LMO is the best one because it does not contains cobalt, but is also the one which requires more lithium. NMO is in between the two. For each GWh the amount of Li required varies from 1360 to 3660 Tons, while of cobalt from 910 to 2500 Tons.

The world reservoirs of the two elements are reported to be about 15 millions of Tons for Li [38]

<sup>8</sup>Mobile phones

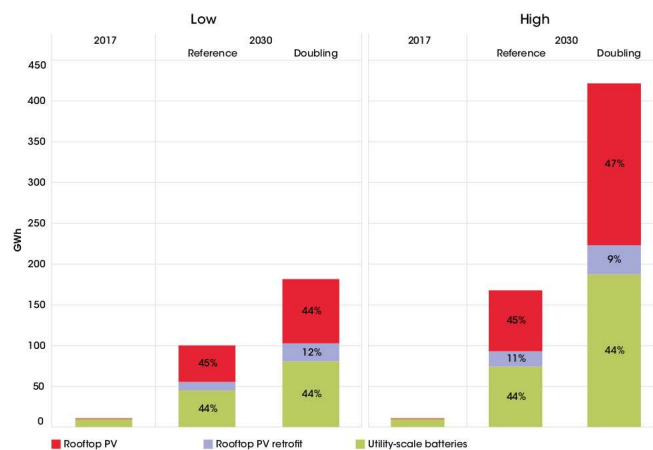


Figure 1.8: Estimated growth of BES per sector 2017-2030. Taken from [16].

## 1.2. STATIONARY ENERGY STORAGE SYSTEMS

and 5 millions of Tons for Cobalt[37].

### Sodium and Precursors

Sodium-ion based commercial devices start to appear on the market during the last years, but no mainstream technology has been established, while lots of promising materials are at the prototyping level[39, 32]. In the following table some of the most promising cathode materials are reported. Hard carbon is assumed as anode material to normalize the power density and for a faster comparison with the lithium-ion table. Even if the reported capacities per Kg seem to be higher with respect to lithium, it has to be considered how the values reported in papers vary a lot among works and tend to be best case capacities. The "paper values" for the same lithium material reported above are about 2 times higher than the commercial device one. The stability of the reported materials is also quite poor, compared to commercial devices. Notwithstanding the comparison aims to be more on the material abundance than on performances. It comes out

Active Material	Wh/Kg (paper work)	Precursors	Kg	Ref.
$Na_2MnP_2O_7$	220			[20]
$Na_2(VO)P_2O_7$	250			[5]
$Na_2FePO_4$	200			[4]
$Na_3V_2(PO_4)_3$	320			[46]
		$Na_2CO_3$	0.35	
		NH <sub>4</sub> VO <sub>3</sub>	0.51	
$NaTi_2(PO_4)_3$	190			[46]
$NaCrO_2$	300			[45]
$Na_2C_2O_6$	700			[19]
$Na_4C_8H_2O_6$	230			[44]
$NaMnO_2$	450			[7]
$Na_2Fe(SO_4)_3$	280			[3]
$Na_{2/3}(Ni_{1/3}Mn_{2/3})O_2$	450			[23]

Table 1.2: Materials for sodium ion batteries

the critical materials to be vanadium and titanium, for which the reservoirs are more than 60 millions of tons each [34, 15, 26, 25]. All other materials may be considered almost unlimited.<sup>9</sup>

### Considerations

All the figures to justify the choice of sodium technology over the lithium one are now available. To answer the forecast growth of about 200 GW h over the next decade, about 4 millions of Tons of lithium and cobalt are needed; it means about 80% of the cobalt reservoirs and 27% of the lithium one.<sup>10</sup>

On the sodium side the same volume is relatively small (5-10% of the available reserve) and hence there is no risk linked to resources shortage in the next decades. Another point is the distribution of each resource. Analysing the provided references, one can observe lithium

<sup>9</sup>For chromium and sodium the reservoirs are hundreds of millions of tons[14]

<sup>10</sup>The availability of reservoirs does not mean that the extraction rate will rise fast enough to permit their exploitation

### 1.3. ELECTROCHEMICAL ENERGY STORAGE DEVICES

and cobalt production to be localized in few countries (China, Congo, Chile) while sodium and vanadium are much more distributed around the world.

## 1.3 Electrochemical Energy Storage Devices

A step backward is now necessary to present in details the batteries energy storage (BES). The BES scenario may be divided into two main families: *primary batteries* or not-rechargeable and *secondary batteries* or rechargeable .

It is important to distinguish from now on the word *cell* from the word *battery*. A cell is a system composed by two working electrodes and electrolyte in between them; it is the building block of a battery and its circuitual element looks like a capacitor, reflecting the similarities between the two. A battery may sometimes be made of a simple cell but that is rarely true: batteries often comprise stacks of cells, a DC-DC converter, and control systems.

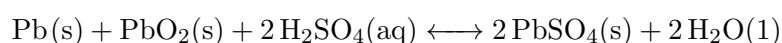
All secondary battery relies on a reversible reaction which is driven in one direction during discharge and in the reverse direction during charge. The reactions can also be split into two parts, taking place at the two opposite electrodes: reduction at the cathode (positive electrode) and oxidation at the anode (negative electrode).

### 1.3.1 Secondary Batteries

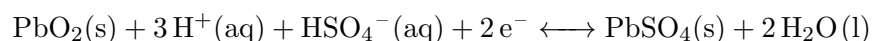
A summary of the major and most successful secondary cells and the exploited reactions is presented below.

#### Lead-acid batteries

Lead acid batteries are the oldest and most used technology. Flooded lead-acid batteries have been developed in the nineteenth century and are composed of lead electrodes flooded with solution of sulphuric acid ( $H_2SO_4$ ). It is peculiar, compared to other secondary battery, how the electrolyte has an active role and it is not just used as ions conductor. During discharge, lead sulfate ( $PbSO_4$ ) is plated on both electrodes and it is consumed during charge. The overall reaction is:

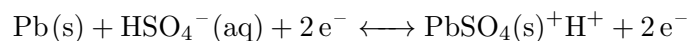


Which can be divided into positive electrode reaction:



### 1.3. ELECTROCHEMICAL ENERGY STORAGE DEVICES

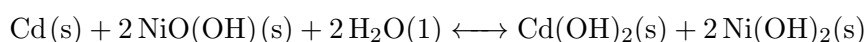
And negative electrode reaction:



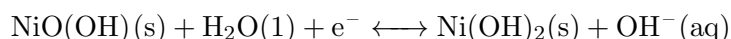
In the common lead acid batteries the electrolyte is a liquid which "floods" the lead plates, but because of the gas formation (oxygen and hydrogen) during reaction, the batteries have to be vented to avoid pressure increase. As side effect the electrolyte evaporates and the life time of the batteries is reduced. The technology evolved with the valve-regulated lead-acid batteries, which are sealed by a valve; this valve is provided in order to avoid pressure to exceed a safety threshold. In this cell the oxygen is reduced back to water and the pressure increase does not cumulate during cycling but it reaches a peak at the end of each cycle. The main advantage of this technology is the low cost, due to maturity of the production process and mass production for automotive applications.

#### **Alkaline Batteries**

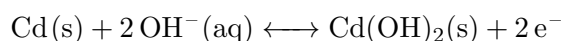
Cadmium-nickel oxide and metal hydride-nickel oxide cells are the two main technologies present in the alkaline batteries technology. The reaction in Cadmium-nickel oxide cells is the following:



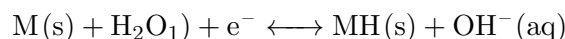
With the positive semi-reaction



And negative one



Those kind of cells can either be vented or sealed and were very popular before the introduction of the sealed hydride-nickel oxide cells. The hydride-nickel oxide cells exploit the same reaction at the positive electrode while at the negative one a metal is used to form an alloy with the hydrogen:



This technology has much more capacity compared with lead acid and is far safer. This is why it has been the preferred choice for portable application. It is not cheaper than lead acid but is anyway cheaper than the far more advanced lithium-ion technology.

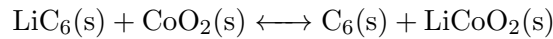
### 1.3. ELECTROCHEMICAL ENERGY STORAGE DEVICES

#### Lithium Ion Batteries

All the batteries so far presented uses an aqueous solution as electrolyte which implies some sort of complication due to gas formation during reaction. The main solution, with the sealed cell, is the incorporation the water hydrolysis in the cell chemistry, in order to revert the effect during the cycling. With lithium-ion water is replaced by organic electrolytes, which can withstand high voltage without producing volatile by-product. The result is much more powerful batteries and a simpler technology. The electrolyte shuttles the ions between the two electrodes and two insertion compounds are used to intercalate and de-intercalate them. The following reaction takes place:



The name of this system is "rocking-chair" because of the motion of ions back and forth the two electrodes. A typical example is the lithium-cobalt-oxide cathode and graphite anode couple:



In the next chapter the physics behind ion-intercalation compounds will be presented in details; while the main parameters used to compare different technology and to model the behaviour of a secondary cell are presented below.

#### 1.3.2 Model and Parameters

People coming from an electrical background are used to looking at batteries as independent voltage sources. The highest non-ideality is a series resistance, which accounts for a voltage drop when connected to a load. A much more realistic model is a controlled voltage generator  $V(\text{SOB})$  in series with a resistor  $R_s(\text{SOB})$  (figure 1.9). Where SOB, the state of battery, is the Pandora's box where all the issue have been hidden into.

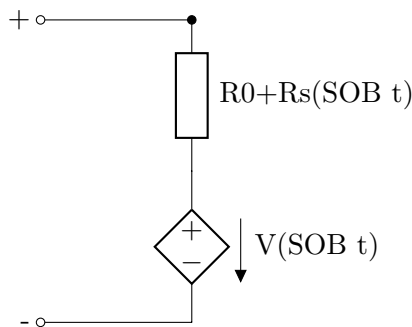


Figure 1.9: The battery model

### 1.3. ELECTROCHEMICAL ENERGY STORAGE DEVICES

Because the SOB is a function of different variables, included the previous history of the battery, it is worthy to spend some times on the parameters which are used in literature to talk about batteries and get a clearer picture.

#### **Open Circuit Voltage (OCV)**

*Open circuit voltage (OCV)* is defined as the voltage measured in between the positive and negative terminal of when no load is present. It is equal to the voltage  $V$  of the ideal generator.

#### **Close Circuit Voltage (CCV)**

On the other side, when a load is connected the *Close circuit voltage (CCV)* is defined, which depends on the load. Both OCV and CCV depend also on the previous history of the battery. The voltage is almost the only parameter which can be directly measured with a certain precision during the operation of a battery. All other parameters has to be estimate from its variation in time.

#### **Capacity (Q)**

The *Capacity (Q)* is define as the sum of current which flows through the battery before the CCV reaches a fixed threshold  $V_{min}$  and is measured in A h or mA h:

$$Q = \int_0^{\bar{t}} I(\tau) d\tau \quad \bar{t} | CCV(\bar{t}) = V_{min}$$

#### **State of Charge (SOC)**

*State of charge (SOC)* can be expressed as the battery capacity  $Q$  minus the charge removed from the battery at the time  $t$ , divided by  $Q$  or, expressed as a function of the current  $I(t)$ :

$$SOC(t) = \frac{Q - \int_0^t I(\tau) d\tau}{Q}$$

It is unit-less and varies between 1 and 0. The state of battery, and hence the voltage and the series resistance, are function of the state of charge and its history: certain technologies face a performances drop if the SOC reach too low or too high value<sup>11</sup>.

---

<sup>11</sup>See Depth of Discharge

### 1.3. ELECTROCHEMICAL ENERGY STORAGE DEVICES

#### Depth of Discharge (DOD)

Related to the SOC can be defined the *Depth of Discharge (DOD)* which is the complementary of the minimum (with respect of time) SOC which the battery reaches during its cycling ( $DOD = 100\% - \min\{SOC\}$ ). If the battery is not discharged completely the *DOD* will be lower than 100. This is usually done with lots in technologies because the full discharge results in a degradation of performances over time. As an example the different life cycle of lead-acid batteries with respect to DOD is reported in figure 1.10.

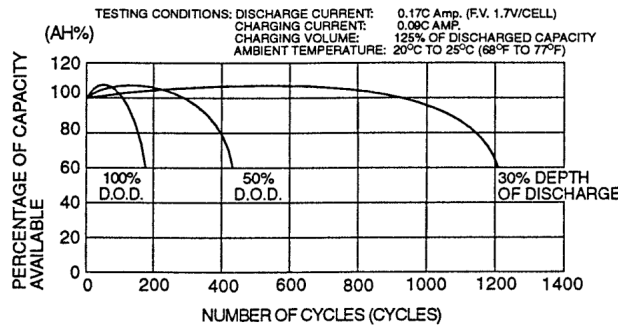


Figure 1.10: Maximum number of cycles of lead acid battery at different DOD. Taken from [9].

#### Nominal Capacity ( $C_r$ )

*Nominal capacity ( $C_r$ )* is the capacity of the battery under a certain nominal condition: fixed load, room temperature, etc. . Every time the battery is operated outside the nominal operation conditions the actual capacity  $Q$  and the *Nominal capacity* may differ of even an order of magnitude (for extreme operation conditions). This is due to the nature of V(SOB): the capacity is defined as the integral between two values of V(SOB), which shape changes at different operation conditions, leading to differences in the calculated capacity, as shown in figure 1.11.

<sup>12</sup> Nominal capacity is measured at room temperature, at low discharge current, and at the beginning of the history of the battery; same measurement conditions but different history (e.g. different DOD) lead to different measured capacity. Nominal Capacity is somehow the maximum capacity the battery can provide, if operated at best conditions.

#### Current Rating (C-rate)

*Current rating* or *C-rate* is a way of expressing the current with respect to *Nominal capacity*. Given a current, which is flowing across the battery, it can be written as the nominal capacity

<sup>12</sup>Temperature and current at which the battery is discharged influence the SOB and hence the measured capacity

### 1.3. ELECTROCHEMICAL ENERGY STORAGE DEVICES

multiplied by a constant, having the unit of  $\text{h}^{-1}$ . For example if a battery has a nominal capacity of 2 A h and a current of 4 A is flowing:

$$I = m \cdot C_r$$

In this example  $m$  is equal to  $2\text{h}^{-1}$  and the  $C$ -rate has the same value of  $m$  but expressed in Ampere; is equivalent to say 4 A or 2C of current. Another way of looking at the  $C$ -rate, is to keep the time unit and to interpret it as the time it takes to discharge the battery at that current level: 2C is the current which fully discharge the nominal capacity in half an hour; 0.5C is the current which fully discharge it in 2 hours, and so on.

It is worth spending some more time on the concept of *Nominal capacity* and  $C$ -rate. The *Nominal capacity* is often considered to be the capacity at low  $C$ -rate as mentioned before; that is to say, the capacity when the cell is not under stress. When someone claims to have found a material with an high capacity he or she is usually speaking about maximum capacity at low  $C$ -rate. This figure-of-merit was good for mobile phones and PCs because the current consumption was carefully controlled ( $C$ -rate from 0.2 to 0.1). If the paradigm shifts from portable devices to stationary power storage, spikes of current are expected, linked with production variation, and current up to 10C or 100C may flow with unpredictable effects. At this condition there are no guarantees that the low- $C$  performances reflect the actual ones.

#### Internal Resistance

The *internal resistance* models the voltage drop, proportional to the current which flows in the battery and is represented by  $R$  in the model. It is an important parameter to assess if a battery is suited for high  $C$ -rate applications. It easy to imagine a big  $R$  results in a big voltage drop

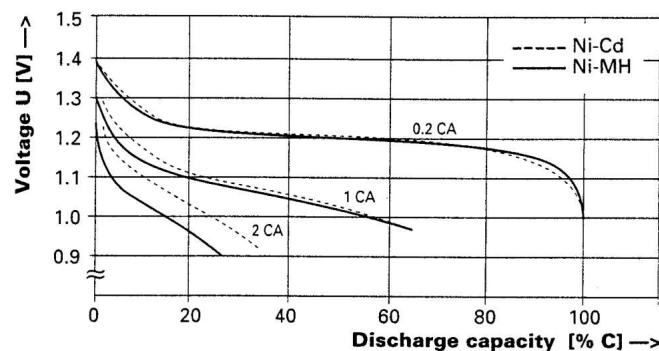


Figure 1.11: Discharge voltage profiles at different discharge currents; on the x axis the corresponding capacitance calculated by time integration. Taken from [9].

### 1.3. ELECTROCHEMICAL ENERGY STORAGE DEVICES

and even if  $V(\text{SOC})$  is bigger than  $V_{min}$ , CCV may be smaller and no current can flow at the appropriate voltage. The battery is a voltage source, not a current source, and even if a current may always flow, that may happen at the wrong voltage.

#### **Energy-to-Power Ratio (E/G)**

Energy-to-Power ratio is the relationship between the energy and power of a device and is expressed in  $\text{kWh kW}^{-1}$ . If the ratio is higher than one, the device is best suited for applications which require high energy devices; a ratio less than one indicate a device with high power performances. PHS are an example of high E/P ratio, because are usually used to store energy, to enhance frequency response the instantaneous power provided is important and devices with smaller E/P ratio are a common choice.

#### **Efficiency (Energy and Power)**

When charging a battery, it happens that more amperes or more watts has to be provided than the one obtained back when discharging the battery. Two types of efficiency can be defined: Ampere-hour efficiency

$$\eta_{Ah} = \frac{\text{Available Capacity in Ah}}{\text{Required Charge Input in Ah}}$$

and Watt-hour efficiency

$$\eta_{Wh} = \frac{\text{Available Energy in Wh}}{\text{Required Input in Wh}}$$

For stationary applications or for big storage systems, those parameters are particularly important for the tailoring of the thermal management system. A low efficiency does not only means waste of energy, but also heat production. If, during operation, lots of heat is produced (low efficiency) the resulting device will be more expensive due to more complex TMS.

#### **Volumetric and Gravimetric Density**

In order to compare different technologies, the capacity or the power (capacity times average discharge voltage) the battery provides are normalized with the total weight or volume. The four parameters obtained are:

$$\text{Volumetric Energy Density} = \frac{\text{Available Capacity (Ah)}}{\text{Volume (cm}^3\text{)}}$$

$$\text{Gravimetric Energy Density} = \frac{\text{Available Capacity (Ah)}}{\text{Weight (Kg)}}$$

### 1.3. ELECTROCHEMICAL ENERGY STORAGE DEVICES

$$\text{Volumetric Power Density} = \frac{\text{Available Energy (Wh)}}{\text{Volume (cm}^3\text{)}}$$

$$\text{Gravimetric Power Density} = \frac{\text{Available Energy Wh}}{\text{Weight (Kg)}}$$

In the lab-perspective, it is the volume and the weight of the sole active material which makes the difference, while in a real systems the management system and the case account for the major part of the weight. This means that materials that differ a lot in terms of volumetric or gravimetric energy or power density in a lab-experiments, may not lead to very different final devices.

#### Voltage Profile

Last but not least V(SOB) as to be somehow defined. One may expect the voltage to be almost constant during discharge or at least to be some kind of monotonic function of SOC in the short period; unluckily none of the two is true: V(SOB), as shown in figure 1.12, is usually an hysteretic function of SOC: charge plateau is slightly higher then discharge one, which results in a not perfectly efficient<sup>13</sup>. This is an important point, because lots of paper report the energy efficiency, which is the ratio between capacity delivered during discharge and capacity provided during charge. Because the voltage of a battery varies during cycling, this parameter is not enough to assess the power efficiency of the battery.

SOB is influenced by temperature and previous history, which makes it rather complex to estimate the SOC and the health of the battery. The complexity of the battery management systems stems from the intrinsic complexity of the V curve altogether with the need of a fine control on the batteries required in big systems.

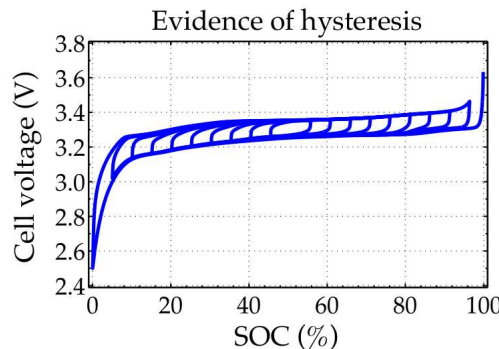


Figure 1.12: Hysteresis of the battery voltage curve with respect to the SOC. Taken from [29].

<sup>13</sup>The power required to charge the battery is bigger then the one provided during discharge

## 1.3. ELECTROCHEMICAL ENERGY STORAGE DEVICES

### 1.3.3 Comparison of Performances

Now that lots of parameters are available, it is useful to compare different secondary battery technologies with each other and with other storage technologies.

#### Ragone Plot

One of the most used tool for comparing storage technologies is the Ragone plot. On the X axis the power density and on the Y axis the energy density are reported. In figure 1.13 a Ragone plot to compare different secondary batteries with other storage technologies is presented. The main piece of information to get from a Ragone plot is about the size of a storage system for a given energy or power requirements. It is clear, at a first glance, that PHS is the bulky one for both power and energy while lithium ion is the best one for balanced performances. Super-capacitors are small if power is required, while a huge volume is necessary to obtain high energy[10, pag 115 fig 4.12].

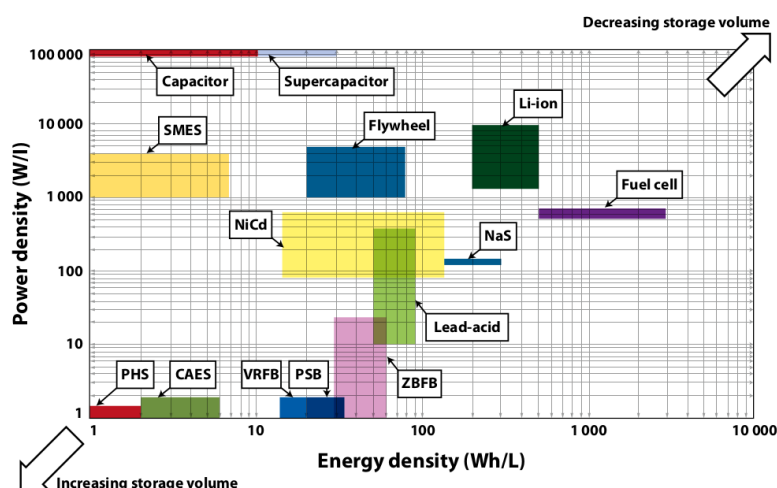


Figure 1.13: Ragone plot of different storage systems. Taken from [16].

#### Energy Efficiency

Because the efficiency is of paramount importance a plot where different storage technologies are compared with respect to this parameter is proposed in figure 1.14. Ion batteries are the best technology in terms of efficiency and hence is a promising candidate for the target application of the present work. Sodium ion, due to the intrinsic similarity to lithium ion, is expected to be able to reach the same efficiency.

### 1.3. ELECTROCHEMICAL ENERGY STORAGE DEVICES

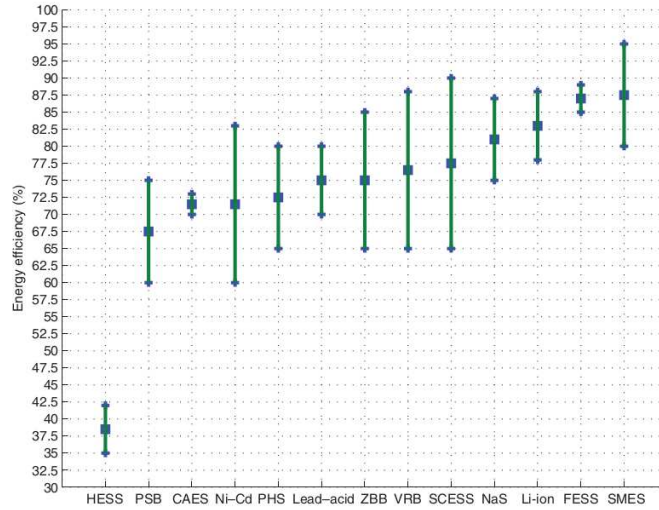


Figure 1.14: Efficiency of different storage systems compared. Taken from [10].

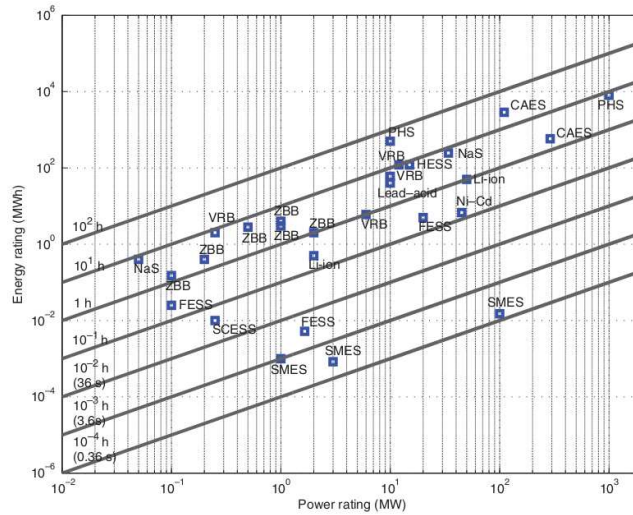


Figure 1.15: Unnormalized Ragone plot refers to actual application of each technology. Taken from [10]

#### Discharge Time

A variation of the Ragone plot, which uses the power and energy without normalization over volume or weight, can be used to group storage technologies according to the discharge time. Because the power and energy are not normalized, this plot is more about the actual performances of the device that can be build out from each technology (figure 1.15). PHS seems to be the worst technology according to Ragone plot, while it is the one with the highest energy and power rating in this second representation. It means that it is possible, both technologically and economically, to build large systems using PHS.

Discharge time can also be directly plotted on the y axis as in figure 1.16. This second plot conveys information about the purpose each technology is used for: the one like PHS, on the right corner, are used for bulk energy storage, while the one which present themselves on the left,

## 1.4. SODIUM-ION BATTERIES TECHNOLOGY

are usually used in a small format, for quality service and other control applications.

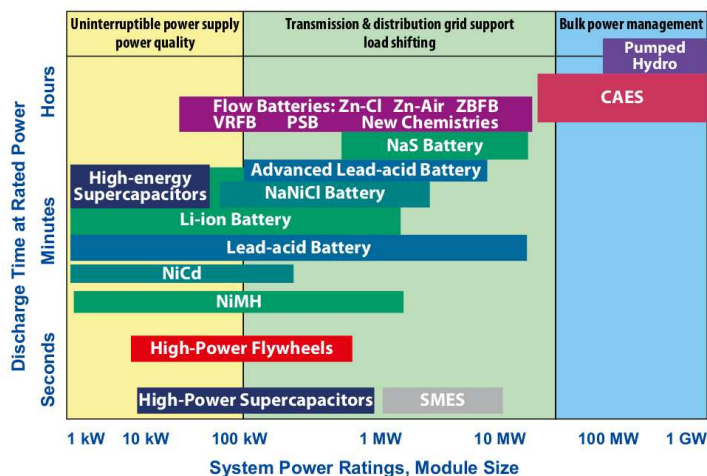


Figure 1.16: Derived from the unnormalized ragone plot the power ratio vs discharge time is a convenient way to group technologies by application. Taken from [16].

## 1.4 Sodium-ion Batteries Technology

The title of this work is a recipe to address the challenges of stationary storage systems. All the considerations and parameters so far listed may be extended to all kind of electrochemical storage device: electrochemical batteries, flow batteries, hydrogen cells. Notwithstanding it is time to shrink the focus and, after a brief introduction to ion-based batteries, a state-the-art review on sodium-ion battery and nanostructures is proposed.

Electrochemical cells store energy in changes in the chemical bonds of materials (metal alloy or crystals) and redox is the tool to store or drain energy from the materials. In electrochemical batteries the amount of energy which the device can store is fixed when the cell is assembled, while in flow batteries and hydrogen cell the redox reaction site and the energy tank are two different elements (the tank can be made bigger without any impact on the active element). In electrochemical cells the red-ox reaction zone is also where ions are stored and this results in a co-dependence between the power provided (linked to the redox mechanism and dynamics) and the total energy (linked to the number of ions available for the reaction). The redox reaction is what is called a surface phenomenon: it takes place at the interface between two phases (the crystal and the electrolyte). The energy of ions in one phase is higher than in the other and energy is released by the spontaneous transition from one phase to the other (during discharge). This means that the power performances of the device are linked to the surface area of the electrodes. On the other hand, the energy stored is proportional to the number of ions in the

## 1.4. SODIUM-ION BATTERIES TECHNOLOGY

crystal, which increases with the volume. higher volume means higher energy but lower power performances: relatively to the total energy stored. The main parameter is the time it takes to deliver the energy stored to the load; one can easily imagine that the surface area to volume ratio is directly linked to the energy to power ratio (E/G). What happens in bulky crystals is that ions at the interface can react and release energy immediately, while ions in the bulk have to wait for the other ions, nearer to the liquid phase, to react, before reacting themselves.

A battery with bulk active material is characterized by an high E/P ratio and is most suited for energy storage and control applications. The target of this work is to increase the power performance and reduce the E/P, without decreasing the energy content. Different solutions have been proposed in literature to address this issue: the growth of crystals with fractal morphology and matrices of supporting material with embedded nanocrystals are the mainstream. Carbon nanofibres (CNFs) is one of the possible supporting structures with the advantage of easy, cheap and tunable production process which can be implemented almost in any lab. The main goal of producing nanoparticles of active material on a supporting matrix is to maximize the area to volume ratio. Notwithstanding it is not enough to increase the area to volume ratio but it is the interface area to volume ratio which determines the performances.<sup>14</sup>

Nowadays many researches focus on the synthesis of high area to volume ratio particles, but then the cell is assembled with the commercial slurry technique which results in a compact layer, and only the top surface is directly exposed to the electrolyte.

CNFs are a valuable option which is not directly linked with a particular material and then it can be reused to enhance a wide range of materials; at the same time CNFs target also other issues which are particular important: they stabilize the active material when subject to mechanical stress and provide conductive path from reaction zone to current collector.

In figure 1.17 three different typologies of electrode are shown: bulky active material with "2D" interface; nanostructured active material, with high surface area "2D" interface; porous matrix with embedded active material and "3D" interface.

For what concerns the active material, sodium-vanadium-phosphate (NVP), used in the present work to test the CNFs nanostructure, is not only one of the possible choice for sodium ion battery cathode but is also one of the best one in terms of stability at high current rate. The choice of this material avoids additional problems linked with material degradation in this early stage of development and it permits to focus on the CNFs structure properties. It has also been already tested with a structure of CNFs and hence it makes it possible a comparison

---

<sup>14</sup> If the second phase (e.g. liquid) cannot reach uniformly the large area provided, the advantages of nano-size or nanostructured particles may be lost

## 1.4. SODIUM-ION BATTERIES TECHNOLOGY

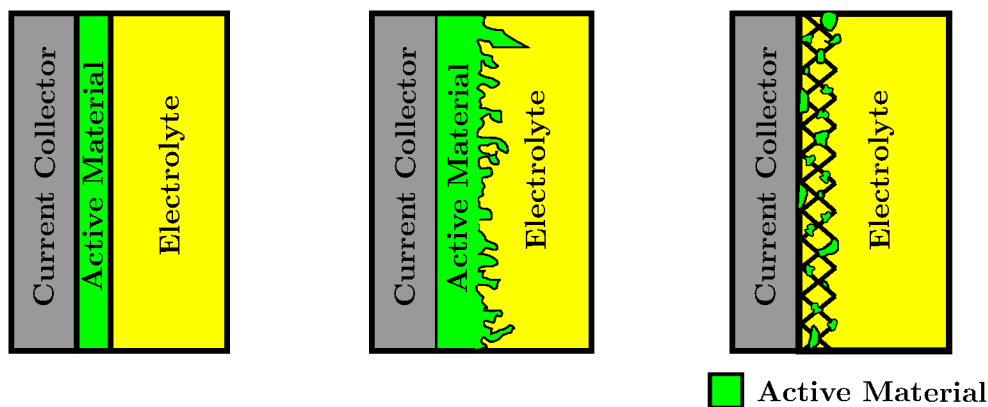


Figure 1.17: a) 2D interface, b) high surface area 2D interface, c) 3D interface .

with literature.

### 1.4.1 Cathode Materials

Following the classical sodium battery material review the different materials are grouped in families, according to their crystalline structure. Refer to [18, 39, 33, 30, 1] for complete review of the sodium-ion materials.

#### Layered Oxides

Layered oxides is a family containing all compounds with formula  $Na_xMO_2$  where M is a transition metal (Ti, V, Co, Mn, Cr, Fe or Ni). Subdivisions of the family refer to the sodium contents and the resulting crystal structure (O3, P2 or P3). The most popular one is the manganese oxide ( $NaMnO_2$ ) which shows an experimental capacity of  $200 \text{ mA h g}^{-1}$  and a potential range between 2 and 4 V[43]. The crystalline structure of those materials is the one shown in figure 1.18, where the large channel between oxide layer permit the intercalation of sodium ions. The main problem with this materials are irreversible phase transitions, which occur when too much sodium is extracted or due to air moisture[12, 43].

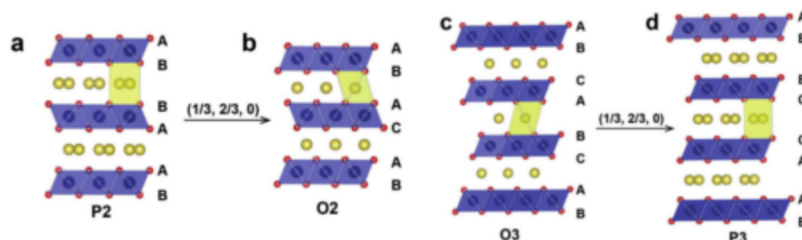


Figure 1.18: Crystal structure of layered oxides. Taken from [43].

## 1.4. SODIUM-ION BATTERIES TECHNOLOGY

### Poly-anionic Compounds

Compared with layered oxides, poly-anionic compounds are characterized by strong covalent bonds between poly-anions units of the form  $(XO_4)^{n-}$ , where X is P, S or Si. Due to the strong bonds the crystal structure is far more stable than the layered oxides one and hence a very good mechanical stability and the absence of irreversible phase transition characterized those kind of compounds. On the other hand those bonds result in low gravimetric and volumetric energy density due to both the intrinsic density of the material and the necessity, due to low conductivity, to use it in form of powders mixed with conductive carbon. The main usage is then high power application. The most used ones are the so called NASICON structures with the formula  $Na_xMM'(XO_4)_3$ . Sodium-vanadium-phosphate ( $Na_3V_2(PO_4)_3$ ) is one of them. NASICON means Na Super Ionic CONductor because those compounds show extremely high ions conductivity. The latter is due to big channels in the crystal structure, which permit the sodium to intercalate without any modification of the crystalline phase. High thermal stability is another advantage of those materials.

### Prussian Blue Analogues

The characteristic group of this family is  $[Fe(CN)_6]$  and the most common ones are in the form  $Na_xM[Fe(CN)_6]$  with  $M = Co, Ni, Fe, Ti, Cu$ . As in NASICON materials, Prussian Blue Analogues (PBAs) are characterized by large channels in the crystal structure which permit the reversible intercalation of Na ions. Notwithstanding, PBAs does not show a good crystal stability during intercalation, due to irreversible phase transition; The hazard linked with thermal degradation is another problem<sup>15</sup>.

#### 1.4.2 Nanostructured Electrodes

The most common technique used to obtain nanostructured electrodes are presented below. All those techniques aim, primarily, to define a conductive path from nanocrystals to the metal electrodes but they make it possible also the introduction of the concept of porous electrodes. As it will be explained in the next chapter, commercial battery relies on a planar technology, which result in a 2 dimensional interface between the electrodes and the electrolyte. With 3D porous structure, like carbon matrices, the contact point between the liquid and the solid gains one dimension, and a degree of freedom. Because the ions diffusion is much faster in the liquid than in solid, the ions can easily access all the active material, directly from the electrolyte, without any of solid diffusion process (which is slower). It means that the reaction is faster

---

<sup>15</sup>Materials particularly sensitive to temperature result in complex thermal management system.

## 1.4. SODIUM-ION BATTERIES TECHNOLOGY

(higher power) not only because the surface area is increased, but also because the physical processes involved are faster (liquid diffusion/solid diffusion). The main drawback is a lower volumetric energy density due to the void inside the support structure. Recalling the main target of this thesis are stationary applications and high C-rate, porous structures seem to be the optimal choice.

### **Nanoparticles Synthesis**

The easiest way of increasing the surface area ratio of a material is by means of nanoparticles synthesis. Hydrothermal procedure can be exploited for the direct synthesis of nanoparticles. Because a conductive path between nanocrystals has to be established nanoparticles are usually mixed with carbonaceous structures. A simple mixture of active material and amorphous carbon is the basic idea, but lots of variations have been tested: coating of nanocrystals with carbon; embedding the crystals into complex structures like graphite electrodes and carbon nanofibres. [27, 35]

### **Carbon Nanofibres**

In order to produce different supporting elements for the nanoparticles, the electro-spun carbon-nanofibres, thanks to the flexibility of the production process, have been extensively used in literature. Carbon nanofibers, as shown in figure 1.19, are a non-woven mat of carbon fibers which can be used as support or even be directly produced with the active material embedded into it[42, 47, 22]. The production process consists in spinning a continuous polymer fibre onto a support and the superposition of different part of the fibre create a mat. The polymer is then carbonized to form the conductive support.

### **Block Copolymers Matrices**

Block copolymers is an alternative technique to electrospinning to produce carbon matrix for active material support[48]. This technique exploits the self-assembly properties of a mixture of two polymers. After the self-assembled nanostructure is formed and the two polymers solidified, one of the two is removed with chemical process while the other is carbonized.[28, 48, 21].

In the next chapter a detailed explanation of the working principles of the design used in this work and the differences with the standard one are presented. Of particular interest, the ad-

## 1.4. SODIUM-ION BATTERIES TECHNOLOGY

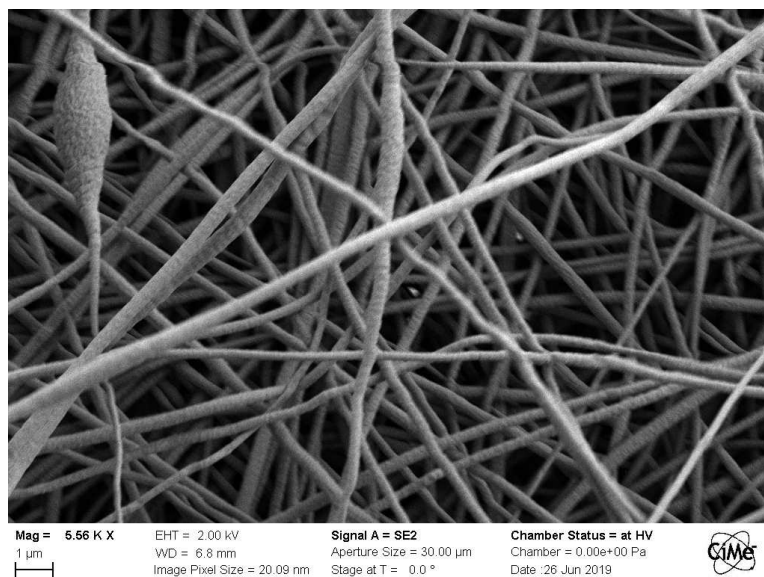


Figure 1.19: Carbon Nano-fibres SEM image.

vantages and potentialities are shown not to depend completely on the particular choice of materials and precursors but to be linked with the physical understanding of the cell. This is to say that the entire work can be transposed, without major changing, to different materials and even to lithium-ion technology.

One of the biggest innovative contribution has been the implementation of the full production chain for those type of devices, starting from scattered works which dealt with subsets of the process. In the next chapter each part of the work is presented separately, and this is the exact panorama to be found in literature. This way the reader will become familiar with the multiplicity of different techniques used in the whole span of the project.

At the end of six months it is possible to assert that it an easy and fast way of development this technology has been found, and it is worthy to continue the research on this path, to realize, as soon as possible, a first sodium-ion battery prototype for stationary application.

## References

- [1] Peter A. van Aken et al. “Recent progress on sodium ion batteries: potential high-performance anodes”. In: (2018). DOI: 10.1039/c8ee01023d.
- [2] Heymi Bahar. *Renewable power:Tracking Clean Energy Progress*. 2019. URL: <https://www.iea.org/tcep/power/renewables/> (visited on 08/12/2019).
- [3] Prabeer Barpanda et al. “A 3.8-V earth-abundant sodium battery electrode”. In: *Nature Communications* 5 (2014), pp. 1–8. DOI: 10.1038/ncomms5358.

#### 1.4. SODIUM-ION BATTERIES TECHNOLOGY

- [4] Prabeer Barpanda et al. “Sodium iron pyrophosphate: A novel 3.0 V iron-based cathode for sodium-ion batteries”. In: *Electrochemistry Communications* 24.1 (2012), pp. 116–119. DOI: 10.1016/j.elecom.2012.08.028.
- [5] Prabeer Barpanda et al. “ $\alpha$ - $\text{Na}_2\text{P}_2\text{O}_7(\text{VO})$ : A 3.8V Pyrophosphate Insertion Material for Sodium-Ion Batteries”. In: *ChemElectroChem* 1.9 (2014), pp. 1488–1491. DOI: 10.1002/ce1c.201402095.
- [6] Roland Berger. “Business models in energy storage”. In: May (2017).
- [7] Juliette Billaud et al. “ $\beta$ - $\text{NaMnO}_2$ : A high-performance cathode for sodium-ion batteries”. In: *Journal of the American Chemical Society* 136.49 (2014), pp. 17243–17248. ISSN: 15205126. DOI: 10.1021/ja509704t.
- [8] O Bolufawi, Omonayo Bolufawi, and Additional. “Renewable Energy Integration with Energy Storage Systems and Safety”. In: *intechopen* (2018).
- [9] Berndt D. *Maintenance-Free Batteries*. Research studies press LTD, 1997.
- [10] Francisco Díaz-gonzález. *Energy Storage in Power Systems*. ISBN: 9781118971321.
- [11] GAO. *Information on Challenges to Deployment for Electricity Grid Operations and Efforts to Address Them*. May. 2018, p. 50. URL: <https://www.gao.gov/products/GAO-18-402>.
- [12] S. Guo et al. “Environmentally stable interface of layered oxide cathodes for sodium-ion batteries”. In: July (). DOI: 10.1038/s41467-017-00157-8.
- [13] Holger C Hesse. *Lithium-Ion Battery Storage for the Grid - A Review of Stationary Battery Storage System Design Tailored for Applications in Modern Power Grids*. 2017. ISBN: 4989289269. DOI: 10.3390/en10122107.
- [14] Martin B Hocking. “7 - Industrial Bases by Chemical Routes”. In: *Handbook of Chemical Technology and Pollution Control (Third Edition)*. Ed. by Martin B Hocking. Third Edition. San Diego: Academic Press, 2005, pp. 201–220. ISBN: 978-0-12-088796-5. DOI: <https://doi.org/10.1016/B978-012088796-5/50010-7>. URL: <http://www.sciencedirect.com/science/article/pii/B9780120887965500107>.
- [15] Jen How Huang et al. “Vanadium: Global (bio)geochemistry”. In: *Chemical Geology* 417 (2015), pp. 68–89. ISSN: 00092541. DOI: 10.1016/j.chemgeo.2015.09.019. URL: <http://dx.doi.org/10.1016/j.chemgeo.2015.09.019>.

#### 1.4. SODIUM-ION BATTERIES TECHNOLOGY

- [16] IRENA. *Electricity storage and renewables: Costs and markets to 2030*. October. 2017, p. 132. ISBN: 9789292600389. DOI: ISBN978-92-9260-038-9(PDF). URL: <http://irena.org/publications/2017/Oct/Electricity-storage-and-renewables-costs-and-markets>.
- [17] Geoff James et al. "Storage Requirements for Reliable Electricity in Australia". In: (2017).
- [18] Mohammed Ibrahim Jamesh and A.S. Prakash. "Advancement of technology towards developing Na-ion batteries". In: *Journal of Power Sources* 378 (2018), pp. 268–300.
- [19] Minah Lee et al. "High-performance sodium-organic battery by realizing four-sodium storage in disodium rhodizonate". In: *Nature Energy* 2.11 (2017), pp. 861–868. ISSN: 20587546. DOI: 10.1038/s41560-017-0014-y. URL: <http://dx.doi.org/10.1038/s41560-017-0014-y>.
- [20] Huangxu Li et al. "Robust graphene layer modified Na<sub>2</sub>MnP<sub>2</sub>O<sub>7</sub> as a durable high-rate and high energy cathode for Na-ion batteries". In: *Energy Storage Materials* 16. June 2018 (2019), pp. 383–390. ISSN: 24058297. DOI: 10.1016/j.ensm.2018.06.013. URL: <https://doi.org/10.1016/j.ensm.2018.06.013>.
- [21] Mingqi Li and Christopher K. Ober. "Block copolymer patterns and templates". In: *Materials Today* 9.9 (2006), pp. 30–39. DOI: 10.1016/S1369-7021(06)71620-0.
- [22] Weihan Li et al. "Nanostructured electrode materials for lithium-ion and sodium-ion batteries via electrospinning". In: *Science China Materials* 59.4 (2016), pp. 287–321. ISSN: 2095-8226. DOI: 10.1007/s40843-016-5039-6. URL: <http://link.springer.com/10.1007/s40843-016-5039-6>.
- [23] Yihang Liu et al. "Layered P<sub>2</sub>-Na<sub>2/3</sub>[Ni<sub>1/3</sub>Mn<sub>2/3</sub>]O<sub>2</sub> as high-voltage cathode for sodium-ion batteries: The capacity decay mechanism and Al<sub>2</sub>O<sub>3</sub> surface modification". In: *Nano Energy* 27 (2016), pp. 27–34. ISSN: 22112855. DOI: 10.1016/j.nanoen.2016.06.026. URL: <http://dx.doi.org/10.1016/j.nanoen.2016.06.026>.
- [24] Abhishek Malhotra et al. "Use cases for stationary battery technologies : A review of the literature and existing projects". In: (2016). DOI: 10.1016/j.rser.2015.11.085.
- [25] Asian Metal. *Titanium resources, reserves and production*. 2019. URL: <http://metalpedia.asianmetal.com/metal/titanium/resources%7B%5C%26%7Dproduction.shtml> (visited on 08/09/2019).
- [26] index mundi. *Vanadium: Estimated World Production, By Country*. 2017. URL: [https://www.indexmundi.com/en/commodities/minerals/vanadium/vanadium\\_t7.html](https://www.indexmundi.com/en/commodities/minerals/vanadium/vanadium_t7.html) (visited on 04/10/2019).

#### 1.4. SODIUM-ION BATTERIES TECHNOLOGY

- [27] *Nanostructured Materials for Electrochemical Energy Production and Storage*. Nanostructure Science and Technology, 2009. ISBN: 9780387493220.
- [28] *Nanostructured Materials for Electrochemical Energy Production and Storage*. 2009. ISBN: 9780387493220.
- [29] L. G. Plett. *Battery Management Systems: Battery Modeling*. ARTECH HOUSE, 2015, p. 390. ISBN: 9781630810238.
- [30] Xiangjun Pu et al. “Recent Progress in Rechargeable Sodium-Ion Batteries : toward High-Power Applications”. In: 1805427 (2019), pp. 1–33. DOI: 10.1002/sm11.201805427.
- [31] E U Roadmap. “Mapping Renewable Energy Pathways towards 2020”. In: (2020).
- [32] Samuel Roberts and Emma Kendrick. “The re-emergence of sodium ion batteries : testing , processing , and manufacturability”. In: (2018), pp. 23–33.
- [33] Paula Serras et al. “Na-ion batteries , recent advances and present challenges to become low cost energy storage systems”. In: *Energy & Environmental Science* (2012), pp. 5884–5901. DOI: 10.1039/c2ee02781j.
- [34] Melissa Shaw. *Vanadium Reserves by Country*. 2019. URL: <https://investingnews.com/daily/resource-investing/battery-metals-investing/vanadium-investing/vanadium-reserves/> (visited on 08/09/2019).
- [35] Laifa Shen et al. “Challenges and Perspectives for NASICON-Type Electrode Materials for Advanced Sodium-Ion Batteries”. In: *Advanced Materials* 29.48 (2017), p. 1700431. DOI: 10.1002/adma.201700431.
- [36] A. M. Skundin, T. L. Kulova, and A. B. Yaroslavtsev. “Sodium-Ion Batteries (a Review)”. In: *Russian Journal of Electrochemistry* 54.2 (2018), pp. 113–152. ISSN: 15698041. DOI: 10.1093/annonc/mdy055. URL: <http://link.springer.com/10.1134/S1023193518020076>.
- [37] statista. *Cobalt reserves worldwide as of 2018, by country (in metric tons)*. 2018. URL: <https://www.statista.com/statistics/264930/global-cobalt-reserves/> (visited on 04/10/2019).
- [38] statista. *Countries with the largest lithium reserves worldwide as of 2018 (in metric tons)*. 2018. URL: <https://www.statista.com/statistics/268790/countries-with-the-largest-lithium-reserves-worldwide/> (visited on 04/10/2019).
- [39] Yang-kook Sun. “Sodium-ion batteries: present and future”. In: 46.12 (2017). DOI: 10.1039/c6cs00776g.

#### 1.4. SODIUM-ION BATTERIES TECHNOLOGY

- [40] Battery University. *Types of Lithium ion*. 2019. URL: [https://batteryuniversity.com/learn/article/types\\_of\\_lithium\\_ion](https://batteryuniversity.com/learn/article/types_of_lithium_ion) (visited on 06/20/2019).
- [41] C. A. Vincen and B. Crosati. *MODERN BATTERIES An Introduction Electrochemical to Power Sources*. Butterworth-Heinemann, 1997.
- [42] Heng Guo Wang et al. “Electrospun materials for lithium and sodium rechargeable batteries: From structure evolution to electrochemical performance”. In: *Energy and Environmental Science* 8.6 (2015), pp. 1660–1681. ISSN: 17545706. DOI: 10.1039/c4ee03912b.
- [43] Peng-Fei Wang et al. “Layered Oxide Cathodes for Sodium-Ion Batteries: Phase Transition, Air Stability, and Performance”. In: *Advanced Energy Materials* 8 (Mar. 2018), p. 1701912. DOI: 10.1002/aenm.201701912.
- [44] Shiwen Wang et al. “All Organic Sodium-Ion Batteries with  $\text{Na}_{4i}\text{C}_{8i}\text{H}_{2i}\text{O}_{6i}$ ”. In: *Angewandte Chemie* 126.23 (2014), pp. 6002–6006. ISSN: 00448249. DOI: 10.1002/ange.201400032. URL: <http://doi.wiley.com/10.1002/ange.201400032>.
- [45] Chan Yeop Yu et al. “ $\text{NaCrO}_2$  cathode for high-rate sodium-ion batteries”. In: *Energy and Environmental Science* 8.7 (2015), pp. 2019–2026. ISSN: 17545706. DOI: 10.1039/c5ee00695c.
- [46] Shicheng Yu et al. “Self-standing NASICON-type electrodes with high mass loading for fast-cycling all-phosphate sodium-ion batteries”. In: *Journal of Materials Chemistry A* 6.37 (2018), pp. 18304–18317. DOI: 10.1039/c8ta07313a.
- [47] Lifeng Zhang et al. “A review: Carbon nanofibers from electrospun polyacrylonitrile and their applications”. In: *Journal of Materials Science* 49.2 (2014), pp. 463–480. ISSN: 00222461. DOI: 10.1007/s10853-013-7705-y.
- [48] Zhengping Zhou et al. “Block copolymer-based porous carbon fibers”. In: *Science Advances* 5.2 (2019), eaau6852. ISSN: 2375-2548. DOI: 10.1126/sciadv.aau6852.

## Chapter 2

# Tools and Theoretical Background

In this second chapter the working principles of batteries are explored and the characterization techniques employed presented. The starting point is the *rocking-chair* principle, which is behind commercial ion-based rechargeable battery, together with the electrode slurry and calendaring production techniques. It follows the introduction to electro-spinning and soaking, as alternatives to the aforementioned techniques to produce electrodes.

The chapter precedes with a comprehensive analysis of the characterization techniques to study and optimize the process, from precursors to final cell test. This chapter provides an overlook of the project flow and deliveries which will be in deep presented in the third chapter.

### 2.1 Ion-Based Cells: Physics and Production

Ion-base cells exploit the rocking-chair principle, which permits stable and efficient charge and discharge: two complementary phase transitions in the anode and cathode materials result in a raising/lowering amount of a certain ion at the two electrodes. During charge the cathode is depleted and anode is enriched of ions. If this reaction is thermodynamically unfavourable, energy, in forms of current, is provided to accomplish it. Once the ions are promoted to an higher energy state (associated to one phase of the materials), they can, theoretically, store the energy for a very long time. When a conductive path is created, a reverse current flows and the equilibrium phase forms back.

## 2.1. ION-BASED CELLS: PHYSICS AND PRODUCTION

### 2.1.1 Electrochemical Cells

The concept of electrochemical cell has been presented in the first chapter, altogether with some examples from commercial technologies. The main components of each cell are the two electrodes where the redox reaction takes place and the electrolyte but some more parts are required for cell to work reliably. In figure 2.1 a schematic view of a laboratory ion-base cell with all its components is proposed. The purpose of each one is exposed below.

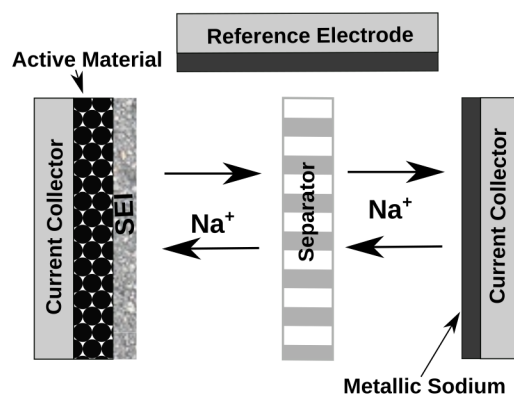


Figure 2.1: Schematic of an ion-base cell with a metallic sodium anode and reference electrode.

### Electrodes

The electrodes are the core of a cell. It is here that the ions are stored and at their interface with electrolyte that the redox reaction takes place. The electrodes are a stack of two layers, of which the outer one is the current collector and the inner one containing the active material. The current collector is the final element of each cell and is used to connect with the external world. It is usually a metal plate, where electrons convey. From this point the voltage of the cell is measured. The constant part of the internal resistance of the cell is usually composed by the resistance of the current collector and the contact resistance between the current collector and the second layer. This second layer, in commercial technology, is a mixture of the active material itself, carbon composites, to improve the electrical conductivity of the layer, and a binder. Exploiting the conductive carbon path, electrons move back and forth the active sites, where the reaction takes place, and the current collector. The resistance due to the path from the active material the current collector depends on the active site where the reaction takes place, and hence is a function of the state of the battery<sup>1</sup>.

<sup>1</sup>It is a function of the SOC, because the discharge happens simultaneously on planes of equal resistance and proceeds gradually to more resistive ones. The history of the battery may lead to change in the local resistance in time.

## 2.1. ION-BASED CELLS: PHYSICS AND PRODUCTION

### Electrolyte

The electrolyte acts as a reservoir where free ions are available for reaction. The most common electrolytes are solution of a salt (e.g.  $NaClO_4$ ); ions conductive polymer or a solid ion conductor are used too. The electrolyte is electrically neutral: for each cation ( $Na^+$ ) an anion is present ( $ClO_4^-$ ).

The two half reactions take place at the two electrodes, and if no link between them were available an unbalance of ions would built up: at one electrode the ions are consumed while at the other generated. The electrolyte permits to shuttle the ions generated at one electrode to the others, to preserve the local electro-neutrality. The electrolyte must be electrically insulating in order to force the electron flow outside of the cell. If it is highly resistive, but not insulating, the cell experiences self discharge: between the two electrodes a potential difference builds up and, if an internal conductive path is available, current flows. High resistance means a Small self discharge current end hence a long retention time.

Another issue to be managed is the chemical stability of the electrolyte: as for the electrons a single path is necessary to ensure a useful current flow, for the same reason, ions must react through a single and controlled chemical reaction. The example of the water electrolysis in the lead-acid cells is an example of a parasitic reaction. In ion-based batteries, the electrolyte can reacts and forms composites with the ions, reducing the cell capacity: if the ions are used for some side reaction they cannot be used for the sustain the current flow.

The next component to be analysed, the SEI, is usually something that naturally builds up as a result of side reactions.

### Solid Electrolyte Interface (SEI)

The interaction between the electrolyte and the electrodes may lead to unwanted side reactions. An example is the formation of composite between organic electrolytes (used in lithium and sodium-ion battery) and the carbon. The reaction consumes a certain amount of ions and hence reduces the capacity of the cell. When the reaction by-products accumulate, a layer between the electrode and the electrolyte (SEI) forms. Luckily this layer often results in a self passivation of the electrodes, which prevents the parasitic reaction to consume all ions. Anyway, it is an unpredictable element and an artificial SEI is often placed as third layer of the electrode. This layer must permit ion diffusion and prevent the electrolyte one.

## 2.1. ION-BASED CELLS: PHYSICS AND PRODUCTION

### Separator

Volumetric and gravimetric characteristics of a cell have already been introduced in the previous chapter. Because a good device has high value of those parameters unnecessary volume and weight must be eliminated. In particular, the electrolyte, being a path for ions transport, should be as thin as possible, to both speed up the transport and increase energy and power density of the cell. Ideally, a gap of few tens of nanometres is enough but what if a pressure is exerted from the outside on the cell? The two electrodes may touch, causing a short circuit. In practice, a highly porous insulating layer is placed between the electrodes, and acts as a sponge for the electrolyte. The two electrodes can be pushed one against the other to minimize the space, without any risk of shorting the cell.

### Reference Electrode

The last component is of particular interest in laboratory setup and only few commercial devices use it. The reference electrode is an additional electrode to be placed inside the cell; it provides an extra point of measurement during characterization. Because through the two main electrodes a current flows, ohmic drop causes change in measured voltage. It is also known that, because reactions are taking place at the surface, the equilibrium concentration is perturbed and Nernst equation is not valid any more, making it rather difficult to link the potential of the two electrodes with the actual situation inside the cell. The reference electrode must be design so that no reactions take place at its interface (stable with respect to the electrolyte and the ions) and no current flow through it. It represent a reference point which does not change during operation.

It is a fundamental element during measurement but it is usually not implemented in commercial device, due to extra cost and weight. Notwithstanding in stationary storage implants, where big batteries are used, the introduction of a reference electrode does not impact so much the final weight: if one small reference electrode results in better understanding of the status of the battery, smaller control units are necessary and the overall system may even be lighter.

### 2.1.2 Thermodynamics of Cells

The understanding of physical mechanism, which drives the electrical force inside the cell, is of paramount importance to improve the performances by means of materials and nanostructures. This section is devoted to the analysis of the formalism behind the redox reaction; it permits

## 2.1. ION-BASED CELLS: PHYSICS AND PRODUCTION

to derive the theoretic potential difference of the cell, given the couples of anode and cathode materials. Starting from this theoretical approach, it is possible to develop a physical model[46] of the cell to be used in the characterization phase.<sup>2</sup> [61, 19]

In order to shed light inside electrochemistry cell some useful quantities have to be introduced:

### Chemical Potential

Let's consider a system composed of multiples interacting chemical species. The energy  $U$  of system is the sum of all the internal energies: kinetic energy linked with particles motion; rotational and vibrational energy of each particle; the interaction energy between different particles; energy linked with electrons at excited energy levels. What happens if one molecule is added to the mixture? Of course the internal energy rises, due to both the energy linked with the added particle (kinetic, vibrational, etc.) and the interaction of the others molecules with the newcomer. The chemical potential ( $\mu_i$ ) of the specie  $i$  is defined as the variation of the internal energy, associated with the addition of molecules of that specie, while all other thermodynamic parameters are kept constant: number of other molecules( $n_j$ ), volume (V), entropy (S).

$$\mu_i = \left( \frac{\delta U}{\delta n_i} \right)_{V,S,n_{j \neq i}}$$

### Gibbs Energy of Reaction

A chemical reaction where the quantities a,b,c of reactants A,B,C are combined to produce the quantities x,y,z of products X,Y,Z is considered.



Because the chemical potential has been define as the energy added (or removed) from the system when there is a change in the number of one species, the energy of a chemical reaction can be determined by summing up the energy of products and remove the energy of reactants. This quantity is called Gibbs energy of reaction ( $\Delta G_{reaction}$ ).

$$\Delta G_{reaction} = \sum_{products} \nu_i \mu_i - \sum_{reactants} \nu_i \mu_i$$

Where  $\nu_i = a, b, c$  are the stoichiometric coefficients

---

<sup>2</sup> This approach is particularly important during the research phase, while models used in control systems are usually simple empirical one, like the one proposed in the previous chapter, easier to implement in microcontrollers[46]

## 2.1. ION-BASED CELLS: PHYSICS AND PRODUCTION

### Electrochemistry and Potential Difference

So far so good but what if the species are charged ones? Stuff gets a little bit more complicated. The species not only interact between each other, but also with electric field from and to the outer of the system. This new contribution, called *outer potential* is added to the total energy  $U^3$ . Also at the interface, phenomena of polarization intervene to change the energy of the phase and another contribution has to be considered in the final expression<sup>4</sup>. Skipping to the conclusion, an electrochemical potential  $\tilde{\mu}_i$  for each charge species  $i$  is defined, which account also for electric field interaction. The electrochemical Gibbs energy of reaction  $\Delta\tilde{G}$  is defined as the sum and difference of the electrochemical potential of reactants and products.

Because the reaction is usually split into two different contributions: reduction and oxidation, the Gibbs energy may be defined as the sum of reduction and oxidation energy plus the net addition/subtraction of  $n$  electrons:

$$\Delta\tilde{G} = \tilde{\mu}_{red} - (n\tilde{\mu}_{e^-} + \tilde{\mu}_{ox})$$

In this expression electrons are explicitly exchanged during a reaction, from and to the system. This is to say that electrons are needed to complete the reaction; because the system is neutral they can only be found outside of the system. Let's now imagine a couple of reactions, one which takes electrons from the outside and the other which produces electrons. One can imagine to take the electrons of the latter and bring them to the former. That is exactly what happens when the two electrodes of a cell are connected. When the voltage between the two electrodes is sensed, with a voltmeter, it is the sum of the "forces" the two electrodes are exerting on the outer world, to move electrons in or out of the system, that is measured.

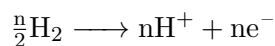
It has to be noticed that the Gibbs energy can be easily turned into a voltage dividing it by the Faraday constant  $F$ :

$$E = \frac{\Delta\tilde{G}}{F}$$

As it will be explained soon, this voltage can be linked to the voltage measured at the end of a cell but still some pieces are missing before coming to this conclusion.

### Standard Hydrogen Electrode (SHE)

Let's consider an electrode where the following reaction is taking place:



---

<sup>3</sup>Following the previous reasoning the extra ion is brought to the system from an infinite distance; During its trip, if charged, it interacts with electric fields

<sup>4</sup>For a rigorous exposition see [19]

## 2.1. ION-BASED CELLS: PHYSICS AND PRODUCTION

It is the redox of hydrogen ( $H/H^+$ ). The Gibbs energy of this reaction has been taken as the zero of a scale: the standard electrode potential, to which all the others Gibbs energy can be referred.

$$\Delta\tilde{G}_{H/H^+} = 0$$

### Nerst Equation and Standard Redox Potential

In the 19<sup>th</sup> century an expression to link the concentration ([red],[ox]) of species in a redox reaction and the potential measured at the end of the cell was discovered, it is called Nerst equation:

$$E = E^0 + \frac{RT}{nF} \ln\left(\frac{[ox]}{[red]}\right)$$

During the measurement no current flows in between the two electrodes. In order to set a scale during the experiment, one electrode (*reference*) was kept fix while the other (*working*) was changed to test different redox reactions. It was in that occasion that the hydrogen reaction was taken as the reference one <sup>5</sup>. It was just years later that the quantity  $E^0$ , called *standard redox potential* was related to the Gibbs energy by the expression:

$$E^0 = -\frac{\Delta\tilde{G}}{nF}$$

Where n is the number of electrons exchanged during the reaction.

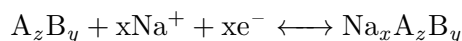
The standard redox potential is so called because it is measured at precise (standard) conditions in term of temperature, Ph, etc. Under those same conditions, if the standard potential is negative the reaction can spontaneously occur and positive if it can not. *The products energy is greater that the reactants one, which means that energy has to be provided from the outside.* As an example, the reduction of metallic sodium ( $Na/Na^+$ ) has a standard potential of  $-2.71$ , and lithium of  $-3.0401$ , hence both of them occur at standard conditions.

### Reaction in Sodium-ion cells

The typical reaction of the ion-based cell can be written as:



It can be split into two redox reactions



---

<sup>5</sup>The reference electrode was metallic platinum.

## 2.1. ION-BASED CELLS: PHYSICS AND PRODUCTION

This second form better represents the physical situation at each electrode, where only one half of the complete reaction takes place. It has to be noticed that during the charge and discharge process the reaction arrow reverts.

The sodium ions generated at one electrode reach the other ones by means of the electrolyte, while an external contact permits the current flow. The force of this flow is determined by the potential ( $E$ ) between the two electrodes, which can be expressed as the difference of the two standard potentials:

$$E = E_{cathode}^0 - E_{anode}^0$$

Because large potential difference means high power, the anode and cathode materials are chosen in order to maximize this difference.

### Out of Equilibrium: Charge/Discharge

So far the potentials considered are referred to a measurement without current flows through the electrodes. Notwithstanding nothing has been said about the behaviour of the cell when it is out of equilibrium, that is to say, during charge or discharge. As long as the two electrodes are not connected by an ohmic contact, the redox reactions at each electrode compensate each others and the cell is at equilibrium. The equilibrium concentration dictates the potential measured, as stated by the Nerst equation. It also means that if a voltage is imposed, the systems is forced to change the equilibrium concentration by increasing one of the two reactions (reduction and oxidation) at the two electrodes to modify the ions concentration. in figure 2.2 a schematic picture of different conditions is reported: zero external potential (equilibrium), positive external potential, negative external potential. In all three cases a dynamic equilibrium is, eventually, established: different processes balance each others to obtain no net changes in the systems.

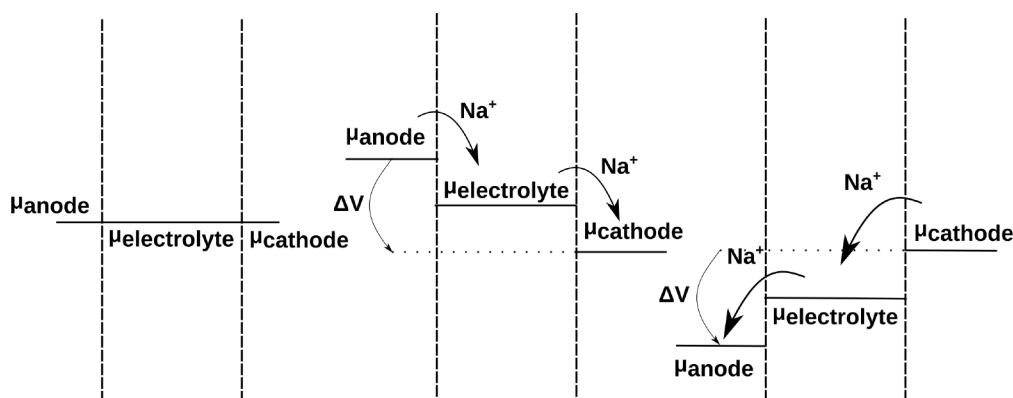


Figure 2.2: Effect of the electrode polarization on the chemical equilibrium.

## 2.1. ION-BASED CELLS: PHYSICS AND PRODUCTION

What happens if the two electrodes are electrically connected? the answer is not that the systems is brought out of equilibrium but that the systems itself is changed. It is because the systems is changed that the former condition is not any more an equilibrium one and electrons and ions start to flow. The motion of electrons produces an unbalance in the rate of redox at the two electrodes and the flow of ions is a consequence of it. Because the electrons accumulate at one electrode while are depleted at the other, the reduction at one electrode does not find enough electrons to keep the same frequency<sup>6</sup>; the oxidation, at the other electrode, sees far more electrons than it was used to consume, and it is forced to increase its frequency. The main difference between charge and discharge is the cause of the electrons unbalance: during discharge the electrons are spontaneously drained from one electrode to the other; discharge is the equilibrium condition of the connected system and hence nothing happens after it is reached: the electrons unbalance is forced by current injection.

The reduction is predominant at positive electrode and the oxidation at the negative one.<sup>7</sup> The condition is quite similar to the case of a potential imposed from the external because it is like each of the two electrodes imposes its potential to the other.

The question to be answered now is: how the electrons and the ions actually reach the point of reaction? So far reactions have been assumed to just take place but all the stuff must be at their place (near enough) for it to actually happen. Let's start with the electrons point of view

### **The Path of Electrons**

It starts from the positive electrode, from which the electrons are drained. After the reaction the electron is inside the active material, which is usually and insulator. The electron "feels" that a low energy states exist at the other electrode, and is pulled toward the current collector by an electric field. This electric field is create by the others electrode which "wants" more electrons. At this point the electron has the maximum possible energy and using it in a circuit guarantees the maximum power. Easier said than done because it is still in the active material. Luckily enough a conductive material nearby can provide a easy (low resistance) path to the current collector. But how to reach it? The electron can not but use part of its energy to "jump" to the conductor from the active material, by means of tunnelling. From the outside electron is seen to lose some energy; the tunnelling process is interpreted as a part of the internal resistance. At this point, if the conductive path can directly bring the electron to the current collector, no additional complexity is added, but if this is not the case, more tunnelling may be necessary and more energy is lost. Of course the journey through the conductive path is

---

<sup>6</sup> Frequency: number of single reactions per second.

<sup>7</sup>during charge and discharge positive and negative electrode switch

## 2.1. ION-BASED CELLS: PHYSICS AND PRODUCTION

not completely painless because it has a certain resistance and some more energy will be lost anyway. In particular, the contact between the active material slurry and the metallic current collector is critical, and its evolution in time (detachment of the slurry) may lead to cell failure. Once in the current collector, the electrons can be used; after that the process described is performed in the inverse direction, to reach the oxidation site where ions and electrons recombine.

### **The Path of Ions**

At the same time the electron starts its journey, an ion is created inside the active material; it feels the urgency to escape from it and to reach the other electrode. The first obstacle, if the reaction takes place in the bulk of the active material, is the active material itself. The ion has to diffuse in the solid, until he reaches the electrolyte. Usually ion diffusion in solid is much slower than in liquid<sup>8</sup>, and the time spent in the active material or other solid, is much longer than the one spent elsewhere.

As the electron, the ion feels an electric field which imposes a drift in the direction of the other electrode. Once it escapes the active material, it is rapidly attracted to the other electrode where a second process of solid diffusion takes place. If the SEI is present the ions must diffuse also through it.

What if the ion is not at its place when a new reaction must<sup>9</sup> take place? the cell is forced to use part of its internal energy to increase the electric field which attracts the ion, to make it move faster. This way the actual Gibbs energy decreases (more energy is needed to create the products) and the available potential is lowered. The potential loss associated with ions diffusion is the second components of the internal resistance.

It is time to shed light on the mysterious  $V(\text{SOB})$  introduced in the previous chapter.

### **$V(\text{SOB})$**

At open circuit, when the cell is charge,  $V(\text{SOB})$  is  $V_{\text{OC}}$  and is also the difference between the Gibbs energy of reaction of the two electrodes. Of course if the conditions change (pH, temperature, etc.), the Gibbs energy changes too; the  $V(\text{SOB})$  is hence a function of the internal variables of the cell.

The very moment the discharge begins,  $\text{SOB}$  suddenly changes and a discontinuity in the voltage is measured: current flows through the internal resistance, leading to a decrease of the voltage from  $V_{\text{OC}}$  to  $V_{\text{CC}}$ . After that, the measured voltage gradually decreases as the resistance in-

---

<sup>8</sup>For lithium the diffusion in LCO is about  $10^{-12} \text{ cm}^2/\text{S}$  while in the electrolyte is about  $10^5 \text{ cm}^2/\text{S}$  [69, 30].

<sup>9</sup>The verb "must" here is important because the cell cannot decide IF a reaction takes place but only where and at which cost in term of potential drop

## 2.1. ION-BASED CELLS: PHYSICS AND PRODUCTION

creases. The main reason of this latter increase is the shift of the reaction from low resistance zones, which corresponds to the most favourable points and hence the first one to react, to higher resistance zones[65]. The change of  $V$  can be linked to the SOC: high SOC correspond to low resistance and vice versa. It has to be noticed that the resistance does not actually increase but simply it is "measured" at different places <sup>10</sup>.

What actually changes the resistance is the formation of SEI, which permanently increases the resistance linked with ion diffusion. Other phenomena of internal degradation may occur: during ion extraction the material may experience mechanical stress and detach from the conductive path (the tunnelling length is increased); the contact between the current collector and the slurry of active material may deteriorate; the electrolyte may decompose leading to slower ion diffusion in liquid. All this phenomena are peculiar of the material under analysis and must be assessed separately, each time a new cell is designed.

### Performances

As final step, it is possible to draw connections between the physical principles and the performances of a cell. For example the power performances of a battery are linked both to the voltage and the internal resistance of the device. The former depends mainly on the choice of material while the latter to the diffusion process of ions and the conductive path of electrons. The dependence of the capacity to the C-rate can also be appreciate: The capacity is a derived quantity, measured between two points of the  $V(\text{SOC})$  curve; when an high current flows in the cell, more and more energy is wasted to drive faster the chemical process inside the cell. In particular, some reaction points, which at low C-rate correspond to a voltage drop inside the integration extreme, at higher current may be considered at too low voltage. In figure 2.3 this situation is depicted. The measurement is stopped before the full capacity is measured, because part of it is extracted at a voltage which is considered too low to power the device.

### 2.1.3 Slurry Electrodes

It is now necessary to present the classical production process used for commercial batteries[57, 24, 38, 51] and understand which kind of structures can be obtain with it, in order to justify the choice of a different process.

---

<sup>10</sup>Those consideration will be extremely useful when analysing CNFs structures

## 2.1. ION-BASED CELLS: PHYSICS AND PRODUCTION

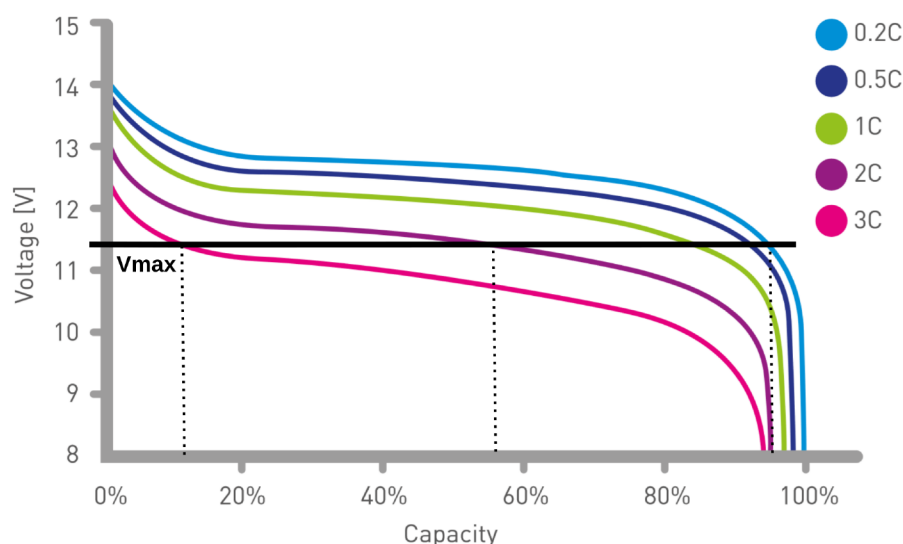


Figure 2.3: Different measured capacities for different C-rate.  $V_{max}$  is the extreme of integration when computing the capacity. Taken from [43].

### Production Process

The process starts with the mixing of the precursor to form a viscous solution. In the solution are mixed the active material, black carbon, if it is necessary to increase the conductivity, and a binder to guarantee mechanical stability once the solvent is evaporated. The solvent may be water or other liquid substance, appropriate for the chosen active material. The mixed solution is then used to coat a metal foil (aluminium or copper), via doctor blade or similar techniques. The coating is then dried and the solvent evaporated. Typical thickness of the coating layer is some tens of micrometers.

Anode and cathode are produced by the same process, in parallel, and are then assembled with the separator. The used technique, calendaring, consists of pressing the three layers, one on the other, with two rollers. The single cell is then cut out of the foil and assembled in a protective case. As last step, before sealing the battery, the electrolyte is filled into the case.

### Advantages

The process has several advantages, among which the fact of being symmetric for the anode and the cathode. It is also particularly suited for mass production, because each step is processed on a metal foil and only at the end the shape and size of the battery are decided. It means that the process is also flexible, and different battery shapes can be produced by changing the cut and assembly steps.

The active material is produced by other companies or in a different implants, hence no major modification to the process are needed but to change the solvent, to change the active material

## 2.1. ION-BASED CELLS: PHYSICS AND PRODUCTION

of one electrode.

### **Limitations**

The slurry is pressed to increase the contact between the active material and the collector, during the calendaring step. As side effect the pressure decreases the porosity of the slurry. The resulting uniform and dense layer of active material, binder, and carbon deposited on the metal foil is difficult for the electrolyte to wet. As a result the soaking phase with electrolyte is the bottleneck of the process; it is also difficult to ensure a good wetting for the whole surface of active material[51, 52]. The effect of poor wetting of the active material near the electrodes lead to poor capacity at high C-rate. In particular the problem has been studied and addressed for lithium-ion batteries with different approaches like laser microstructuring of electrodes[2, 51, 22].

The whole problem becomes critical when the slurry get thicker. In particular, one cannot increase the thickness of the slurry, in order to increase the total energy content of the cell, without decreasing the capacity at high C-rate[12, 53, 54]: The deeper part of the slurry is reached by few electrolyte or not reached at all; because of the high voltage drop necessary to increase the ion motion it cannot be used at high current. In order to reach thicknesses of hundreds of microns nanostructured electrodes must be employed[2, 56, 68].

### **2.1.4 Porous Electrodes Theory**

For a more quantitative analysis of the influence of porosity and wetting of the electrode on the electrochemical performances, the porous electrodes theory is one of the most useful tool. The model has been developed and applied at the university of Berkeley, starting from the sixties, in the group of J. S. Newman[41, 42, 10]. The interest in this model is testified by a number of publications which use it to model and optimize cells[60]. In 2019 the topic of porous electrode theory, applied to ion batteries, still requires further development to reach a fully understanding of the actual phenomena[51, 52]. Notwithstanding, the advantages of a porous electrode reported in literature include: higher stability and high current rate; fast ion diffusion and better electric path; high mechanical stability due to easier volume expansion accommodation[37, 71, 33, 45].

### **Macroscopic Description**

In picture 2.4 is reported the structure of a porous electrode, as the one considered in the theory developed by Newman[10, 41].

## 2.1. ION-BASED CELLS: PHYSICS AND PRODUCTION

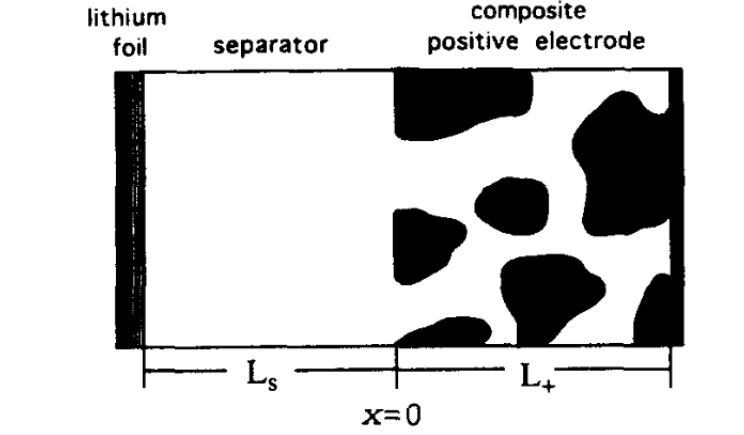


Figure 2.4: Porous electrode schematic. Taken from [11].

In the model, the redox reaction is restricted to the interface between the solid and liquid phase; the electrolyte is assumed to penetrate everywhere into the porous electrode. The reaction rate, at any given time and place, depends on the particular physical properties of the solid phase and of the electrolyte. In order to simplify the problem, the actual geometry of the electrode is disregarded and macroscopic parameters are used: in the one dimensional problem, the electrode is considered as a continuous mixture of solid and liquid phase. An average conductivity along the  $x$  axis is defined, as an average ions conductivity. Equations for solid and liquid phase potential ( $\phi_1, \phi_2$ ) and current ( $i$ ) are derived from ohm law, diffusion and drift motion of ions. The electrochemical reaction is introduced to guarantee the conservation of the number of particles in the system. The core of the model is the polarization equation, which links the local current density to the potential in the two phases and the concentration of ions ( $C$ ):

$$\nabla \cdot i = f(\phi_1 - \phi_2, C)$$

The actual form of this equation has to be chosen among different models, proposed in literature, to obtain the best fit for the system under study [15].

### Reaction Zone Model

One of the possible application of the porous electrode theory is the study and optimization of thickness and porosity for a given cell [40]. In particular, given the value for average resistivity on the  $x$  axis, due to either the conductive path or the ion diffusion, the reaction zone model [42] can be introduced. In this model, the reaction is confined in a small neighbourhood of a point  $X_0$ . While the active material is consumed by the reaction, the point shifts. In the case of a porous electrode, with low ion transport resistance, the reaction starts from the current collector, because it is the point of lowest resistivity; during time the reaction zone shifts in the

## 2.2. CNFS PRODUCTION AND CHARACTERIZATION

direction of the interior of the cell[65]. In the case the ion diffusion in the electrodes results in a resistance higher than the one of the active material matrix, the reaction starts at the exact opposite position: as far as possible from the electrode[40]. With this simple model, it is possible to define the voltage drop at each point of the electrodes, and to determine the optimal thickness: once the maximum current is fixed, at each point on the x axis corresponds a voltage drop; the point which corresponds to the maximum drop the system can handle is the optimal value. Of course the model can also be used to determine the porosity and the conductivity of the electrodes, given a constrain on the energy per square centimeters[65].

## 2.2 CNFs Production and Characterization

Following the reasoning of the previous section, the control of porosity and conductivity, of both active material matrix and electrolyte, represent the design tool to optimize the performances of electrochemical cells.

The study and design of electrolyte has not been treated during this thesis but is anyway a central element of a good battery. In order to really understand and control the characteristics of the device, the present work should be accompanied by a work on electrolyte<sup>11</sup>[52, 34, 29, 63, 25, 5].

Carbon Nanofibres (CNFs) studied in the first workload of the present thesis represent a possible way of tailoring the conductivity and porosity of the electrodes.

### 2.2.1 CNFs and their Application

CNFs are widely use in research, due to their interesting properties and easy fabrication procedure. They appear, as shown in figure 2.5, as a non-woven mat of fibres; the mat can be

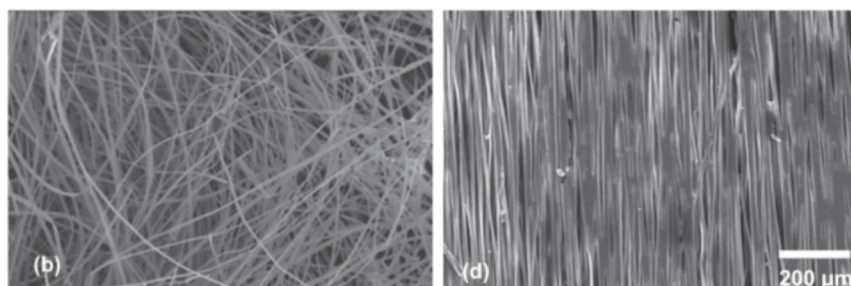


Figure 2.5: Ordered and disordered CNFs mats produced by electrospinning. Adapted from [58].

<sup>11</sup>Diffusion of ions; wetting of the electrolyte; formation of SEI and electrolyte degradation.

## 2.2. CNFS PRODUCTION AND CHARACTERIZATION

regular or randomly oriented, with large or small gaps. Those structures are mainly realized with polymers precursors. Fiber's diameters can range from tens of nanometers to tens of micrometers[20, 16, 77, 73]. The main physical characteristics with reference values and the main applications found in literature are reported above.

### **Physical Characteristics**

The mean diameter of the fibres is of course the main parameter in order to control the dimension of the pores of the mat. It can be controlled by means of different precursors or process parameters.

The internal and external morphology and structure is also of great importance: it is possible to embed particles inside and outside of the fibres; roughness and chemical composition can be used to promote crystal growth. The possibility of a core-shell structure is also exploited to place the active material inside the fibre while the outer carbon shell ensures a conductive path. The electrical conductivity itself is of major concern when porous electrode has to be realized. This parameter, altogether with the ion diffusion, dictates the dynamic evolution of the reaction zone model.

The conductivity is influenced by the carbon allotropes in the fibers: if graphite is present, higher conductivity is expected with respect to amorphous carbon. Carbon nanotubes can be either added to or growth on the carbon fibers to increase the conductivity. Adding metal particles is also effective[26, 73]. Typical values of electrical conductivity range from  $10^{-2}$  to  $10^3 - 10^4$  S/cm, depending on the content of graphite and conductive particles [7, 49, 73].

### **Main Applications**

CNFs first application, in 1981, was a dust filter for industrial purpose, followed by filters for cars and trucks. In the nineties CNFs popularity grown, due to application in biomedical and electronics fields: scaffolds for tissue engineering, drug delivery, fuel cells and gas sensors[20].

CNFs are today a mainstream technology and they are widely used also in energy storage systems. Carbon can intercalate lithium and CNFs are used as porous anode; with embedded particles of active material they serve as cathode too. Because graphite cannot intercalate sodium, amorphous carbon fibers used as sodium anode result in poor conductivity[73]. CNFs has been widely studied as conductive matrix for SIB active materials[72, 9, 64, 23].

## 2.2. CNFS PRODUCTION AND CHARACTERIZATION

### Electro-spun CNFs

CNFs can be produced with different processes, like block copolymers[78], thermal chemical vapor deposition[16] and electrospinning [26, 59]. The latter technique is widely used and the one chosen in the present work. In figure 2.6 the typical electro-spinning setup is shown. It

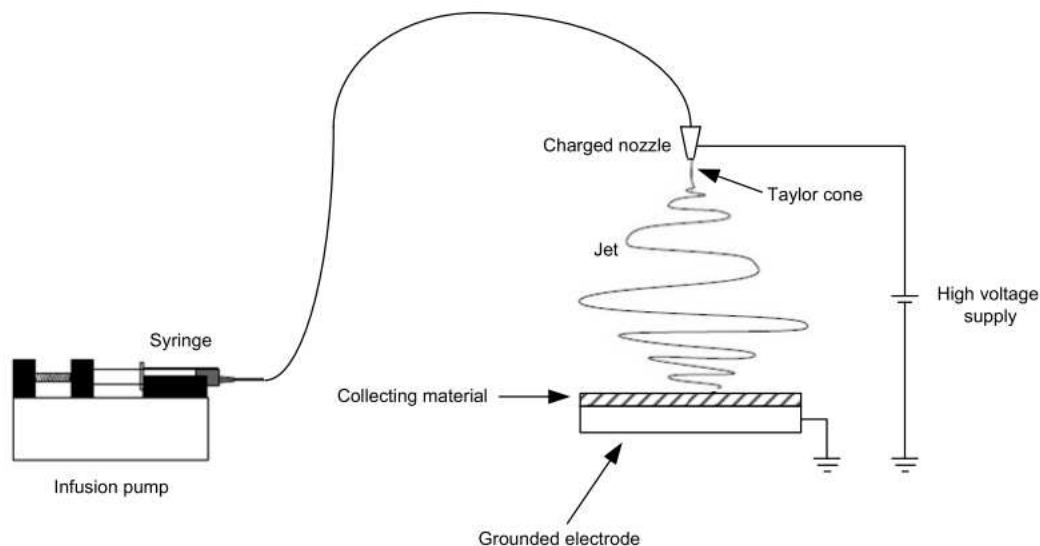


Figure 2.6: Typical electrospinning setup. Taken from [3]

consists of a syringe, loaded with the precursor solution, usually a polymer and a polar solvent; a syringe pump to control the precursor flow; a metallic needle connected to an high voltage supply, and a metallic target connected to ground[59]. The solution, at the end of the metallic needle, accepts electrons and gets charged. The charges repulse each others and tend to accumulate near the edges of a droplet, at the needle aperture. When the charge repulsion is higher than the surface tension, the drop tip is broken and a continuous jet of polymer and solution is drawn towards the current collector by the electric field. In figure 2.7 the formation of the so called Taylor cone[55] and the fibres spinning are shown.

During the flight, the solvent starts to evaporate and an almost solid fibre is deposited. Because the fibre is not conductive, charges are trapped for a long time and the repulsion between the already deposited fibre and the flying one leads to a random deposition. Different parts of the flying fibre also interact and spread in space the fibre, before it touches the metallic collector. Engineering the electric field and the metallic collector is a valuable tool to control the deposition of the fibres: it is possible to increase the uniformity of the fibre deposition or to impose an order to the fibres (figure 2.5). The easiest way of controlling the electric field is by means of the voltage difference and the distance between the needle and the collector. Also the humidity is an important parameter and, together with the temperature, controls the evaporation rate

## 2.2. CNFS PRODUCTION AND CHARACTERIZATION

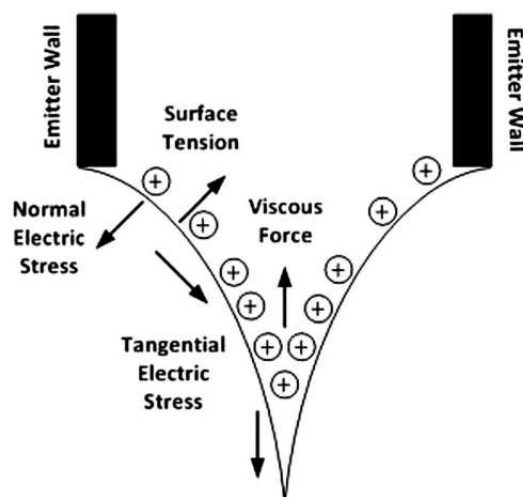


Figure 2.7: Taylor cone formation principle. Taken from [6].

of the solvent. An higher evaporation rate leads to thicker fibers because the electric field has less time to stretch the fibers before they solidify. Also the electrostatic interaction between charges in the fiber is influenced by humidity: water molecules in the air neutralize the trapped charges and decrease the repulsion, leading to smaller deposition spot[32, 62, 58].

### Stabilization and Carbonization

Once the polymer fibres have been deposited onto the collector, some additional process steps are required to transform them into carbon nanofibres.

First, the solvent has to be completely evaporated, usually in a ventilated oven at about 70 °C, for 1-2 hours. After that, a process called stabilization is performed with a slow ramp of temperature first at 100-200°C and then to 260 °C, with dwelling time of 1-2 hours[14, 18]. This process is critical for the mechanical properties of the fibres. During this step the chemical structure of the polymer is changed, and some chemical bonds are broken and other formed. It guarantees the flexibility of the fibres after the carbonization; without stabilization the carbonized fibres are usually very brittle. The very same stabilization process has to be accomplished with smooth ramps and long dwelling time, in order to prevent thermal shock which forms cracks into the final fibres.

Once the fibers have been stabilized, an high temperature process is performed to carbonize them. Above 600 °C the polymer decomposes and hydrogen, nitrogen, and oxygen are released. Only the carbon is preserved, leading to the formation of carbon fibres. The process must take place in an inert atmosphere of nitrogen or argon, to prevent the polymer from burning. The process can last as long as 2 to 10 hours. Longer the thermal plateau and higher the

## 2.2. CNFS PRODUCTION AND CHARACTERIZATION

temperature, higher the degree of graphitization and more brittle the fibers. It is then a trade off between electrical and mechanical properties which has to be made, when optimizing the carbonization step[18, 14, 48].

### 2.2.2 CNFs Characterization

The whole process must be carefully characterized and different techniques are employed. Each technique and of the information each one can convey are presented below.

#### Fourier Transform Infrared Spectroscopy (FTIR)

During the stabilization and carbonization phase the main events to be monitored are the changes in the molecular structure of the polymer. In particular, the correlation between chemical structure and electro-mechanical properties of the final fibres mat is of paramount importance. The same analysis is used in order to assess the effect of changes in the time, temperature, and temperature curve during the annealing process. It is then possible to determine the minimum time and temperature to obtain a certain result, in term of final CNFs properties. In particular the study of molecular bonds is performed through Fourier Transform Infrared Resonance [21, 31]. The molecular bonds length can be excited by means of an EM radiation: energy is provided to promote to an higher energy states the molecules; it usually corresponds to an EM wave of frequency  $10^{13} - 10^{14}$  Hz, that is the infrared band (IR). When a sample is irradiated by the full IR spectrum, the output signal contains all the frequency but the absorbed ones, which correspond to the vibrational states of the bonds. A Michelson interferometer is exploited to excite the sample with a single frequency at each sampling time<sup>12</sup>. The detector output is the amplitude of the signal transmitted through the sample at a given time. The Fourier transform is used to convert back the acquired signal from time domain to frequency domain. Peaks in absorption at different wavelength can be easily related to different bonds types, using data present in literature.

#### Microscopy

Fibres diameter is the main parameter which affects the porosity of the electrode. Different approaches, at the level of precursors preparation and electro-spinning setup, permit to modify it. The diameter is also observed to shrink during the annealing process. The final diameter

---

<sup>12</sup>Of course it is impossible to obtain a single frequency. The sample is excited by a small part of the spectrum near a certain frequency

## 2.2. CNFS PRODUCTION AND CHARACTERIZATION

is hence influence by the whole process and optical microscopy imaging is the best technique to monitor it. This technique is very fast and samples from any stage of the process can be obtained. The acquisition of large portions of fibres permits to determine average quantity, like pores dimension and mean diameter, with automatic image processing procedures. No need of samples preparation or complex measurement results in large amount of data from each batch[31].

### **Scanning Electron Microscopy (SEM)**

While optical microscopy is best suited for large field imaging and for rough parameters extraction, SEM is the ideal tool for an in deep analysis of the sample and the estimation of fine grain features of the fibres. Estimation of fibres roughness and cross section analysis are two of the main characterizations performed with secondary electrons . Because a conductive sample is needed to acquire a clear images, pre-carbonization fibres are coated with carbon or gold. The preparation of samples and cross sections, altogether with the necessity to fine tune the microscopy parameters to obtain good results, may takes several hours. The acquisition of large number of images is a slow procedure, and the results may not be as meaningful as others characterization techniques available[31]. Notwithstanding the possibility of a close look to the fibres can shed light on hidden feature, and lead to a better understanding of the process. For example, a low conductivity may be linked with too high evaporation rate during the spinning process, after a SEM analysis: if the fibres already deposited are completely dry when new spun fibres deposit on them, a poor contact may form; on the other hand if the fibres are soften by the presence of the solvent, they can fuse together and result in a lower resistivity. The two different morphologies can be easily observed at SEM but are invisible if observed with optical microscopy.

### **Four Probe**

Because of the particular morphology of the fibres, a good ohmic contact can be hard to establish between a metal and the fibres, unless a certain pressure is exerted. The roughness of the mat may result in large contact resistance which masks the actual resistance due to the fibre thickness. Both for in plane and across plane resistance is essential to use the four probe technique in order to suppress the contact contribution. In figure 2.8 a typical setup is shown; it consists of four electrodes: two are used to impose a current, the other two to measure

## 2.2. CNFS PRODUCTION AND CHARACTERIZATION

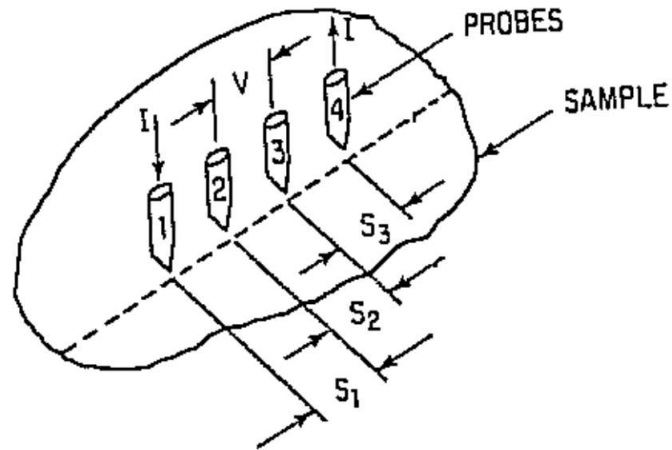


Figure 2.8: Four probe setup for resistance measurement. Taken from [67].

the voltage drop in between. With this configuration, because no current flows between the two inner electrodes, the voltage drop due to contact resistance is eliminated[67, pag 119]. The theory behind this measurement is not as easy as the Ohm's law and, depending on the characteristics of the sample under analysis, different formulas must be considered. For semi infinite sample the resistivity is given by

$$\rho = \frac{V}{I} 2\pi s$$

with  $s$  the spacing between the probes. In the case of a thin film the resistance does not depend any more on the distance and the formula reduce to

$$\rho = \frac{V \cdot t \cdot \pi}{I \cdot \ln 2}$$

where  $t$  is the thickness of the thin film, much smaller than the distance between the probes.

### Raman Spectroscopy

The resistivity measured with four probe must be related to the process variable, in particular with the carbonization temperature. As already explained, the conductivity of the fibres can be enhanced by means of metal doping or with an higher degree of graphitization. The latter is controlled by the annealing temperature and time. In order to obtain a quantitative measurement, the Raman spectroscopy is used. This technique is closely related to the infrared adsorption. As for FTIR, the used frequency are of the order of  $10^{13} - 10^{14}$  Hz ( $10^{-4} - 10^{-6}$   $m^{-1}$ ) and the interactions between EM waves and molecular bonds is observed. The Raman

## 2.3. ACTIVE MATERIAL

spectroscopy focus on the scattering of the EM waves during interaction. The scattering can be both elastic (scattered EM at the same frequency as the exciting one) and inelastic (scattered EM at different frequency): *Rayleigh scattering* and *Raman scattering*, which is the one observed with this technique.

In Raman spectroscopy the sample is excited with a certain spectrum of EM and the frequency shift between the input and output signal is recorded. The shifts can be related to particular molecular bonds; in particular, carbon is characterized by two scattering peaks in the visible at 560 and 1360  $cm^{-1}$  called G and D peaks. The two are related to different carbon-carbon bonds: the G peak is related to bond stretching in carbon rings or chains [17]; the D is related to single carbon atom resonance. Because graphene planes are composed by rings of carbon, the G peak can be related to the quantity of order graphene structure. The ratio between D and G peak is often used as quantitative measurement of the degree of graphitization of the carbon fibres [66].

## 2.3 Active Material

While in the previous chapter the choice of the active material has been justified, a deeper analysis of the sodium-vanadium-phosphate and its properties is proposed below.

### 2.3.1 NVP

$Na_3V_2(PO_4)_3$  is a typical example of the NASICON type materials. The electrodes, based on it, show an high solid ions diffusion, a pronounced structural stability, and high cycling performances[76]. The main drawback is a low electric conductance which imposes the exploitation of carbon coating and conductive matrices. The usage of CNFs is among the proposed solution in literature and a very effective one: one of the best performing NVP cathode has been realized embedding NVP nanoparticles into CNFs[72]. Even more complex structures, using carbon nanotubes and graphene, have been tested but with poorer results[79].

The storage mechanism of NVP exploits the change in oxidation state of vanadium. The sodium atom can be divided into two types ( $Na_1$  and  $Na_2$ ) depending on the occupation state with respect to the group  $V_2(PO_4)_3$ . 2/3 of the sodium atoms are in the  $Na_2$  occupation state. The redox reaction linked to the release of sodium ions from this site



corresponds to a standard potential of 0.70 V, or 3.40 V if the couple  $Na/Na^+$  is considered as reference. During the reaction, the oxidation state of vanadium atoms change from 3+ to 4+.

## 2.3. ACTIVE MATERIAL

The  $Na_2$  sites can be fully desodiate and a theoretical capacity of  $117.60 \text{ mA h g}^{-1}$  is reported[50]. The  $Na_1$  ions can also be removed at a potential as low as 1.60 V with respect to sodium reference. The theoretical capacity is only one half of the  $Na_2$  sites one. The lower capacity and the intermediate voltage make the second reaction useless for either cathode or anode reaction<sup>13</sup>, although the possibility of a fully symmetric cell based on NVP cathode and anode has been proposed[44, 76].

The NVP can be produced by conventional synthesis techniques: co-precipitation; hydrothermal synthesis; solid reaction. High temperature processes may be used to improve the crystallinity of the particles at temperature as high as  $900^\circ\text{C}$ [36].

### 2.3.2 Loading of CNFs

Of particular interest for the present work are the different strategies reported to load the NVP into carbonaceous structures.

#### Co-spinning

An exploited procedure to load the NVP into the CNFs is the co-spinning method. NVP nanoparticles are added to the polymer solution and spun altogether with the fibres. With this technique different structures can be realized: nanoparticles inside the fibres or core-shell configuration. [35]. After the spinning, the CNFs and the NVP are annealed together at  $800^\circ\text{C}$  to improve the crystallinity and to carbonize the fibres. This process is not particularly flexible from the point of view of loading control: once the concentration of NVP in solution is fixed, it is constant through all the mat. Notwithstanding is very fast and can be adapted to other materials.

#### Dip Coating

The dip coating consists of soaking the fibers with a liquid precursor of the active material and evaporating the solvent, trapping the particles into the fibers[72]. Once again the loading is fixed by the concentration and few control on the distribution can be achieved. The procedure can be performed either on stabilized or carbonized fibres. The latter are far more hydrophilic than the former and the soaking takes place in few minutes instead of hours.

---

<sup>13</sup>The power content of a cell is given by the product of the maximum current times the mean voltage. An intermediate voltage at anode or cathode leads to low power cells.

## 2.3. ACTIVE MATERIAL

### **Buchner Filtration**

Buchner filtration is a well known vacuum assisted filtration technique: the vacuum is used to draw the solution thorough a filter in order to speed up the process. If the carbon fibers are used instead of the filter, the active material particles dispersed in solution get trapped[74]. With this procedure the distribution profile can be controlled: depending on the size of particles, the major part of the NVP is retained in the top part of the filter; if multiple filtration steps are performed the concentration of active material in the fibres is increased. If the crystals are small enough, a continuous flux of water drags them in the deep of the mat, resulting in a peak of concentration at a given height. The process is very fast and can be performed either on stabilized or carbonized fibres.

### **Hydrothermal Synthesis**

The hydrothermal synthesis is an alternative to crystallization at high temperature. Instead of 800 °C, a temperature as low as 100-200°C, combined with high pressure, leads to the crystallization of the NVP precursor. The CNFs, plunged into the solution, catalyse the crystallization on their surface. The crystals are directly grown onto the CNFs and no high temperature process is necessary. This process works better with the carbonized fibres because they are much more resistant and can easily stand the high pressure. No control of the crystallization sites leads to a random distribution of the NVP but the dimension of the crystals can be easily tuned by process parameters. [36]

### **2.3.3 NVP Characterization**

The characterization of the NVP is a crucial phase. The crystallinity of the NVP is a fundamental parameter to obtain good electrochemical activity and ion conductivity. Because the crystallization process, by means of high temperature treatment, may need several hours to be completed, its optimization is mandatory.

### **X-Rays Diffraction Spectroscopy (XRD)**

In the study of crystal structures X-rays diffraction spectroscopy is recognized to be an excellent technique. The X-rays wavelength is of the order of magnitude of the crystal lattice and phenomena of diffraction appears when atoms and EM waves interact. Because each crystal structure results in a different diffraction pattern, a huge database have been developed, in the years, to collect the footprint of every possible structure. By means of automatic softwares, the

## 2.4. ELECTROCHEMICAL CELLS TESTING

recorded pattern is compared with the database and the crystal structures, and phases, present in the alleged synthesized material, can be assessed. Conclusions about the mean crystal size and the percentage of each crystalline phase can be also drawn[31].

### SEM

The SEM is of great interest for the characterization of the active material. As for the fibres, the measurement of secondary electrons (SEs) is a valuable tool for the morphological characterization of the crystals: dimension; cross section distribution; position with respect to the fibres. Notwithstanding, much more informations can be obtained by back scattering electrons (BSE) and energy dispersive spectroscopy (EDS or EDX). The former technique exploits the difference in energy of BSE emitted by different materials: high atomic number elements result in high energy BSE and vice-versa; by means of a potential difference, the energy of the observed BSE can be selected, increasing the contrast between carbon and active material. It is used to confirm the nature of different particles, inside the fibres, observed with SEs.

The EDS is a more complex technique but provides details about the spatial distribution of each atomic species, with great precision. EDS excitation signal is the very same of the SEM (electrons) but the observed quantity are X-rays. The primary electrons of the SEM can excite, with scattering, the electrons of an atom; once the electrons return to the non excited state X-rays are emitted. Because emitted X-rays are linked to the energy gap between two states, the wavelength can be easily related to the energy difference and hence to particular species with can emit that particular wavelength[31].

This technique is of particular interest in post-mortem analysis of electrodes: the presence of unexpected atoms inside the electrodes or near it surface can be related to the formation of SEI and to parasitic reactions.

## 2.4 Electrochemical Cells Testing

The core of this work is the electrochemical characterization of cells, which use CNFs as supporting matrix for NVP active material. Once the electrochemical parameters, presented in the first chapter, have been determined, it is possible to draw considerations about the effect of the nanostructure on the cell. It is of particular interest to demonstrated the consistency of the porous electrode model with the acquired data and to confirm the results reported in literature. The fully understanding of the characterization techniques used is fundamental to reach the right conclusions, therefore this whole section is devoted to the test setup, the possible measurements

## 2.4. ELECTROCHEMICAL CELLS TESTING

to be performed, and the issues than may be encountered.

### 2.4.1 Typical Cell Setup

Different possible setups can be found in literature. Some of them are commercial setups, while others are custom made ones. It has to be noticed how the production of the electrodes and the mounting of the cell can be less or more automated. Higher automatic is characteristic of advanced stage of development, when only smaller optimization are required and the reproducibility is the major concern. In the early stage of development smaller volume of production are required and flexible production lines are most suited for frequent design modifications.

The list of setups presented below starts with lab scale ones, which are characterized by low throughput and low cost, and ends with the industrial ones.

#### Swagelok

Among the custom setup, the Swagelok is a very popular one. It is a two or three electrodes setup<sup>14</sup> as shown in figure 2.9. The name comes from the brand of fluid connectors producer.

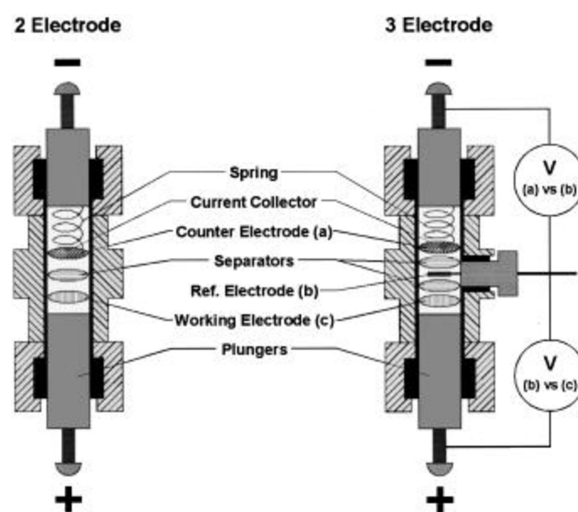


Figure 2.9: Two and Three electrodes Swagelok cell schematic. Taken from[1].

Usually the device is built from a plastic connector for pipes and metallic electrodes are placed at the three holes. The sealing of the structure is guaranteed with plastic o-rings and Parafilm. The popularity of this setup stems from the simple design and low cost. With respect to commercial solutions it is far cheaper and sometimes even more convenient to use when a three electrodes setup is necessary. On the other hand, the sealing may not be perfect, resulting in stability issues, and the pressure exerted on the cell may vary in time and among different mounts.

<sup>14</sup>For some measurements three electrodes are mandatory

## 2.4. ELECTROCHEMICAL CELLS TESTING

### El-cell®

The El-cell®, among the commercial setups, is the most popular one. As shown in figure 2.10 a spring and a metallic case are used to guarantee a good sealing and a constant and reproducible pressure on the cell. The main drawbacks are the high cost and the difficulty of implementing the reference electrode. As depicted in figure it has to be introduced through a small hole in the bottom part of the test cell.

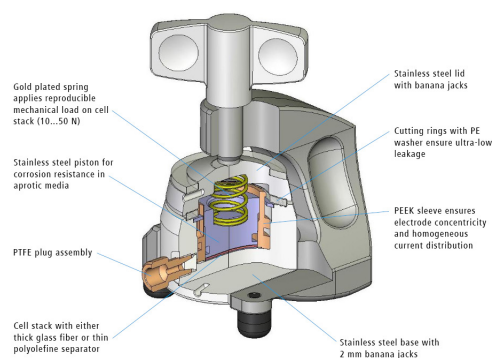


Figure 2.10: El-cell schematic. Taken from [8].

### Coin Cell

The coin cell is the simplest industrial setup. Because lab scale mounting setups are available, it is often used when lots of cells have to be mounted. As shown in figure 2.11 it is similar to the El-cell but the sealing is achieved by pressing the top and bottom case. The setup is usually a two electrodes one and each cell can be used only once. In the early phase of testing this setup is not particularly convenient and is also quite expensive due to the mounting machine to be purchased. Also for the testing a dedicated setup is needed because of flat electrodes.

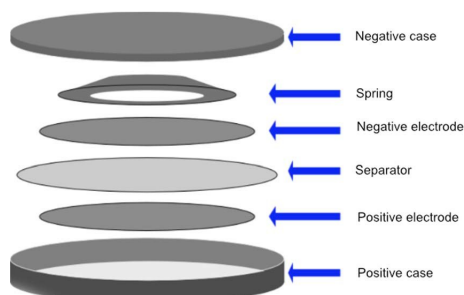


Figure 2.11: Coin cell schematic. Taken from [28].

## 2.4. ELECTROCHEMICAL CELLS TESTING

### Pouch Battery

The pouch battery setup is the most advanced one, close to the one used in big commercial batteries. It is usually exploited only when the technology has been optimized, in order to test stack of cells, close to the final product. The setup is a two electrodes one. Once again, a dedicated mounting setup is necessary as the cell cannot be reused. As shown in figure 2.12, up to 7-8 cells can be mounted in a single pouch battery. The automatic sealing guarantees a high stability and reproducibility.

Small pouch batteries can also be mounted with a minimum expense (only the sealing setup is necessary), but the two electrodes setup makes them less appealing in the early stage of development.

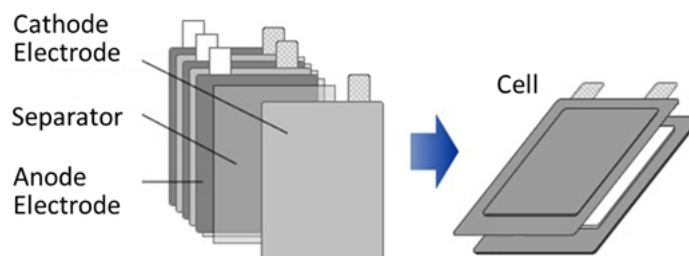


Figure 2.12: Pouch battery schematic. Taken from [28].

### 2.4.2 Cyclic Voltammetry (CV)

The first electrochemical technique to be explored is the cyclic voltammetry. It is used, together with XRD, in the early phase of characterization, in order to confirm the chemical activity of the synthesized crystals.

#### Physical Principles

In order to understand the working principles of the CV, the Nerst equation has to be recalled. The equation links the potential between two electrodes and the concentration of the redox specie in the electrolyte:

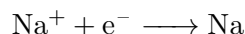
$$E = E^0 + \frac{RT}{nF} \ln \left( \frac{[ox]}{[red]} \right)$$

Redox in the way the ratio between  $[ox]$  and  $[red]$  can be changed. If the reduction is predominant the number of ions is increased, the ratio decreased.



## 2.4. ELECTROCHEMICAL CELLS TESTING

On the other hand the oxidation increases the concentration of the reduction specie and decreases the oxidizing one, decreasing the potential.



Each time the ratio between the two species is changed, electrons must be transferred from or to the cell in order to balance the reaction. This is to say, a current must flow each time a change in the potential occurs. In particular, the current must be proportional to the change in the ratio: for each ion generated one electron must be removed from the electrode:

$$i \propto \frac{\delta \frac{[ox]}{[red]}}{\delta t}$$

After substitution in the Nerst equation, the dependence between voltage and current can be expressed as

$$i \propto e^{(E-E^0)\frac{nF}{RT}}$$

Where  $E^0$  is the standard redox potential for the redox and  $E$  the voltage drop between the two electrodes. This equation predicts an infinity raise in current, while the potential drop is increased, but various phenomena take place, in the real case, which stop the increase in current. First of all, because, in order to react, the species need to be near the electrolyte, and are consumed after reaction, a constant flux of ions is required to sustain the reaction. Those ions motion is limited by the diffusion laws in the liquid and, eventually, limits the maximum number of reactions that can take place per second. A maximum equilibrium value for the current should then be established. Notwithstanding another players enters the stage at this point. The electrical double layer is also modified due to change in surface potential of electrodes. While the voltage increases, the diffusion zone of the double layer expands deeper and deeper into the electrolyte, slowing down the ions transport. Hence, the current, after a maximum is reached, starts to decrease.

A more basic reason for the current to drop is the finite amount of one specie: if the active material sites are fully exploited the reaction simply stops and the current goes back to zero. The cyclic voltammetry measurement consists of sweeping the voltage between the two electrodes and monitoring the current flow. Far from the redox potential, the current is the tail of an exponential and almost zero amperes are measured. When the potential difference approaches  $E^0$ , the current rises up to the maximum value and then decreases. Because each redox couple is linked to a particular potential, different reactions can be separately observed and clearly characterized.

The sweep, after a maximum voltage value is reached, is reversed and the potential goes back

## 2.4. ELECTROCHEMICAL CELLS TESTING

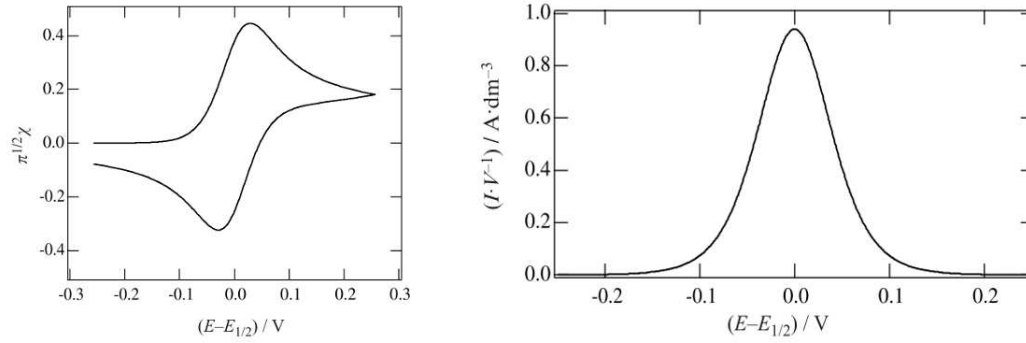


Figure 2.13: Two examples of CV curve: diffusion limited process and reaction limited process. Adapted from [19].

to the starting one. Many cycles are performed in order to observe differences due to parasitic effect, like electrolyte degradation.

Because the potential between the two electrodes must be precisely fixed, a reference electrode is necessary for the measurement.

In figure 2.13 two classical examples of CV are presented: in the first one the diffusion behaviour is clearly visible; in the second one the current suddenly drops, after the complete consumption of active material [13, 19]. An in deep analysis of the technique is possible, starting from physical equations and thermodynamics considerations. It is possible to express analytically the shape of the CVs reported above [19]. The diffusion limited one is modelled by the recursive formula

$$2\sqrt{\delta} \left[ \chi(\delta)\sqrt{k} + \sum_{i=1}^{k-1} \sqrt{k-1} [\chi((i+1)\delta) - \chi(i\delta)] \right] = \frac{1}{1 + \zeta \theta S(\delta)}$$

Where

$$k\delta = \frac{nF}{RT} \nu t$$

With  $\nu$  the scan rate in  $V s^{-1}$  and  $t$  the time.

$$\chi(z) = \frac{I(\sigma t)}{nFAc_R\sqrt{\pi D_R\sigma}}$$

With  $\sigma = \frac{nF}{RT} \nu$  and  $c_R$ ,  $D_R$  the initial concentration of the reduction species and its diffusion rate.

$$\theta S(t) = \frac{c_R}{c_O} e^{-\sigma t}$$

And  $\zeta = \sqrt{\frac{D_R}{D_O}}$  is the ratio between the red and ox species diffusion coefficients.

The following equations can be manipulated to obtain more meaningful expressions: the current

## 2.4. ELECTROCHEMICAL CELLS TESTING

as a function of the scan rate

$$I(\sigma t) = nFAc_R \sqrt{\pi D_R \frac{nF}{RT} \nu} \chi(\sigma t)$$

And the peak current as a function of the scan rate.

$$I_p = 0.4463nFAc_R \sqrt{\frac{nF\nu D_R}{RT}}$$

From the latter equation, it is possible to determine the diffusion coefficient  $D_R$ .

The potential value, at which the reaction takes place, is shifted with respect to the standard potential of  $\frac{59}{n}$  mV and does not depend on the scan rate as long as the reaction kinetics is faster than the ion diffusion. If the reaction is slower than the mass transport, the separation increases with the scan rate.

### Measurement Setup

The cell setup for the CV is a three electrodes one: the voltage on the electrode under test (working electrode) is fixed with respect to the reference electrode; the current can circulate between the working electrode and the counter one. In figure 2.14 both the cell and the measurement instrumentation are schematically reported.

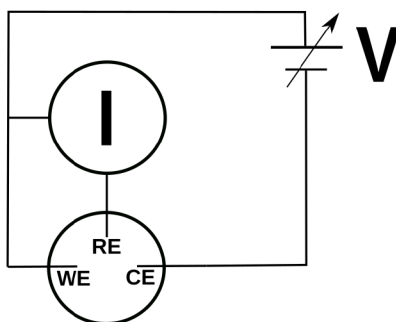


Figure 2.14: Cyclic voltammetry measurement setup schematic.

### Data Analysis Techniques

The purpose of the CV is mainly to determine which kind of reaction are taking place, at which voltage, and to provide some information about the dynamics of the processes. Because high sweep rate results in high current, to obtain good results and to avoid the saturation of the

## 2.4. ELECTROCHEMICAL CELLS TESTING

measurement setup, scan rates as slow as  $0.1\text{-}1\text{mV s}^{-1}$  are used<sup>15</sup>. Performing the measurement at different scan rates, it permit to acquire the  $I_p(\nu)$  function and to determine the diffusion coefficient.

The electrolyte degradation is monitored by repeating the sweep back and forth for many cycles. Because the electrolyte redox potential is usually far from the active material one, only the exponential tail can be observed, superimposed to the main signal. If the electrolyte redox is reversible, the CV curve, and in particular the final parts, should be similar among different cycles. Any difference in the extreme parts of the CV can be related to electrolyte degradation (irreversible reaction), which modifies the chemistry of the cell at each cycle. The formation of the SEI is one of those phenomena and can be monitored during the early cycles: the SEI forms a self passivating layer and hence its growth stops after 3-4 cycles.

This tool is particular interesting at the beginning of the test phase, to confirm the electro-activity of the synthesized material and the behaviour of the electrolyte.

### 2.4.3 Electrochemical Impedance Spectroscopy (EIS)

Another technique used to study the cell and its reactions is the EIS. As the name suggests, the cell is modelled by its impedance at different frequencies (spectroscopy) as a result of the measurement. Each contribution, in order to be accounted in the impedance at a certain frequency, must have a time constant compatible with the frequency itself: the phenomena taking place into the cell are separated according to their dynamic. As for the CV, it is possible to observe different physical effects (e.g. diffusion, charge transfer) separately and hence to characterized them [19].

#### Physical Principles

In figure 2.15 a schematic of an electrode is reported together with the main processes than may take place on its surface. Those processes are characterized by a time constant which represent the average time to be waited before each process takes place.

If a periodic current signal (sine wave), with zero mean, is fed into the electrode, the surface reactions neutralize the excess charge (e.g. growth of the double layer). Because after half period the current starts to flow in the opposite direction, the reactions accommodate it by reverting their effects (e.g. reduction of the double layer). For a given frequency of the input signal, only the reactions with a time constant of the order of, or smaller then, the semi-period contribute to the neutralization of the injected charges. The effect of chemical processes is observed in

---

<sup>15</sup>It result typical in some milliamperes of current.

## 2.4. ELECTROCHEMICAL CELLS TESTING

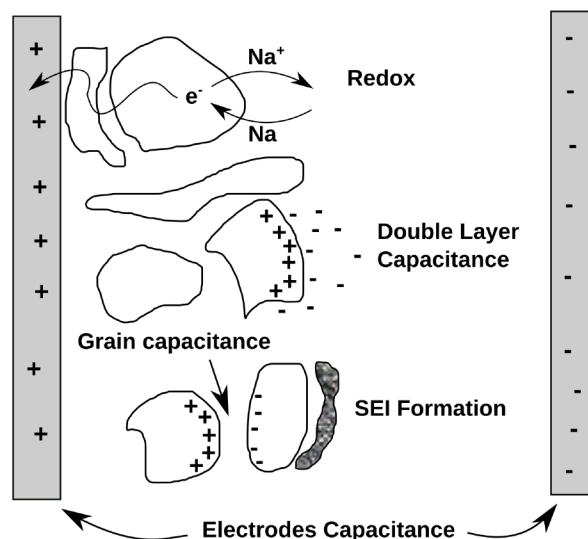


Figure 2.15: Schematic of electrode processes which influence the impedance.

the voltage between two electrodes (working and counter). The impedance modulus is the ratio between the amplitude of input current and output voltage, while its phase is the phase difference between the two signals [27, 4].

The main contributions that can be observed are:

- Capacity of the two electrodes.
- Capacity between different particles of active material.
- Capacity due to the electrical double layer.
- Contact resistance between current collector and active material.
- Resistance of the active material.
- Resistance associated with ion diffusion.

All of them can be easily represented by classical circuitual elements, like resistors and capacitors but the ion diffusion one. This latter must be associated to an ad-hoc circuitual element called *constant phase element* (PCE). It is characterized, in the Nyquist plane, by a constant slope[4]. In figure 2.16 a typical equivalent circuit with all the above mentioned contribution is reported. The PCE is modelled with a W: Warburg element, linked with semi-infinite linear diffusion. Because each element has a physical counter part, a link between the process parameters and the circuitual element can be drawn. For example, the slope of the constant phase element and its frequency parametrization are associated to the diffusion coefficient.

## 2.4. ELECTROCHEMICAL CELLS TESTING

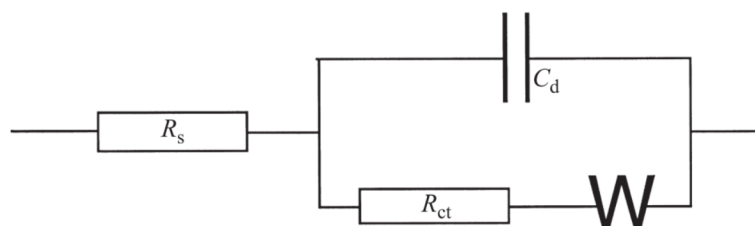


Figure 2.16: Equivalent circuit of an electrode. Taken from [19].

### Measurement Setup

The measurement setup is shown in figure 2.17 and consists of a three electrodes setup, a sinusoidal current source and a voltmeter. The sine frequency is changed after 3-4 periods and swept between 0.01 Hz and 100 Hz 100 kHz.

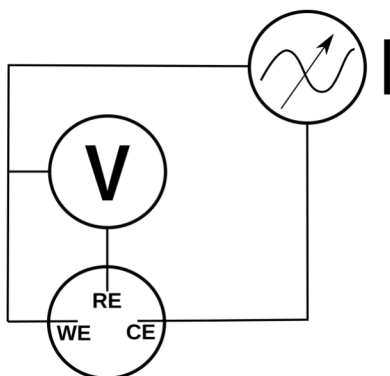


Figure 2.17: EIS measurement setup schematic.

### Data Analysis Techniques

The impedance data acquired are usually reported on the Nyquist plane. Different shapes can be recognized and linked to particular circuit systems: The semi-circular shape is associated to RC circuits; depressed semi-circles are distributed RC; straight line are associated to diffusion phenomena. In figure 2.18 a typical result is reported.

Once a possible collection of simple circuits, to explain the single features, has been established, the full circuit can be realized. This model is not unique and it depends on the initial choice of elements and the way they are assembled in the final circuit. Once the fitting is satisfactory, informations about each part of the circuit can be easily extracted<sup>16</sup>.

<sup>16</sup>Separation of the contact resistance and the charge transfer resistance; diffusion coefficient.

## 2.4. ELECTROCHEMICAL CELLS TESTING

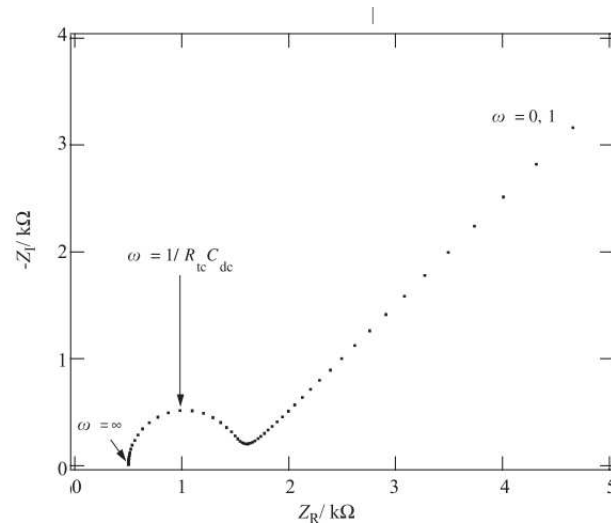


Figure 2.18: Impedance spectrum of an electrochemical cell. Taken from [19].

### 2.4.4 Galvanostatic Cycling (GC)

The last electrochemical technique used in the present work is Galvanostatic Cycling. This is the more intuitive type of test to be performed on a battery. It consists of repeated charge and discharge steps of the battery, at constant current. The battery voltage is monitored and each cycle is stopped when a fixed threshold is reached.

#### Physical Principles

The physical principles behind this kind of measurement are the very same listed in the previous chapter in order to explain the V(SOC) curve. At different current rate the drop increase due to ohmic resistance. The limitation of chemical reactions due to ion diffusion in solid and liquid can be observed, as higher and higher voltage drop, while the current is increased. Those two contributions can be easily separated, by mean of the time scale: the ohmic drop manifests as soon as the current starts to flow and is constant for the all timespan of the measurement. The diffusion induced voltage drop is invisible at the beginning, because the ions are already near the active material, and increases during time: the depletion of ions near the electrodes induces the ions motion.

#### Measurement Setup

The setup is the same as for EIS but the current source is constant as shown in figure 2.19.

## 2.4. ELECTROCHEMICAL CELLS TESTING

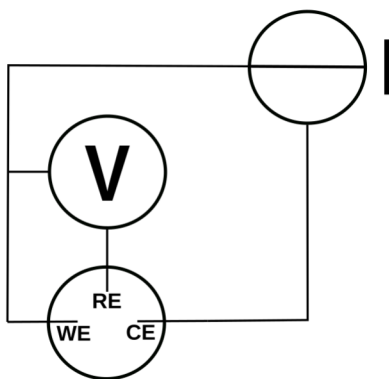


Figure 2.19: GC measurement setup schematic.

### Data Analysis Techniques

The  $V(\text{SOC})$  is acquired at each cycle and lots of informations can be extracted from it. The capacity at the experimental C-rate is promptly calculated as the integral of the current over time. The ratio between charge and discharge capacity is the charge efficiency. From the charge efficiency and the mean voltage the power efficiency is obtained.

The macro parameters linked with the duration of the cycle and its mean value are extremely useful for a fast characterization of the cell. At advance stage of development those informations are the best figure-of-merit to compare different batches of cells.

More qualitative informations can be extracted and integrated with CV and EIS results. For example, the shape of the GC can be associated with more or less distribute process: a constant slope indicate a distribute resistance, while a plateau means constant one.

Apart from the informations a single cycle of GC can provide, the long term evolution of the same parameters and their variation at different C-rates is far more interesting: Capacity and efficiency evolution over different cycles is used to monitor the degradation phenomena of the cell (e.g. electrolyte degradation); analysis at different C-rates are used to determine the optimal current, and to acquire additional informations on processes limiting the cell performances.

### 2.4.5 Reference Electrode and Half-Cell

The setup used in the present work for electrochemical characterization is the Swagelok cell with counter and reference electrode made of metallic sodium. This configuration is frequently encountered in literature but it is sometimes criticized. A brief review of problems linked with this setup is proposed below.

## 2.4. ELECTROCHEMICAL CELLS TESTING

### Reference Electrode

The reference electrode is used to define an absolute reference during the measurement. Because the current does not flow through it, no shift of the reference due to ohmic drop can happen. Notwithstanding, the potential at an electrode, recalling the Nerst equation, can change also if the concentration of species changes. The fundamental quantity is the effective ion concentration (or activity). With respect to standard condition, a decrease in the temperature of the experiment, lead to an increase in the energy needed to perform a certain reaction<sup>17</sup>. It is like less ions are ready to react at a given time and the effective concentration is reduced.

Because all the thermodynamic quantities (pH, pressure, etc) influence the activity of ions, it is extremely difficult to realize reliable reference electrodes. In practice it is enough the reference is stable in the range of the experimental conditions. Anyway, electrolyte degradation and other unexpected processes can result in a drift of the reference voltage[47, 39].

As it is explained below, defective reference electrodes lead to the impossibility of clearly separate anode and cathode contribution and to wrong conclusions about the material under test.

### Half Cell

The half cell used during the experiment is composed of the NVP cathode, a sodium anode, and a reference electrode. Several artefacts can result from this configuration.

Apart from the already mentioned issues with the sodium reference, the presence of metallic sodium at the anode may hide the presence of irreversible reaction: if a reaction at the cathode consumes the sodium ions, in a real cell, with active material at both anode and cathode, the total sodium content decreases at each cycle. In a full cell the effect of the reaction is observed as a fade of the capacity but, because the anode of the half cell can replace the lost ions, the same effect is not measurable in the latter setup.

If the half cell may lead to an overestimation of the cell performances, also the reverse can happen: metallic sodium can cycle at a maximum current of some  $\mu\text{A cm}^{-2}$ , at higher current the cell performances decrease, but the effect may be due only to the anode and not to the material under investigation. Also low efficiency and capacity fade may be due to the metallic anode and not to the NVP cathode, when sodium degradation takes place at the anode and at the reference[75, 70]. Because both reference and anode are made of sodium, it is not possible to properly isolate the cathode dynamics and properties.

Even if some issues derive from the usage of metallic sodium reference electrode, it is the

---

<sup>17</sup>Less energy comes from thermal motion.

## 2.5. SUMMARY

mainstream choice in literature and the chosen one for this work (to achieve consistency with paper results).

### 2.5 Summary

The working principle of an electrochemical cell may be summed up into few elements: the extraction/insertion of an ions inside a crystal structure result in a phase change of the crystal structure itself. During this process one or more electrons are also extracted/provided to the reaction site. This electron represent the current the battery provides while the binding energy of the ions to the crystal determines the voltage of the cell. The conductive path from the reaction zone to the current collector and the diffusion of the ions in the electrolyte and the crystal, altogether with the chemical reaction dynamics, are responsible for the internal resistance of the cell and hence for the dynamic response (higher the resistance higher the voltage drop at high current). Because a big voltage drop means more complex control system, in order to exploit the cell at higher C-rate a low internal resistance is fundamental. This is our first target and the choice of a particular nanostructured electrode where to grow the active crystal is the first step to accomplish the result. Porous structures with embedded nanocrystals have the following advantages:

- Provide a conductive path from the crystal to the current collector.
- Reducing the diffusion path inside the active material (which may be slow compared to the on on the electrolyte).
- Provide a path for the electrolyte and hence for the ions to reach the crystal (all reaction zone are reached by the electrolyte directly).
- Provide space for the phase change related crystal expansion (enhance life cycle).

The CNFs are one of the possible solution to obtain this kind of structure, with the advantage of fast production and lots of parameters to tune the fibre morphology and porosity (nickel or carbon foams are viable alternatives).

The production of CNF exploits the very well known techniques of electro-spinning, widespread in the carbon fibre and textile industry. A very high electric field is used to produce thin fibres starting from a solution containing a polymer. The polymer fibre, during the flight to the collector, spread in order to minimize the electrostatic interaction of charges trapped in it. The result on the collector is a non-woven mat of polymer. Following thermal treatments result only

## 2.5. SUMMARY

in carbon to remain and the formation of carbon fibres mat is achieved.

Different characterization techniques are useful to control and tune the process.

- Optical microscopy is a first check for the morphology of the spun fibre (diameter of the fibre and beads formation).
- Scanning Electron Microscopy (SEM) is used to characterize the process: thickness of the fibre versus spin time; mean dimension of the fibres; morphological analysis.
- Fourier Transform Infrared Spectroscopy (FTIR) is fundamental to monitor the evolution of the polymer and to optimize the thermal process.
- Four probe measure is used for resistance measurement of the fibre: higher temperature results in lower resistance due to graphene formation.
- Raman spectroscopy can add more quantitative information about graphene formation in order to fine tune the thermal process.

Once the fibre is realized it has to be loaded with the active material. It is important to have a good control of this process in order to fully exploit the freedom of this kind of cell design: total weight loading; non-homogeneous distribution.

- X-ray Powder Diffraction (XRD) is used to assess the proper crystal structure of the material inside the CNF.
- SEM cross section is used to determine mean grain size and distribution.
- Weighing g before and after active material loading to determine the active material content.

The characterization is then carried on with an electrochemical cell. The main characterization to carry on are the following:

- Cyclic Voltammetry (CV) is used to check the electrochemical behaviour of the material: reaction voltage; diffusion coefficient of the ions.
- Charge/Discharge Cycling is used to test the cycling stability and the behaviour at different C-rate.
- Electrochemical Impedance Spectroscopy (EIS) is a fine grain tool to determine an equivalent circuit of the device and to explore different electrochemical process inside the cell.

## 2.5. SUMMARY

The whole set of characterization is necessary to establish a causal link between the complex process of production of the cell and the final electrochemical performance. In particular data collection from the beginning to the end of production line with enough statistical sampling is the key to optimize the final device.

## Reference of Chapter 2

- [1] Glenn G Amatucci et al. “An Asymmetric Hybrid Nonaqueous Energy Storage Cell”. In: *Journal of The Electrochemical Society* (2001), pp. 930–939. DOI: 10.1149/1.1383553.
- [2] Jan B. Habedank et al. “Increasing the Discharge Rate Capability of Lithium-Ion Cells with Laser-Structured Graphite Anodes: Modeling and Simulation”. In: *Journal of The Electrochemical Society* 165 (Jan. 2018), A1563–A1573. DOI: 10.1149/2.1181807jes.
- [3] T a Baede. “Towards a new position- controlled electrospinning setup”. In: (2009), pp. 1–52.
- [4] Evgenij Barsoukov and J. Ross Macdonald. *Impedance Spectroscopy*. 2018. ISBN: 9781119333173.
- [5] Clement Bommier and Xiulei Ji. “Electrolytes, SEI Formation, and Binders: A Review of Nonelectrode Factors for Sodium-Ion Battery Anodes”. In: *Small* 14.16 (2018), pp. 1–20. ISSN: 16136829. DOI: 10.1002/sm11.201703576.
- [6] Natalie M Cann, Xinyun Wu, and Richard D. Oleschuk. “Characterization of microstructured fibre emitters: in pursuit of improved nano electrospray ionization performance”. In: *Analyst* 137.18 (2012). DOI: 10.1039/c2an35249d.
- [7] Pablo Carballeira Pol. “Mechanical and electrical properties of carbon nanofiber-ceramic nanoparticle-polymer composites”. PhD thesis. Verbundwerkstoffe GmbH, Jan. 2010.
- [8] EL-CELL. *lectrochemical test cell for two-electrode battery testing*. 2019. URL: <https://el-cell.com/products/test-cells/standard-test-cells/ecc-std> (visited on 07/22/2019).
- [9] Taiqiang Chen et al. “Electrospun carbon nanofibers as anode materials for sodium ion batteries with excellent cycle performance”. In: *Journal of Materials Chemistry A* 2.12 (2014), pp. 4117–4121. ISSN: 20507488. DOI: 10.1039/c3ta14806h.
- [10] Marc Doyle, Thomas F Fuller, and John Newman. “Modeling of Galvanostatic Charge and Discharge of the Lithium/Polyme/Insertion Cell”. In: 140.6 (1993), pp. 1526–1533.

## 2.5. SUMMARY

- [11] Marc Doyle and John Newman. “Modeling the performance of rechargeable lithium-based cells: design correlations for limiting cases”. In: *Journal of Power Sources* 54.1 (1995), pp. 46–51. ISSN: 03787753. DOI: 10.1016/0378-7753(94)02038-5.
- [12] Zhijia Du et al. “Understanding limiting factors in thick electrode performance as applied to high energy density Li-ion batteries”. In: *Journal of Applied Electrochemistry* 47.3 (2017), pp. 405–415. ISSN: 15728838. DOI: 10.1007/s10800-017-1047-4.
- [13] Noémie Elgrishi et al. “A Practical Beginner’s Guide to Cyclic Voltammetry”. In: *Journal of Chemical Education* 95.2 (2018), pp. 197–206. ISSN: 19381328. DOI: 10.1021/acs.jchemed.7b00361.
- [14] Reza Eslami Farsani, Ali Shokuhfar, and Arman Sedghi. “Stabilization of commercial polyacrylonitrile fibres for fabrication of low-cost medium-strength carbon fibres”. In: *e-Polymers* 6.1 (2014). ISSN: 2197-4586. DOI: 10.1515/epoly.2006.6.1.1.
- [15] R. Larry Faulkner and Allen J. Bard. *Electrochemical method, Fundamentals and Applications*. Ed. by JOHN WILEY and SONS. 2002.
- [16] Lichao Feng, Ning Xie, and Jing Zhong. “Carbon nanofibers and their composites: A review of synthesizing, properties and applications”. In: *Materials* 7.5 (2014), pp. 3919–3945. ISSN: 19961944. DOI: 10.3390/ma7053919.
- [17] Andrea C Ferrari. “Raman spectroscopy of graphene and graphite : Disorder , electron - phonon coupling , doping and nonadiabatic effects”. In: 143 (2007), pp. 47–57. DOI: 10.1016/j.ssc.2007.03.052.
- [18] W Frohs, M Heine, and E Fitzer. “Optimization of stabilization and carbonization treatment of PAN fibers and structural characterization of the resulting carbon fibers”. In: *Carbon* 24.4 (1986), pp. 387–395.
- [19] H. H. Girault. *Analytical and Physical Electrochemistry*. Vol. 96. 1. 2004.
- [20] Yury Gogotsi. *Nanotubes and Nanofibers*. 2006. ISBN: 9780849393877.
- [21] J. A Griffiths, P. R. and de Haset. *Fourier Transform Infrared Spectrometry*. 2011, pp. 614–614. ISBN: 9780471194040. DOI: 10.1007/978-3-642-11274-4\_3256.
- [22] Jan Bernd Habedank et al. “Rapid electrolyte wetting of lithium-ion batteries containing laser structured electrodes: in situ visualization by neutron radiography”. In: *The International Journal of Advanced Manufacturing Technology* 102.9 (June 2019), pp. 2769–2778. ISSN: 1433-3015. DOI: 10.1007/s00170-019-03347-4.

## 2.5. SUMMARY

- [23] Ivana Hasa, Jusef Hassoun, and Stefano Passerini. “Nanostructured Na-ion and Li-ion anodes for battery application: A comparative overview”. In: *Nano Research* 10.12 (2017), pp. 3942–3969. ISSN: 19980000. DOI: 10.1007/s12274-017-1513-7.
- [24] Heiner Heimes et al. *LITHIUM-ION BATTERY CELL PRODUCTION PROCESS*. Feb. 2019. ISBN: 978-3-947920-03-7.
- [25] Roksana Hossain and Kazimierz Adamiak. “Dynamic properties of the electric double layer in electrolytes”. In: *Journal of Electrostatics* 71.5 (2013), pp. 829–838. ISSN: 03043886. DOI: 10.1016/j.elstat.2013.06.006. URL: <http://dx.doi.org/10.1016/j.elstat.2013.06.006>.
- [26] Michio Inagaki, Ying Yang, and Feiyu Kang. “Carbon nanofibers prepared via electrospinning”. In: *Advanced Materials* 24.19 (2012), pp. 2547–2566. ISSN: 09359648. DOI: 10.1002/adma.201104940.
- [27] By John T S Irvine, Derek C Sinclair, and Anthony R West. “Electroceraamics Characterisation by impedance spectroscopy”. In: 2.3 (1990), pp. 132–138. ISSN: 15214095. DOI: 10.1002/adma.19900020304.
- [28] Wathanyu Kao-ian et al. “Rechargeable Zinc-Ion Battery Based on Choline Chloride-Urea Deep Eutectic Solvent”. In: *Journal of The Electrochemical Society* 166 (Jan. 2019), A1063–A1069. DOI: 10.1149/2.0641906jes.
- [29] Jin Il Kim, Kyung Yoon Chung, and Jong Hyeok Park. “Design of a porous gel polymer electrolyte for sodium ion batteries”. In: *Journal of Membrane Science* 566.August (2018), pp. 122–128. ISSN: 18733123. DOI: 10.1016/j.memsci.2018.08.066. URL: <https://doi.org/10.1016/j.memsci.2018.08.066>.
- [30] Shung-Ik Lee et al. “A study of electrochemical kinetics of lithium ion in organic electrolytes”. In: *Korean Journal of Chemical Engineering* 19 (July 2002), pp. 638–644. DOI: 10.1007/BF02699310.
- [31] Yang Leng. *Materials Characterization*. Wiley-VCH Verlag GmbH & Co., 2013. ISBN: 9783527317608.
- [32] Dan Li, Yuliang Wang, and Younan Xia. “Electrospinning of polymeric and ceramic nanofibers as uniaxially aligned arrays”. In: *Nano Letters* 3.8 (2003), pp. 1167–1171. ISSN: 15306984. DOI: 10.1021/nl0344256.
- [33] J I Liang and G U O Zhansheng. “Electrochemomechanical performance of porous electrode incorporating binder network”. In: 62.8 (2019), pp. 1331–1340.

## 2.5. SUMMARY

- [34] Shishuo Liang et al. “Gel polymer electrolytes for lithium ion batteries: Fabrication, characterization and performance”. In: *Solid State Ionics* 318.December 2017 (2018), pp. 2–18. ISSN: 01672738. DOI: 10.1016/j.ssi.2017.12.023.
- [35] Hua-Kun Liu et al. “Na<sub>3</sub>V<sub>2</sub>(PO<sub>4</sub>)<sub>3</sub> particles partly embedded in carbon nanofibers with superb kinetics for ultra-high power sodium ion batteries”. In: *Journal of Materials Chemistry A* 3.3 (2014), pp. 1005–1009. ISSN: 2050-7488. DOI: 10.1039/c4ta06001f.
- [36] Yongchang Liu, Fanfan Wang, and Li Zhen Fan. “Self standing Na storage anode of Fe<sub>2</sub>O<sub>3</sub> nanodots encapsulated in porous N-doped carbon nanofibers with ultra high cyclic stability”. In: *Nano Research* 11.8 (2018), pp. 4026–4037.
- [37] Zaichun Liu et al. “Three-dimensional ordered porous electrode materials for electrochemical energy storage”. In: *NPG Asia Materials* (2019). ISSN: 1884-4057. DOI: 10.1038/s41427-019-0112-3. URL: <http://dx.doi.org/10.1038/s41427-019-0112-3>.
- [38] Mitsubishi Electric. “Lithium Ion Battery Production Line Solution Catalog”. In: *Factory Automation* (2019).
- [39] Gholam-Abbas Nazri and Gianfranco Pistoia. *Lithium Batteries*. Springer, 2009.
- [40] John Newman. “Optimization of Porosity and Thickness of a Battery Electrode by Means of a Reaction-Zone Model”. In: *Journal of The Electrochemical Society* 142.1 (2006), p. 97. ISSN: 00134651. DOI: 10.1149/1.2043956.
- [41] John S Newman and Charles W Tobias. “Theoretical Analysis of Current Distribution in Porous Electrodes”. In: (1962).
- [42] John Newman and William Tiedemann. “Porous-electrode theory with battery applications”. In: *AIChE Journal* 21.1 (1975), pp. 25–41. DOI: 10.1002/aic.690210103. eprint: <https://aiche.onlinelibrary.wiley.com/doi/pdf/10.1002/aic.690210103>. URL: <https://aiche.onlinelibrary.wiley.com/doi/abs/10.1002/aic.690210103>.
- [43] Nilar. *Performance*. 2019. URL: <http://www.nilar.com/factory-technology/performance/> (visited on 08/22/2019).
- [44] Yoshinori Noguchi et al. “Fabrication and performances of all solid-state symmetric sodium battery based on NASICON-related compounds”. In: *Electrochimica Acta* 101 (2013), pp. 59–65. DOI: 10.1016/j.electacta.2012.11.038. URL: <http://dx.doi.org/10.1016/j.electacta.2012.11.038>.

## 2.5. SUMMARY

- [45] Nobuhiro Ogihara et al. “Theoretical and Experimental Analysis of Porous Electrodes for Lithium-Ion Batteries by Electrochemical Impedance Spectroscopy Using a Symmetric Cell”. In: 159.7 (2012), pp. 1034–1039. DOI: 10.1149/2.057207jes.
- [46] L. G. Plett. *Battery Management Systems: Battery Modeling*. ARTECH HOUSE, 2015, p. 390. ISBN: 9781630810238.
- [47] Rinaldo Raccichini, Marco Amores, and Gareth Hinds. “Critical Review of the Use of Reference Electrodes in Li-Ion Batteries : A Diagnostic Perspective”. In: ii (2019), pp. 1–24. DOI: 10.3390/batteries5010012.
- [48] M.S.A. Rahaman, A.F. Ismail, and A. Mustafa. “A review of heat treatment on polyacrylonitrile fiber”. In: *Polymer Degradation and Stability* 92.8 (Aug. 2007), pp. 1421–1432. ISSN: 01413910. DOI: 10.1016/j.polyimdegstab.2007.03.023. URL: <https://linkinghub.elsevier.com/retrieve/pii/S0141391007001279>.
- [49] Marialuigia Raimondo et al. “Electrical conductivity of carbon nanofiber reinforced resins: Potentiality of Tunneling Atomic Force Microscopy (TUNA) technique”. In: *Composites Part B: Engineering* 143 (2018). DOI: <https://doi.org/10.1016/j.compositesb.2018.02.005>.
- [50] Laifa Shen et al. “Challenges and Perspectives for NASICON-Type Electrode Materials for Advanced Sodium-Ion Batteries”. In: *Advanced Materials* 29.48 (2017), p. 1700431. DOI: 10.1002/adma.201700431.
- [51] Yangping Sheng. “Investigation of Electrolyte Wetting in Lithium Ion Batteries : Effects of Electrode Pore Structures and Solution”. PhD thesis. University of Wisconsin Milwaukee, Dec. 2015.
- [52] Yangping Sheng et al. “Effect of Calendering on Electrode Wettability in Lithium-Ion Batteries”. In: *Frontiers in Energy Research* 2 (2014), p. 56. ISSN: 2296-598X. DOI: 10.3389/fenrg.2014.00056. URL: <https://www.frontiersin.org/article/10.3389/fenrg.2014.00056>.
- [53] Madhav Singh, Jörg Kaiser, and Horst Hahn. “A systematic study of thick electrodes for high energy lithium ion batteries”. In: *Journal of Electroanalytical Chemistry* 782 (2016), pp. 245–249. ISSN: 15726657. DOI: 10.1016/j.jelechem.2016.10.040. URL: <http://dx.doi.org/10.1016/j.jelechem.2016.10.040>.
- [54] Madhav Singh, Jörg Kaiser, and Horst Hahn. “Effect of Porosity on the Thick Electrodes for High Energy Density Lithium Ion Batteries for Stationary Applications”. In: *Batteries* 2.4 (2016), p. 35. ISSN: 0013-4651. DOI: 10.3390/batteries2040035.

## 2.5. SUMMARY

- [55] F. R. S. Sir Geoffrey Taylor. “Electrically Driven Jets”. In: *Proceedings of the Royal Society A: Mathematical, Physical and Engineering Sciences* 313.1515 (1969), pp. 453–475. ISSN: 1364-5021. DOI: 10.1098/rspa.1969.0205. URL: <http://rspa.royalsocietypublishing.org/cgi/doi/10.1098/rspa.1969.0205>.
- [56] M. E. Sotomayor et al. “Additive-free Li<sub>4</sub>Ti<sub>5</sub>O<sub>12</sub> thick electrodes for Li-ion batteries with high electrochemical performance”. In: *J. Mater. Chem. A* 6 (14 2018), pp. 5952–5961. DOI: 10.1039/C7TA10683A.
- [57] Adrian Spillmann. “From Coin Cell to Gigafactory - Scale-Up of LIB Slurry Processing”. In: (2017).
- [58] Ben Zhong Tang. *Electrospinning: Principles, Practice and Possibilities*. RCS. RSC Polymer Chemistry Series Editor-in-Chief: 2014. ISBN: 9781849735568. URL: [, %20www.rsc.org](http://www.rsc.org).
- [59] W. E. Teo and S. Ramakrishna. “A review on electrospinning design and nanofibre assemblies”. In: *Nanotechnology* 17.14 (2006). ISSN: 09574484. DOI: 10.1088/0957-4484/17/14/R01.
- [60] William Tiedemann. “orty Years of Porous Electrode Theory with Battery Applications”. In: *ECS Transactions* 16.13 (2008), pp. 23–37.
- [61] C. A. Vincen and B. Crosati. *MODERN BATTERIES An Introduction Electrochemical to Power Sources*. Butterworth-Heinemann, 1997.
- [62] Goutham Viswanadam and George G. Chase. “Modified electric fields to control the direction of electrospinning jets”. In: *Polymer* 54.4 (2013), pp. 1397–1404. ISSN: 00323861. DOI: 10.1016/j.polymer.2012.12.082.
- [63] Aiping Wang et al. “Review on modeling of the anode solid electrolyte interphase (SEI) for lithium-ion batteries”. In: *npj Computational Materials* 4.1 (2018). ISSN: 20573960. DOI: 10.1038/s41524-018-0064-0. URL: <http://dx.doi.org/10.1038/s41524-018-0064-0>.
- [64] Heng Guo Wang et al. “Electrospun materials for lithium and sodium rechargeable batteries: From structure evolution to electrochemical performance”. In: *Energy and Environmental Science* 8.6 (2015), pp. 1660–1681. ISSN: 17545706. DOI: 10.1039/c4ee03912b.
- [65] Ming Wang et al. “The effect of local current density on electrode design for lithium-ion batteries”. In: *Journal of Power Sources* 207 (2012), pp. 127–133. DOI: 10.1016/j.jpowsour.2011.12.063. URL: <http://dx.doi.org/10.1016/j.jpowsour.2011.12.063>.

## 2.5. SUMMARY

- [66] Yu Wang, Santiago Serrano, and Jorge J. Santiago-Avilés. “Raman characterization of carbon nanofibers prepared using electrospinning”. In: *Synthetic Metals* 138.3 (2003), pp. 423–427. DOI: 10.1016/S0379-6779(02)00472-1.
- [67] Stanley Wolf and Richard N. Tauber. “Silicon Processing for the VLSI Era Volume 1: Process Technology”. In: (1986).
- [68] Mao-Sung Wu et al. “Assessment of the Wettability of Porous Electrodes for Lithium-Ion Batteries”. In: *Journal of Applied Electrochemistry* 34.8 (2004), pp. 797–805. ISSN: 1572-8838. DOI: 10.1023/B:JACH.0000035599.56679.15.
- [69] Hui Xia et al. “Electrochemical Behavior and Li Diffusion Study of LiCoO<sub>2</sub> Thin Film Electrodes Prepared by PLD”. In: (Jan. 2007).
- [70] Zhixin Xu et al. “Stable Na Metal Anode Enabled by a Reinforced Multistructural SEI Layer”. In: 1901924 (2019), pp. 1–10. DOI: 10.1002/adfm.201901924.
- [71] Jianchao Ye et al. “Structural Optimization of 3D Porous Electrodes for High-Rate Performance Lithium Ion Batteries”. In: 2 (2015), pp. 2194–2202. DOI: 10.1021/nm505490u.
- [72] Shicheng Yu et al. “Self-standing NASICON-type electrodes with high mass loading for fast-cycling all-phosphate sodium-ion batteries”. In: *Journal of Materials Chemistry A* 6.37 (2018), pp. 18304–18317. DOI: 10.1039/c8ta07313a.
- [73] Biao Zhang et al. “Recent Advances in Electrospun Carbon Nanofibers and Their Application in Electrochemical Energy Storage”. In: *Progress in Materials Science* 76 (Oct. 2015). DOI: 10.1016/j.pmatsci.2015.08.002.
- [74] Xianghua Zhang et al. “Na<sub>3</sub>V<sub>2</sub>(PO<sub>4</sub>)<sub>3</sub>: an advanced cathode for sodium-ion batteries”. In: (2019), pp. 2556–2576. DOI: 10.1039/c8nr09391a.
- [75] Yang Zhao, Keegan R. Adair, and Xueliang Sun. “Recent developments and insights into the understanding of Na metal anodes for Na-metal batteries”. In: *Energy Environ. Sci.* 11 (10 2018), pp. 2673–2695. DOI: 10.1039/C8EE01373J. URL: <http://dx.doi.org/10.1039/C8EE01373J>.
- [76] Qiong Zheng et al. “Progress and prospect for NASICON-type Na<sub>3</sub>V<sub>2</sub>(PO<sub>4</sub>)<sub>3</sub> for electrochemical energy storage”. In: *Journal of Energy Chemistry* 27.6 (2018), pp. 1597–1617. DOI: 10.1016/j.jechem.2018.05.001.
- [77] Weijia Zhou et al. *Nanomaterials in Advanced Batteries and Supercapacitors*. 2016, pp. 271–316. ISBN: 978-3-319-26080-8. DOI: 10.1007/978-3-319-26082-2. URL: <http://link.springer.com/10.1007/978-3-319-26082-2>.

## 2.5. SUMMARY

- [78] Zhengping Zhou et al. “Block copolymer-based porous carbon fibers”. In: *Science Advances* 5.2 (2019), eaau6852. ISSN: 2375-2548. DOI: 10.1126/sciadv.aau6852.
- [79] Changbao Zhu et al. “High Power-High Energy Sodium Battery Based on Threefold Interpenetrating Network”. In: *Advanced Materials* 28.12 (Mar. 2016), pp. 2409–2416. DOI: 10.1002/adma.201505943. URL: <http://doi.wiley.com/10.1002/adma.201505943>.

## Chapter 3

# Experiments and Results

The toolbox is now complete and it is possible to easily go through the process flow and its results. It starts with the design of the setup for CNFs production and its optimization. The electro-spun fibres are then analysed with optical microscopy for a first assessment of morphology and tuning of e-spin parameters. The process is characterized and the function which links the volume of polymer spun and the thickness of the mat is defined. Once the process is fixed, the fibres are stabilized at 260 °C. This phase is optimized by testing different dwelling temperatures and temperature ramps. FTIR is used to determine the degree of stabilization and to determine the best procedure. The stabilized fibres can then be carbonized at 800 °C. Fibres from each phase are analysed with SEM to monitor the fibre morphology changes during the process. Average contraction of circular disks of fibres is determined and its dependence on the mat thickness verified. The whole production is a self-standing process and it has been studied in [16].

In parallel with fibres production, researches on active material loading have been conducted. Different techniques are available and have been tested: dip coating, Buchner filtration. The main analysis tool at this stage, apart from weighing, is SEM, used to determine the in-plane and cross-section distribution of the active material. XRD have been used to confirm the crystal phase synthesized.

Once the CNFs with embedded NVP particles are characterized, they are used to mount sodium-ion half cells. Electrochemical testing is conducted with a Swagelok setup, with metallic sodium anode and reference electrode. The cells are mounted in glove-box, with argon atmosphere. The electrochemical testing is performed with Gamry potentiostat *Reference 600+*.

## 3.1 CNFs Production

### 3.1.1 E-spin setup and parameters control

In this section the final electro-spinning setup is reported but more than 5 setups have been designed before a satisfactory result was achieved.

#### Setup and Procedure

The electro-spinning setup used, is schematically presented in figure 3.1. A plastic box surrounds the needle tip and the metallic target. Inside the box a thermometer and humidity sensor are used to control the environmental conditions. A nitrogen flow lowers the humidity to a fixed value (between 40 and 60 % RH). The high voltage supply and the syringe pump are placed outside the box. An high resolution camera is used to monitor, in real time, the formation of the Taylor cone at the needle tip.

Before starting the electro-spinning, the precursor is prepared: it consists of a solution of

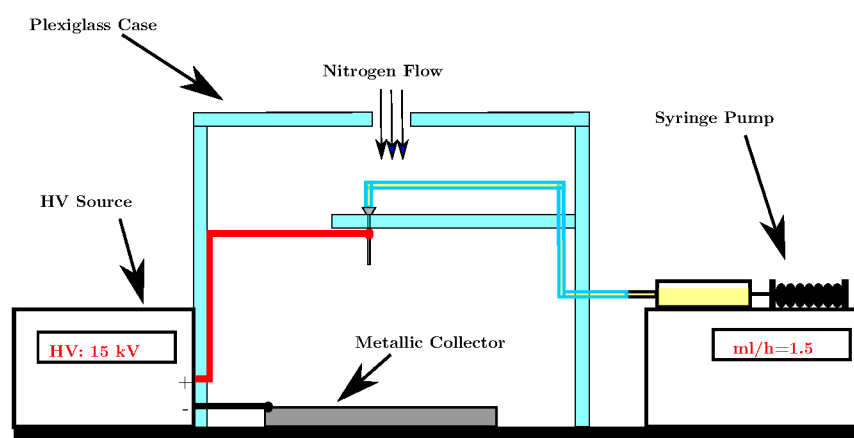


Figure 3.1: Electro-spinning setup.

polyacrylonitrile (PAN) in dimethylacetamide (DMAc). It takes about 12 h to reach a perfectly homogeneous solution, depending on the quantity of PAN dispersed. According to successfully applied formula, a solution of 7% in weight PAN in DMA is prepared[24, 9, 8, 6].

Once the solution is ready, a syringe is loaded with it and placed in a syringe pump for flux

### 3.1. CNFS PRODUCTION

control. The syringe is connected through a PVF pipe<sup>1</sup> to a metallic blunt-end needle. The needle points towards a flat metallic target and the high voltage source is connected between the two.

In order to start the spinning the following step are executed after the setup is mounted:

1. With a nitrogen flow the humidity of the box is reduced to 40% RH.
2. While the HV supply is turned off, the polymer solution is driven from the syringe to the needle and a small droplet is formed on the needle tip. This step is performed manually.
3. The HV source is turned on to a voltage of about 15 kV<sup>2</sup>.
4. The syringe pump is turned on with a pre-set constant flux (e.g. 1.50 ml h<sup>-1</sup>).
5. The formation of the Taylor cone is monitored through the camera.
6. Once the spinning begin, the voltage is adjusted to avoid accumulation or depletion of solution at the tip: the drop should remain constant for all duration of the spinning.
7. Long term drifts are corrected by monitoring the Taylor cone every 30 minutes.

After the spinning, optical microscope is used to confirm the formation of fibres and to verify the correctness of the spinning setups: wrong parameters result in electro-spray and beads formation. It is also possible to determine the average fibres diameter using an image processing tool: *Imagej* with the plug-in *DiameterJ*.

SEM is used to determine the thickness of the mat and the diameter of the fibres with high precision.

## Results

From SEM and optical imaging the result of the spinning can be monitored. In figure 3.2 an optical and a SEM image are reported.

To control the process it is necessary to determine the sample thickness as a function of the spun volume. In figure 3.3 the results of the SEM cross section measurements are reported.

### 3.1.2 Stabilization and FTIR

The second process step is the stabilization: the fibres structure is changed by mean of temperature. The resulting chain structure, shown in figure 3.4, guarantees a better stability during carbonization: stress linked to shrinkage is reduced and the final CNFs are more flexible.

---

<sup>1</sup>DMAC is a solvent for plastic and PVP is melt down in few minutes. Only Fluorine reinforced plastic can stand it.

<sup>2</sup>For each electro-spinning setup the optimal voltage has to be established.

### 3.1. CNFS PRODUCTION

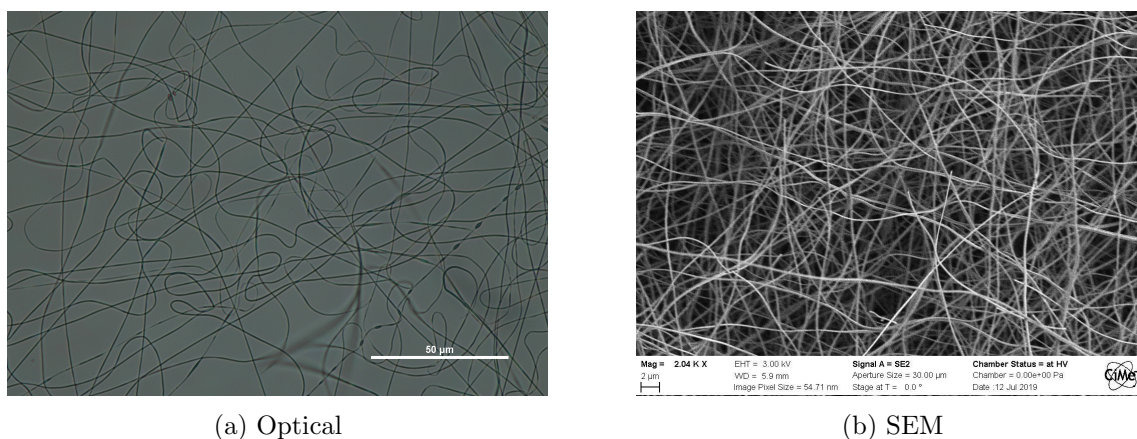
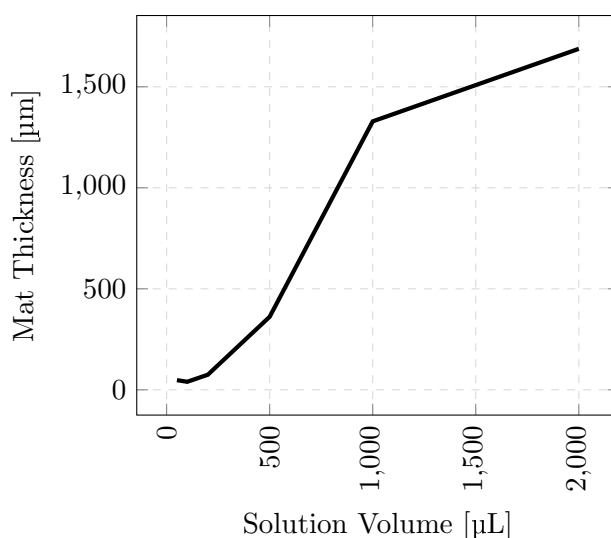


Figure 3.2: Optical and SEM imaging of the spun fibres.



— CNFs thickness as a function of the spun volume. Taken from [16].

Figure 3.3: SEM measurement of the thickness as a function of the spun volume.

#### Setup and Procedure

The fibres are placed in a ventilated oven and a temperature ramp is applied to bring the temperature first to 150 °C and after 1 hour to 260 °C. It takes 2 hours to complete the process and a final ramp down brings the fibres back to room temperature .

#### Results

An early visual inspection can be done to assess qualitatively the degree of stabilization: the white fibres turn gold when stabilized. Pink or pale brown means partially stabilization, while dark brown, overcooked fibres. The FTIR is used for a more quantitative analysis: as shown in figure 3.4 the triple nitrogen bond is eliminated, and its peak, at about 3000  $\text{cm}^{-1}$ , disappears from FTIR spectrum. In figure 3.5 the FTIR spectra after stabilization at different tempera-

### 3.1. CNFS PRODUCTION

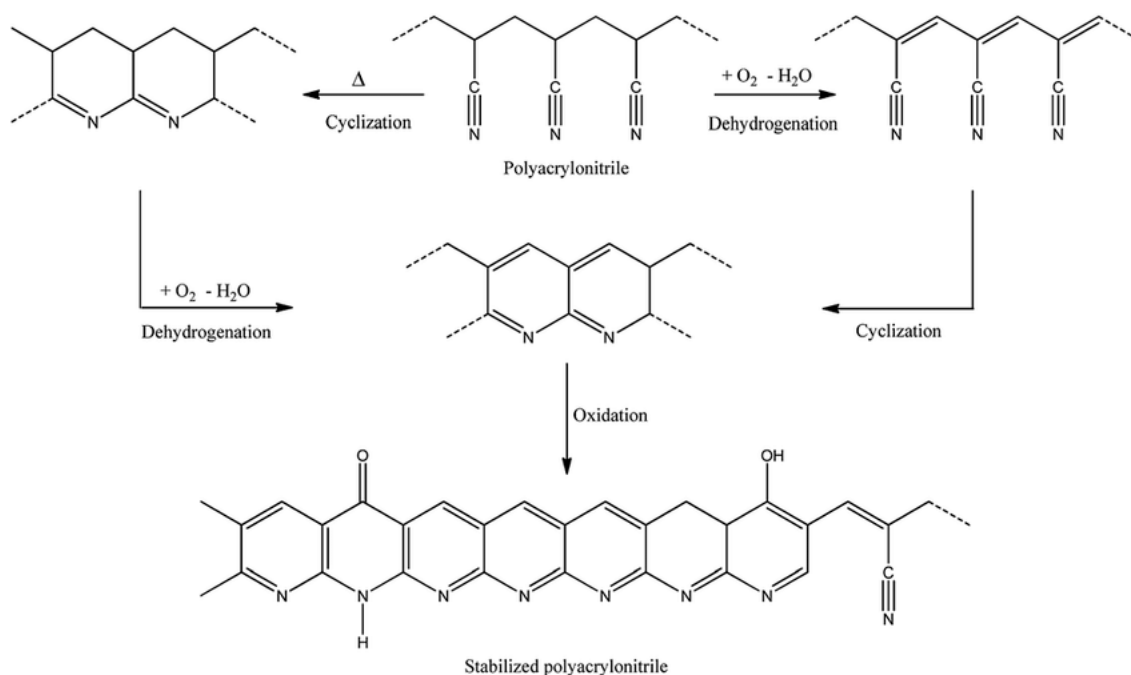


Figure 3.4: Chemical evolution of the PAN during stabilization. Taken from [11].

tures are reported. At 230 °C the triple nitrogen bond is not visible: it is the optimal process temperature. Higher temperature does not affect the structure while lower one results in an partial stabilization.

#### 3.1.3 Carbonization SEM and Optical

##### Setup and Procedure

The final carbonization process takes place as soon as the stabilization ends, to avoid moisture absorption. If it is not the case, the fibres should remain for at least 12 hours in a dry box before being carbonized.

A tubular furnace filled with argon is used; the samples are loaded into the furnace inside alumina crucibles and 30 minutes of purging is necessary to completely remove the oxygen before starting the annealing. A ramp of 5 °C min<sup>-1</sup> is set to reach the dwelling temperature of 800 °C. The carbonization takes about 2 hours to be completed<sup>3</sup> and a ramp down brings the furnace back to room temperature.

A visual inspection permits a first assessment: wrinkles or too much shrinkage are linked to a wrong stabilization process or to the presence of moisture. Following, the SEM imaging is used to determine the final properties of the mat before being used into an electrochemical cell: diameter, pores size, and mat thickness are the three main parameters. The final step is the electrical characterization of the fibres with a four probe measurement.

<sup>3</sup>A longer process results in brittle CNFs due to the total removal of nitrogen and oxygen.

### 3.2. NVP SYNTHESIS AND LOADING

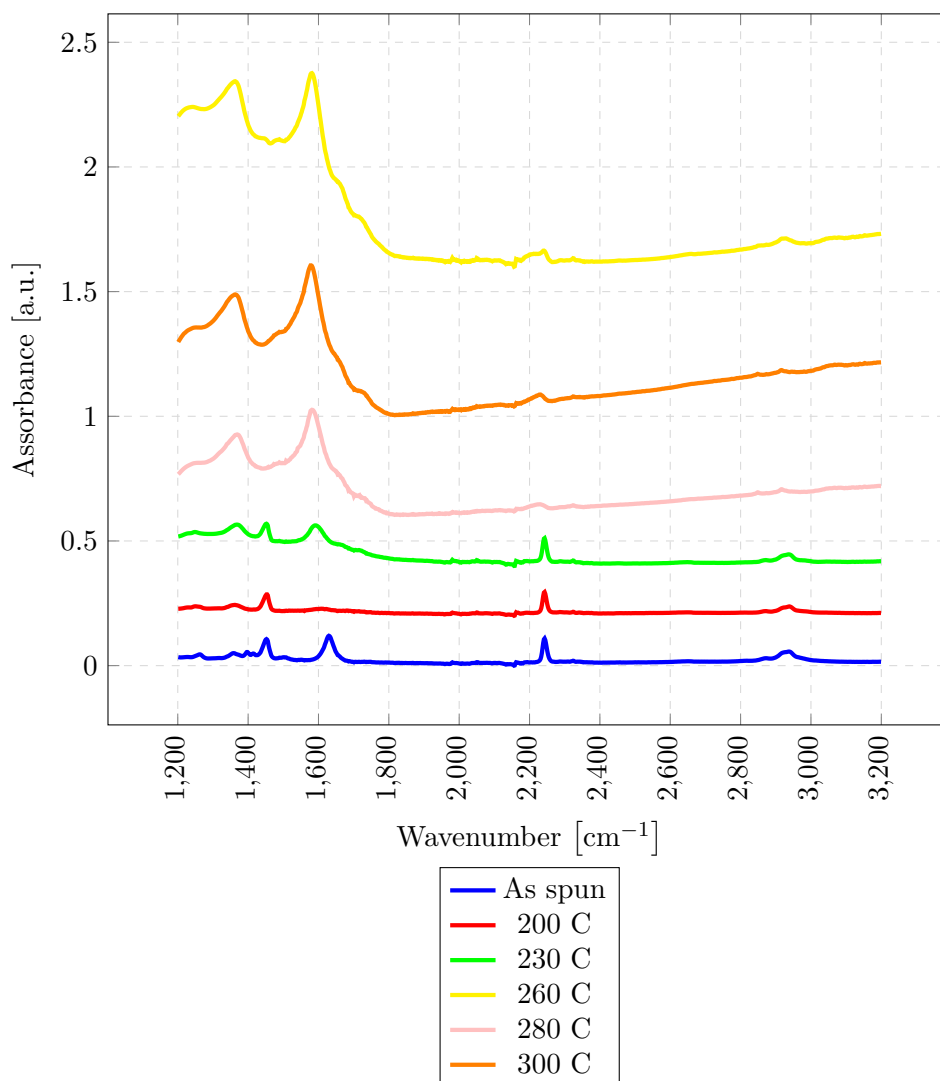


Figure 3.5: FTIR spectra for PAN stabilization at different temperature (2 hours stabilization).

### Results

In table 3.1 the resistance measured is reported for several fibres thicknesses. The mean value is around  $10^{-2} \text{S cm}^{-1}$ .

### 3.2 NVP Synthesis and Loading

The second workload starts from the final deliveries of the first one.

The produced CNFs are loaded with the active material and characterized with SEM to determine the loading profile and the crystals size. Two loading procedures have been explored in the present work: the dip-coating and the Buchner filtration. In both cases a co-precipitation technique is used for the synthesis in solution.

## 3.2. NVP SYNTHESIS AND LOADING

sample	S cm <sup>-1</sup>
1	0.014
2	0.011
3	0.013
4	0.014
5	0.015

Table 3.1: Resistance measurement on CNFs. Taken from [16].

### 3.2.1 NVP Synthesis

The synthesis of NVP is achieved through co-precipitation technique, already presented in the former chapter and adapted from [23]. The procedure adopted and the main characterization results are presented above.

#### Setup and Procedure

In order to synthesize the NVP the following precursors are used:

- 230 g deionized water.
- 8.63 g ammonium metavanadate (0.05 mol).
- 13.50 g oxalic acid (0.15 mol).
- 6.15 g sodium acetate (0.75 mol).
- 8.63 g ammonium dihydrogen phosphate (0.75 mol).

The following step have been performed to produce NVP crystals for XRD analysis:

- Ammonium metavanadate is dissolved in 200 ml of deionized water: a yellow solution is visible. The color is linked to the vanadium oxidation state 5+[20, 12].
- Oxalic acid is added to lower the pH and change the oxidation state of vanadium to 4+ [12, 4]. The solution is observed to turn blue as described by [21].
- After 12 hours of magnetic stirring at 50 °C the dissolution is completed.
- The sodium acetate and the ammonium phosphate are added after being separately dissolved into 30 ml of deionized water.
- After 6 hours of stirring at 80 °C, the liquid precursor is evaporated and a green paste is deposited. The green is associated to the oxidation state of vanadium 3+ in NVP.

### 3.2. NVP SYNTHESIS AND LOADING

- The paste is completely dried in oven at 120 °C for 2 hours and kept in a drier until further use.

At this stage the NVP paste contains nano-crystalline domains. In order to form bigger ones, an high temperature process is performed at 800 °C in Ar atmosphere. Two crystallization procedures have been tested: for 2 and 8 hours. Once extracted from the tubular furnace, the NVP is characterized with power diffraction XRD to confirm the crystal structure.

#### Results

In figure 4.3, reported in Appendix A, the solution of NVP precursor at different stages of preparation is reported.

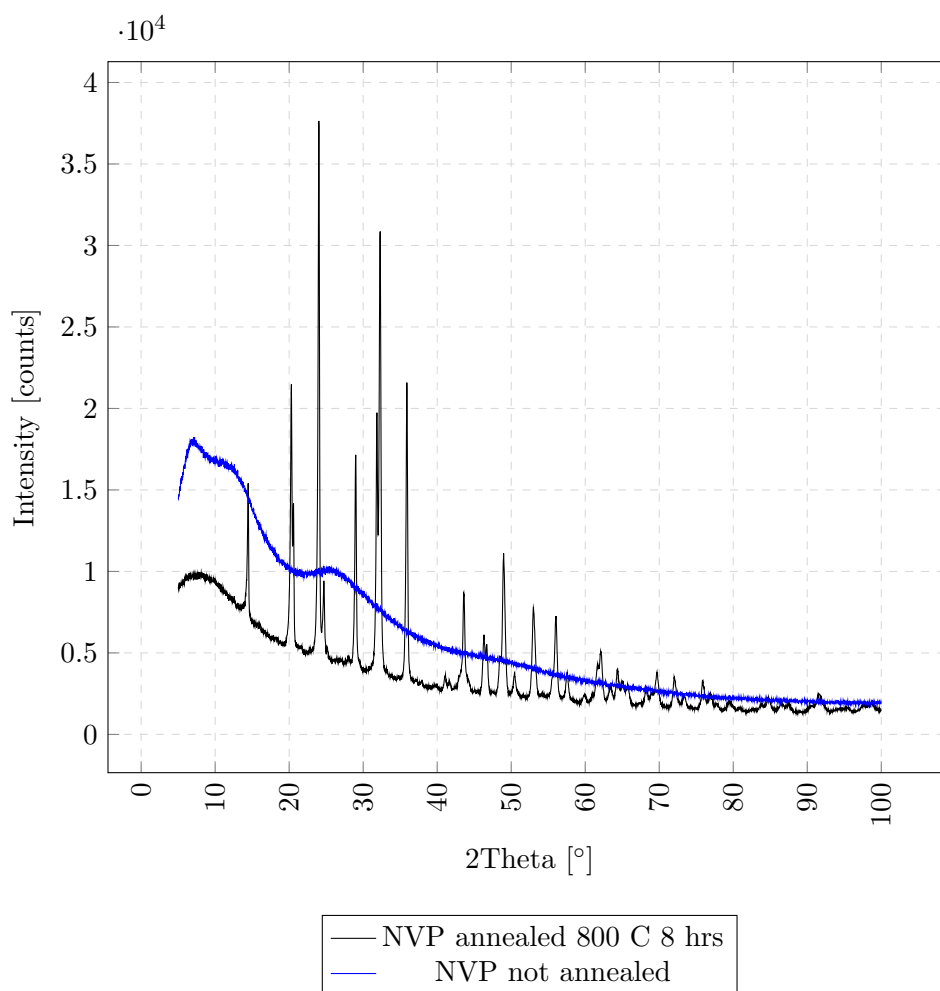


Figure 3.6: XRD data of NVP annealed for 8 hours at 800 C. Pre and post treatment XRD data show the formation of the crystalline phase.

The XRD spectrum of NVP, before and after 8 hours annealing, is proposed in figure 3.6. In Appendix A at figure 4.2 reports the superposition of XRD spectrum and the theoretical

## 3.2. NVP SYNTHESIS AND LOADING

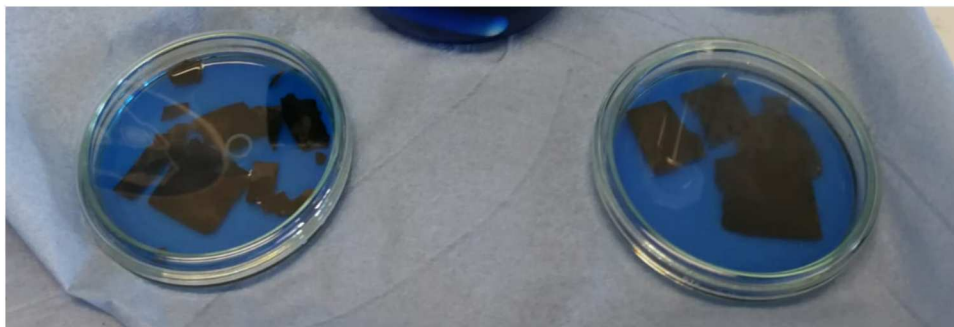


Figure 3.7: Dip-coating of carbonized fibres.

peaks of NVP.

The 2 hours process XRD data (reported at figure 4.1 in Appendix A) show no diffraction peaks, hence no crystalline structure has been synthesized.

### Considerations

The analysis confirms the synthesis of the right crystalline structure for the 8 hours process with a very good match. The shape of the peak suggests the formation of small crystal domains. According to Rietveld refinement theory the diameter of the crystals can be determined with the equation

$$D = \frac{k \cdot \lambda}{\beta \cdot \cos(t)}$$

Where  $\beta$  is the FWHM of the gaussian fit of the peaks<sup>4</sup>[2]. Broader the peaks, bigger the FWHM, and smaller the crystalline domains.

### 3.2.2 CNFs Loading (I): Dip-coating

Once the synthesis process of NVP is confirmed and the CNFs produced, it is possible to proceed with the loading of the active material.

The dip-coating technique has been tested first, because is the one used in the reference paper [23].

#### Setup and Procedure

This procedure uses the liquid precursor of NVP as described above. 4 ml of the solution are spilled into a Petri dish. After being cut in small pieces of about 3 cm<sup>2</sup>, the carbonized or stabilized fibres are dipped into the solution. In figure 3.7 the setup is shown.

The carbonized fibres are left overnight in the solution, while the stabilized one only few minutes. The latter are highly hydrophilic and the solution is almost completely drained in half

---

<sup>4</sup> $\lambda$  is the x-ray frequency and t the measurement angle.

### 3.2. NVP SYNTHESIS AND LOADING

an hour. After the soaking, the fibres are dried in the fume hood or in the oven at 120 °C for 2-3 hours.

#### Results

The first measurement is the weighing of the sample before and after dip-coating. In table 3.2 are reported the data for two different batches of carbonized fibres. In both cases the fibres are

<b>Before (mg)</b>	<b>After (mg)</b>		
1.9	6.8		
9.6	35.7	<b>Before (mg)</b>	<b>After (mg)</b>
3.9	4.5	9.8	12
8.4	15.9	7.7	12
3.6	4.7	7.6	11
18.3	227		
3.2	76.5		

Table 3.2: Weights of CNFs samples before and after dip-coating process. The second measurement is taken after 2 hours of drying under fume hood.

cut before the process.

In the first case the cutting has been performed on the already carbonized fibres. Because the fibres were fragile, the final shape varies a lot among fibres and hence the weight. In the second case the fibres have been punched with a stainless steel puncher after stabilization. This second approach permits a reproducible cut and weight, which reflects on the quality of the data.

The second important parameter is the distribution of the active material along the cross section of the mat. The SEM imaging has been exploited and the results are reported above. During the drying process the fibres are locked in two different orientations: lying on a Petri Dish or hang from one extreme in a vertical position. An unexpected phenomenon has been observed: depending on the drying orientation the active material segregates in a particular zone of the mat.

In figure 3.8 the cross section of the fibres dried in a horizontal position is reported. The active material concentrates on one side of the CNFs. In figure 3.9 two different zones of the vertically dried fibres are reported. It is a top view at the two edges: the one where the fibres were attached and the one far from the hanging point. In the top part (sub-figure a) few active material particles are visible while in the bottom part (sub-figure b) the fibres are completely surrounded by active material crystals.

### 3.2. NVP SYNTHESIS AND LOADING

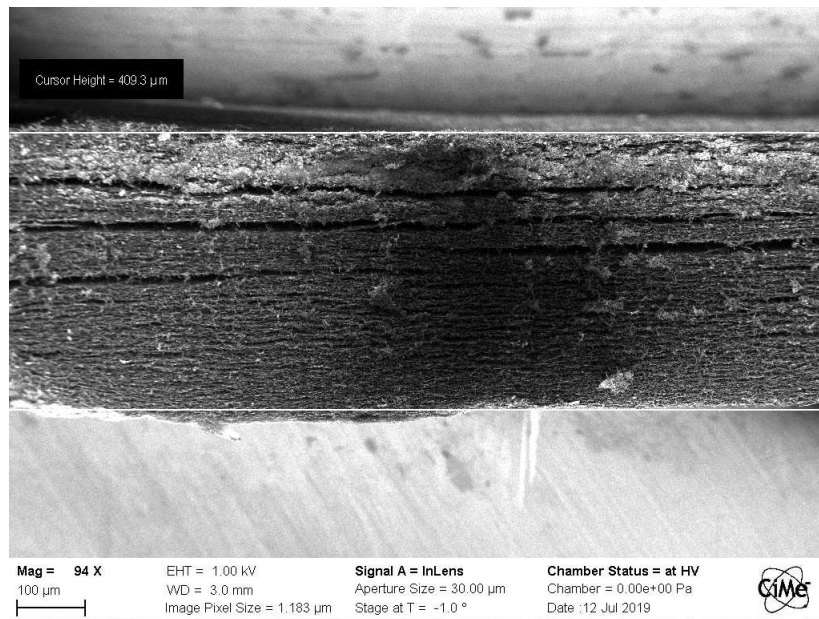
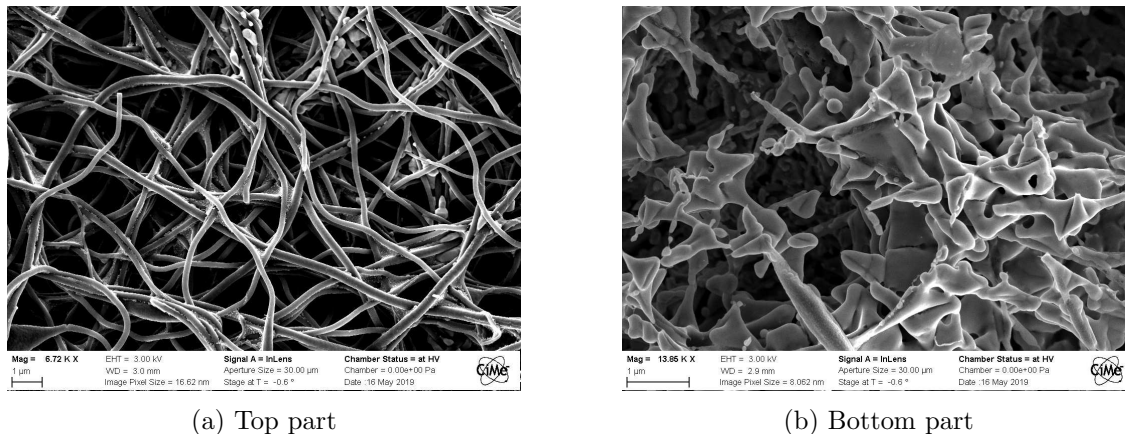


Figure 3.8: Caption



(a) Top part

(b) Bottom part

Figure 3.9: SEM image: top view of CNFs after dip-coating with vertical drying. Upper and bottom part of the fibres.

#### Considerations

For what concerns the amount of active material the dip-coating permits reproducible results but the profile of deposition depends on the drying position. The quantity of active material deposited depends on the soaking time and the solution concentration. This latter dependence fixes an upper limit to the maximum loading.

#### 3.2.3 CNFs Loading (II): Buchner Filtration

The second technique exploited has been introduced in the process flow after the SEM results of dip-coating. The main advantages of this technique are the possibility of increase the loading, and extra degree of freedom for what concerns the distribution.

## 3.2. NVP SYNTHESIS AND LOADING

Before (mg)	After (mg)
3.0	4.8
3.7	4.6
2.8	6.4
9.2	12.8

Table 3.3: Weight of CNFs samples before and after Buchner filtration process.

### Setup and Procedure

As for dip-coating the loading procedure is performed with the liquid precursor. The fibres are used as a filtering paper while vacuum is created in a filtration flask. With this setup, either entire pieces of CNFs or already cut ones can be used. In the former case the filtration is faster and more controllable.

The solution is dropped onto the fibres and is absorbed in less than 30 seconds. The solution from dark blue becomes light blue after filtration. Small crystals cannot be trapped into the fibres and remain in solution.

After some more minutes the vacuum is removed and the fibres are dried in oven. After drying the fibres can be cut with a puncher and carbonized in the furnace.

The process flow, which uses the stabilized fibres as filter, results in a carbonization process which is also used for crystallize the NVP.

### Results

The first analysis is the weighting of the fibres, as for dip-coating. In table 3.3 the weights of fibres before and after filtration is reported. Those data have been produced only for the cut fibres. The SEM cross section analysis is shown in figure 3.10.

### Considerations

The first consideration to be drawn is the possibility of controlling the loading on the cut CNFs. As reported in the data, the process is hard to reproduce on small samples. On the other hand it is not possible to know the local amount of active material if the loading is performed on a sheet of CNFs. Notwithstanding, the process is particularly suited for the loading of big sheet of CNFs and hence it should be preferred in the final process flow. It is also much faster than dip-coating and the amount of material can be increased with multiples filtrations.

For what concerns the distribution, as shown in figure 3.10, the loading is maximum at the interface and only small crystals are deposited in the central part of the mat. It demonstrates the high efficiency of the fibres as filter; it is possible to increase the penetration if smaller

### 3.3. ELECTROCHEMICAL CELL ASSEMBLY AND TESTING

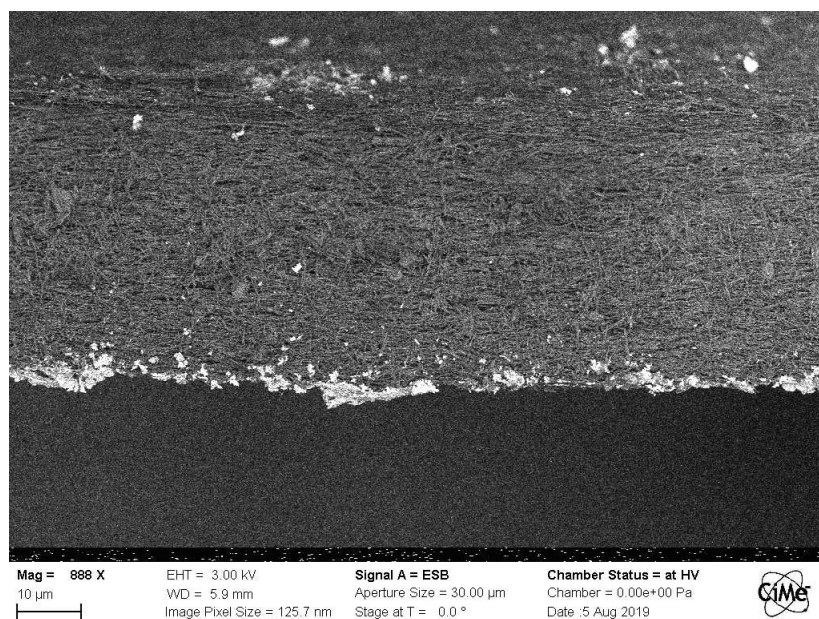


Figure 3.10: SEM cross section of the CNFs loaded with Buchner filtration.

crystals are synthesized and with water flux, to drag the particles.

## 3.3 Electrochemical Cell Assembly and Testing

After the characterization of the NVP, the CNFs are used as cathode for electrochemical cells. As anode a metallic sodium disc is used and fiber glass as separator. The electrolyte is sodium perchlorate ( $NaClO_4$ ) in 50:50 weight mixture of ethylene carbonate and poly(ethylene carbonate); the recipe is taken from literature[3].

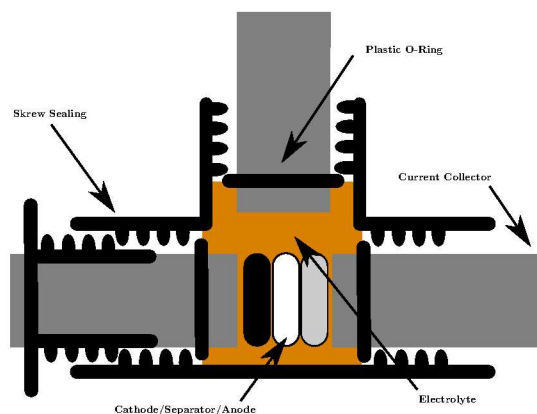
### 3.3.1 Setups

For the testing, two setups have been realized. The first one is a classical three electrodes Swagelok, actually used for the test phase; the second one is a brand new setup, which has been tested but sealing problem makes it necessary some design improvements.

#### Swagelok Setup

In figure 3.11 the schematic and the photo of the Swagelok setup are reported. As described in the previous chapter, the setup is composed by three metallic current collectors, one for each electrode. The plastic case seals the electrolyte, which is sensitive to light. Plastic rings are used to seal the three holes to prevent electrolyte evaporation and to preserve the inert atmosphere

### 3.3. ELECTROCHEMICAL CELL ASSEMBLY AND TESTING



(a) Schematic view



(b) Photo of the used setup.

Figure 3.11: The Swagelok setup

inside the cell: oxygen degrades the sodium and a drift in the potential results.

The available surface at the three electrodes is about  $3 \text{ cm}^2$ .

#### Multi-Electrodes Setup

The testing of multiple cells requires an expensive setup: a multichannel potentiostat altogether with multiple test cells. Notwithstanding, GC and EIS can be implemented with cheap integrated circuits on a PCB. The design of a cell setup, based on ICs components, to tests multiple cells at the same time is proposed below.

In figure 3.12 the schematic the multi-electrodes setup is reported. It consists of two PCBs, where the electrodes have been designed. In figure 3.13 one of the two specular PCBs is shown. The central part, where the space for the electrode is carved out, is made of opaque plexiglass. The same stack of the coin cell is inserted in the holes: the spring guarantees a constant pressure on the electrodes. Two plastic rings are placed in between the PCBs and the plexiglass to obtain a good sealing. The signal of each couple of electrodes is collected on a single flat wire connector, to be linked with another PCB or a measuring device.

During early testing, the stack has proven to be conductive and two cells have been assembled.

### 3.3. ELECTROCHEMICAL CELL ASSEMBLY AND TESTING

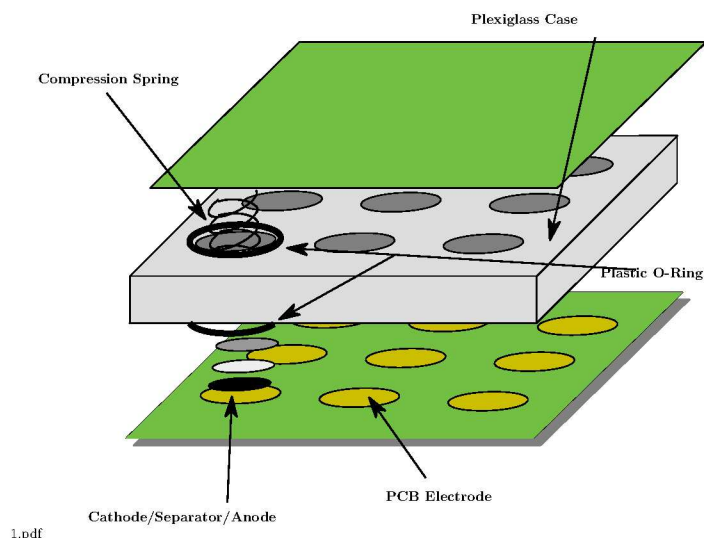


Figure 3.12: Multi-electrodes setup.

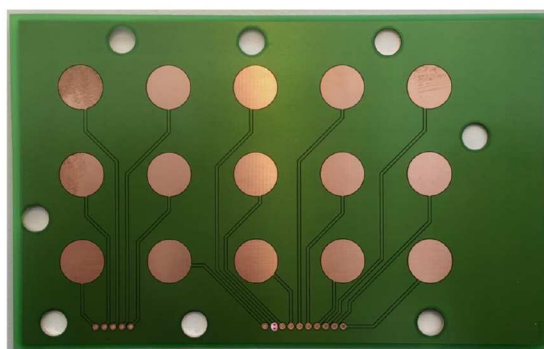


Figure 3.13: Multi electrode PCB.

At the beginning the right voltage is measured at the end of the two electrodes, but over time it fades. Opening the device, after 2 days, no more electrolyte is found.

The prototype has shown the possibility of realizing such a device but some extra work is needed to guarantee the sealing.

In the next sections the characterization results of different batches of electrodes are reported. Each one starts with the characteristics of the used fibres and the loading procedure report. After that, the results of CV, EIS and GC are commented and linked to the CNFs morphology.

#### 3.3.2 Batch 1

The following section refers to the first batch of electrodes. First, the informations about the cathodes are presented. Then the three electrochemical tests and their results. The final section is dedicated to the discussion about the overall device.

### 3.3. ELECTROCHEMICAL CELL ASSEMBLY AND TESTING

#### Fibres Characteristics

For the first batch (NVP1) the CNFs are synthesized with the following steps:

- Spinning of 7% wg PAN in DMAc.
- Stabilization at 260 °C without intermediate plateau.
- Carbonization for 2 hours at 900 °C.

In figure 3.14 the cross section of CNFs is shown.

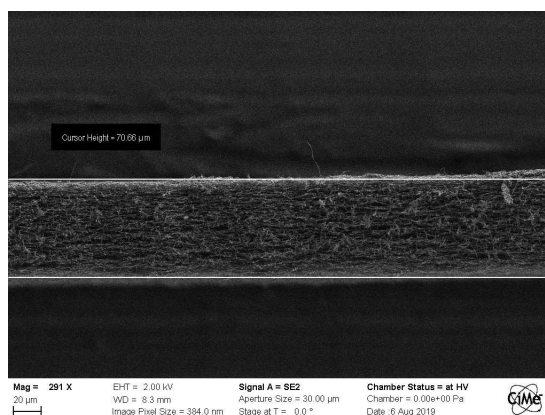


Figure 3.14: Thickness measurement of the CNFs electrode.

#### NVP loading

The active material loading is performed with dip-coating technique on the carbonized fibres. The mat is left for 12 hours in a Petri dish with the liquid precursor. As already shown, in the section related to dip-coating, the active material concentrates in the first 100 μm of CNFs. Because the used mat was thinner (70 μm), the active material is assumed to be almost uniformly distributed. The total active material weight of the tested cell was around 2 mg. It corresponds to 220 μA h<sup>-1</sup> of theoretical capacity.

#### CV Results

As first test, 3 cycles of CV are performed on the cell, to confirm the electro-activity of the synthesized material. The sweep rate is 0.10 mV s<sup>-1</sup> in the range from 1.60 V to 4 V. In figure 3.15 the result is reported: four peaks are visible, two around 3.40 V and two around 1.60 V. Both reaction sites are confirmed. The exact position of the two peaks, linked to the site  $Na_2$ , is 3.46 V, during oxidation, and 3.30 V during reduction. The distance between the two peaks with respect to the standard potential is: 55 mV and 100 mV. The oxidation peak is almost perfectly in line with the theoretical model, which predicts a shift of 59 mV. With respect to

### 3.3. ELECTROCHEMICAL CELL ASSEMBLY AND TESTING

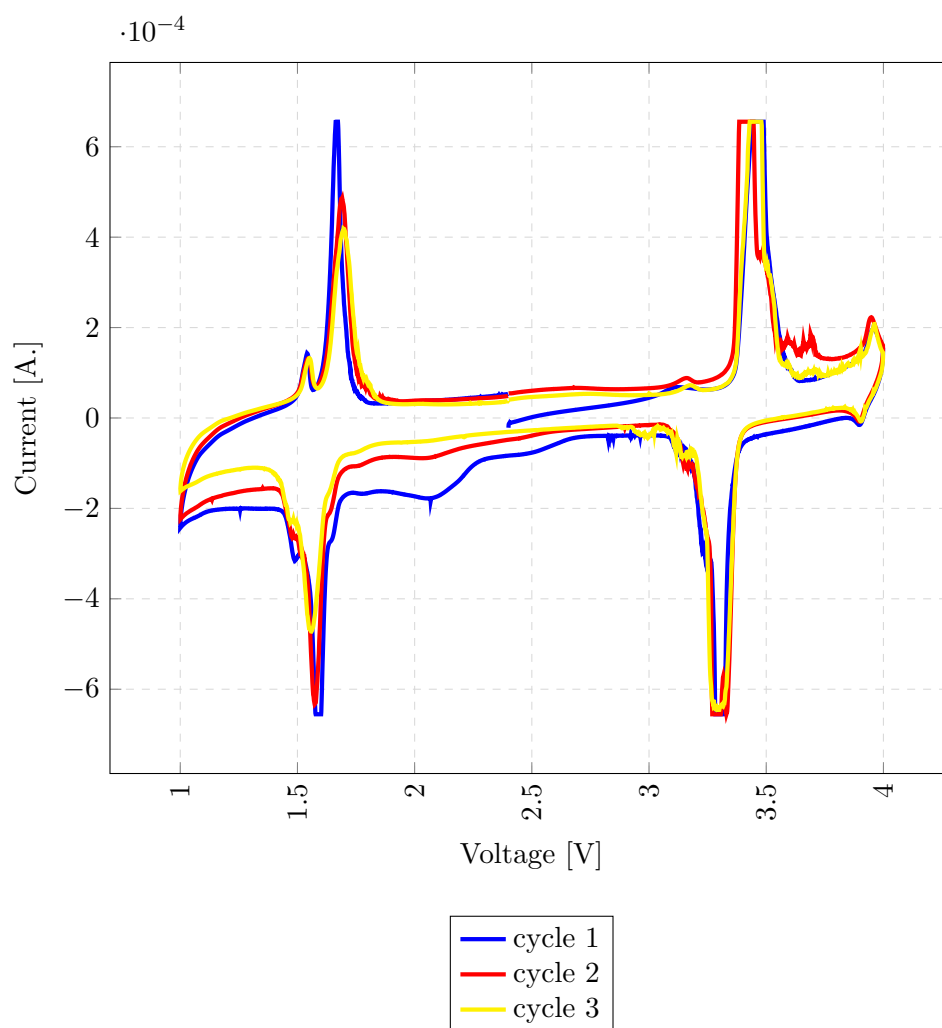


Figure 3.15: Cyclic voltammetry of the first batch.

the shape, the CV is limited by the total amount of active material. By integrating the area under the first peak, with a python script, it results in a total capacity of  $265 \mu\text{A h}^{-1}$ . In figure 3.16 the fitting is reported.

#### EIS Results

EIS has been performed multiple times at different SOC. It has proven constant with respect to SOC and also with respect with time: after 2 weeks, the shape is pretty close to the starting one. In figure 3.17, on the Nyquist plane, three different spectra are reported: before cycling, at SOC 100 after 10 cycles, and SOC 0 after 100 cycles. The main difference between the first and the last, it is the slope of the constant phase element. Curves at different SOC are characterized by the same resistance but different capacitance.

The difference in the constant slope element means the diffusion process in the cycled battery is different. The formation of SEI and the degradation of the electrolyte can be linked to a

### 3.3. ELECTROCHEMICAL CELL ASSEMBLY AND TESTING

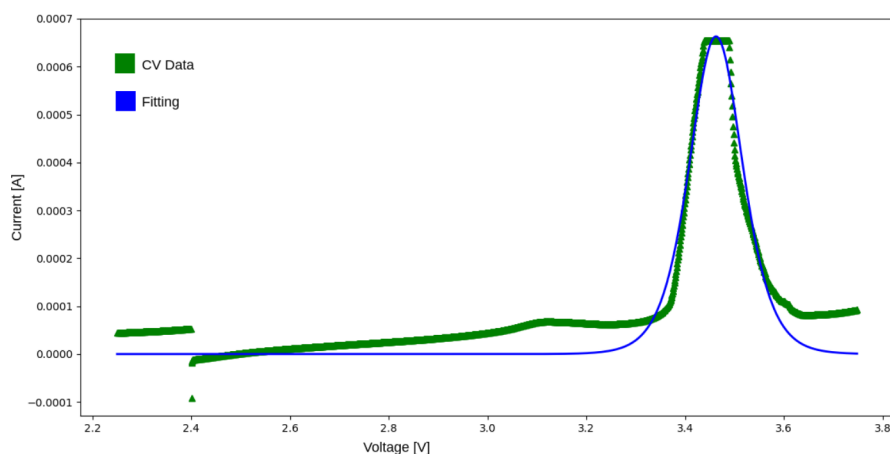


Figure 3.16: Fitting of the CV curve.

decrease in the diffusion coefficient, which is inversely proportional to the slope on the Nyquist plot. This explanation is consistent with the higher slope after 100 cycles<sup>5</sup>.

The last point to be analysed is the decrease in the reactive part when the cell is totally charged. Because it is possible to distinguish two different depressed circles, the model suggested in [7, 1, 17] can be adopted. It is then reasonable to imagine the smaller feature to be present also in the other cases but masked. Following the reasoning of [17] the two elements are linked to the SEI and the EDL. The one at higher frequency, which is also the dominant one, is related to the electrical double layer. The other is due to the solid ion diffusion through the SEI, to reach the electrolyte. It is still to clarify if the reaction starts from the outer or inner part of the electrode. Because the CNFs are quite resistive ( $10^{-2} \text{ S cm}^{-1}$ ) compared with typical value for diffusion ( $10^4 \text{ S cm}^{-1}$ ), it can be assumed the reaction starts near the electrode.

For a cathode, the ions are present when the cell is fully discharge. While at almost SOC 100 only the ions further from the electrode are available. The scenario can be summarized as: at SOC 0 the reaction takes place near the electrode and a SEI as thick as the electrode itself has to be crossed; at SOC 100 the reaction takes place near the bulk electrolyte and hence it takes less time to the ions to reach the electrolyte. Post-mortem SEM confirms the presence of a thick layer of SEI around the fibres.

#### GC Results

The galvanostatic cycling is of paramount importance to characterize the performances of the cell. On the other hand it is more difficult to isolate the single components and hence, if some-

<sup>5</sup>It is also the same slope than after 10 cycles, which is again consistent with SEI formation in the first 3-4 cycles.

### 3.3. ELECTROCHEMICAL CELL ASSEMBLY AND TESTING

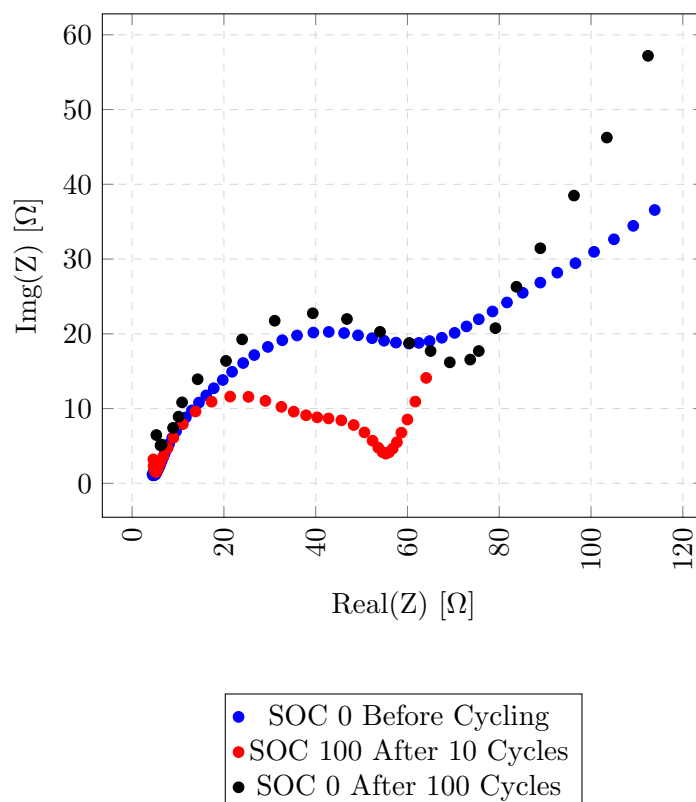


Figure 3.17: EIS spectrum of batch 1.

thing is not working properly, it is difficult to "debug" the device.

The cell has been cycled more than 150 times. It is particularly worthy to report the values of the capacity of the first and last cycles at a C-rate of 1.5C. In figure 3.18 the results are shown: the first charge capacity is equal to the one measured by the fitting of the CV ( $250 \mu\text{A h}^{-1}$ ) but it decreases to 200 as soon as the second cycle. After 70 cycles the capacity is stable around  $200 \mu\text{A h}^{-1}$ , with an energy efficiency of 95%.

An important result to be shown is the shape of the discharge curve at different C-rates. In figure 3.19 the discharge profiles, from 0.1 to 10 C, is reported. Before each discharge, the cell has been charged at 0.1 C. In order to highlight the differences, the voltage axis is restricted from 3.50 V to 3.20 V. All curves reach 80 % of theoretical capacity if a voltage as low as 2.70 V is allowed.

It is possible to identify three contributions of potential drop: IR drop, activation polarization, and concentration polarization[18]. The IR drop is measurable in the early part of the curve (about 1 and 5%). It is then the activation polarization which determines the slope of the curve: increase in path resistance due to consumption of active material. In the final part,

### 3.3. ELECTROCHEMICAL CELL ASSEMBLY AND TESTING

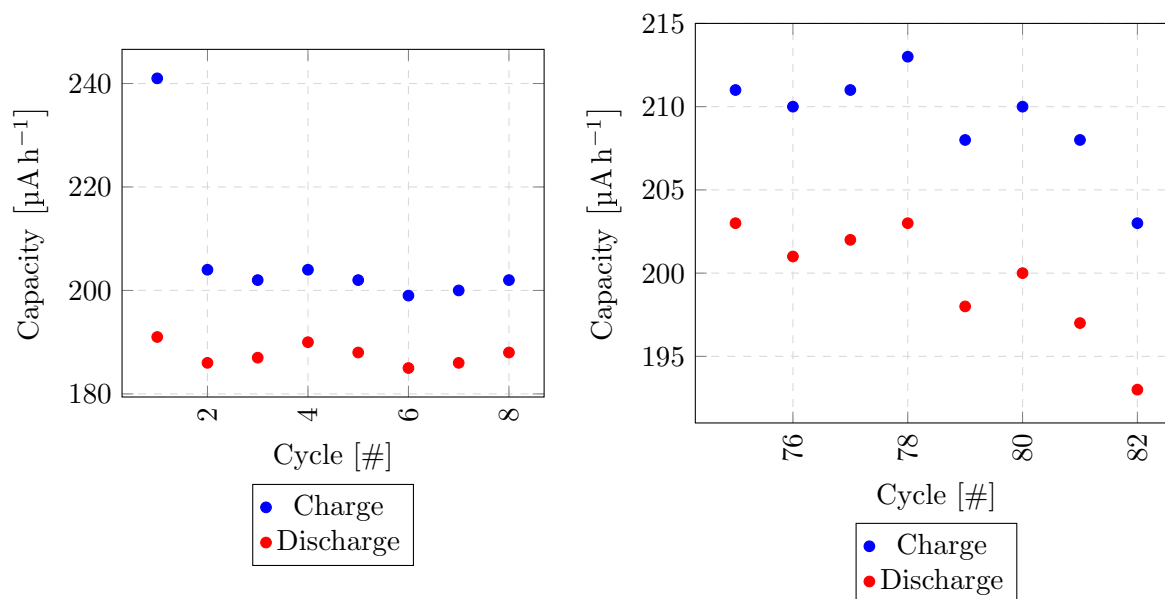


Figure 3.18: Galvanostatic cycling of batch 1.

C-rate	Drop at 5% [V]	Drop at 25[V]%	Drop at 40% [V]
0.5	0.028	0.035	0.040
1.0	0.040	0.051	0.058
2.0	0.05	0.059	0.073
5.0	0.075	0.096	0.127
10	0.115	0.156	0.195

Table 3.4: Voltage Drop Contributions.

the depletion of ions near the electrodes leads to a second drop in the voltage (at about 30 % of discharge). They can all be expressed as resistances. It is possible to fit the three parts with three lines but also taking a single point is meaningful to compare different curve. In table 3.4 the values are reported. The IR drop is also plotted (figure 3.20) to better visualized its linear behaviour.

#### Post Mortem SEM

As final analysis the cathode is extracted from the cell and a SEM analysis performed. In figure 3.21. The occlusion of the pores of the CNFs can be attributed to the formation of SEI, which leads, as anticipated, to and higher capacitance when the cell is fully discharged. Notwithstanding, lots of pores are still open, which justifies the stability in performances and the good cycling at high C-rate.

### 3.3. ELECTROCHEMICAL CELL ASSEMBLY AND TESTING

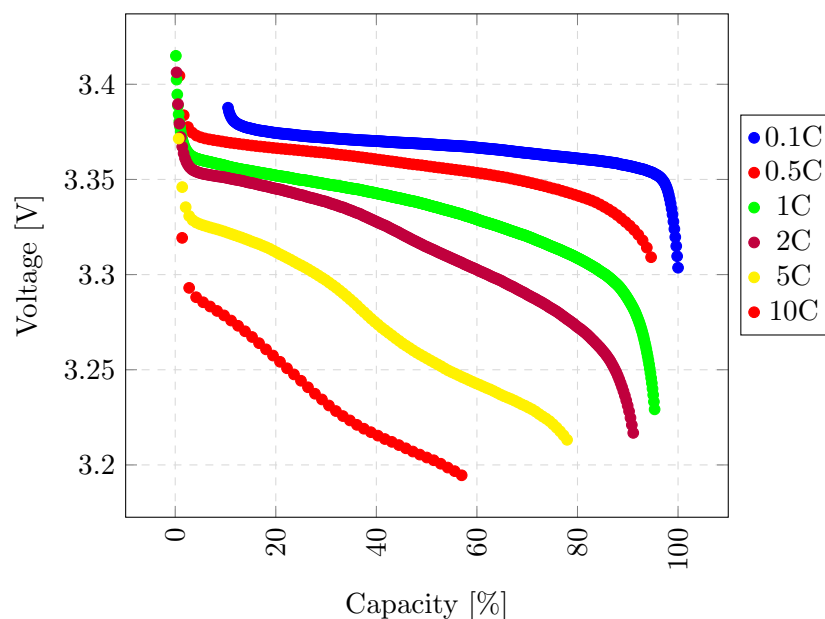


Figure 3.19: Discharge curve at different C-rate (batch 1).

## Conclusions

It is possible to affirm that the porous structure was intact during the whole cycling. Good cycling performance and stability confirm the working principles of the porous electrode. The NVP is completely exploited also at high C-rate with a voltage drop of 0.80 V. The activation polarization accounts for 0.10 V at 2 mA (10C), which corresponds to 50  $\Omega$  as measured with EIS.

The mat is as thick as a normal slurry electrode and no anomalous capacitive effects are observed. The shape of the discharge curve shows constant slope in the zone linked with active material activation energy; it can be related to an homogeneous distribution of the active material.

### 3.3.3 Batch 2

For the second batch a thicker electrode is tested. The overall process is the same as for batch 1 for both CNFs production and loading. Because the active material activity was confirmed by the first batch, the electrochemical analysis was limited to galvanostatic cycling.

### CNFs and Loading

In figure 3.22 the measured thickness for the batch 2 is about 500  $\mu\text{m}$ . The loading of active material is performed with dip-coating and the result is a segregation of the active material on one side of the mat, as already shown in figure 3.8.

### 3.3. ELECTROCHEMICAL CELL ASSEMBLY AND TESTING

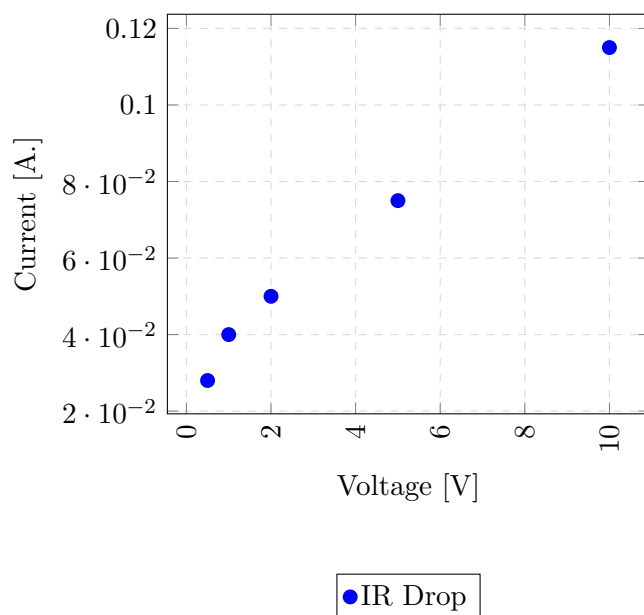


Figure 3.20: IR Drop measured at 5% of discharge.

#### GC Results

The only measurement performed on this batch is the galvanostatic cycling. The reason of this choice is the result of the GC itself. As shown in figure 3.23 the charge process takes three times the charge one (efficiency less than 30%). The explanation has been found in the thickness of the mat and the poor loading: more than two-thirds of the CNFs are not coated, but the huge surface area results in a big capacitance.

#### Conclusions

The second batch results are not satisfactory neither from the point of view of loading, due to evaporation issue of dip-coating, nor the cycling performances. The process has been changed to achieve better results.

#### 3.3.4 Batch 3

The third batch has been realized to solve the issues linked with loading. Buchner filtration is introduced in the process flow instead of dip-coating. Because the major concern was the analysis of the distribution of active material, the carbonization process has also been changed: 2 hours of dwelling at 800 °C instead of 8 hours to preserve the good mechanical properties of CNFs.

### 3.3. ELECTROCHEMICAL CELL ASSEMBLY AND TESTING

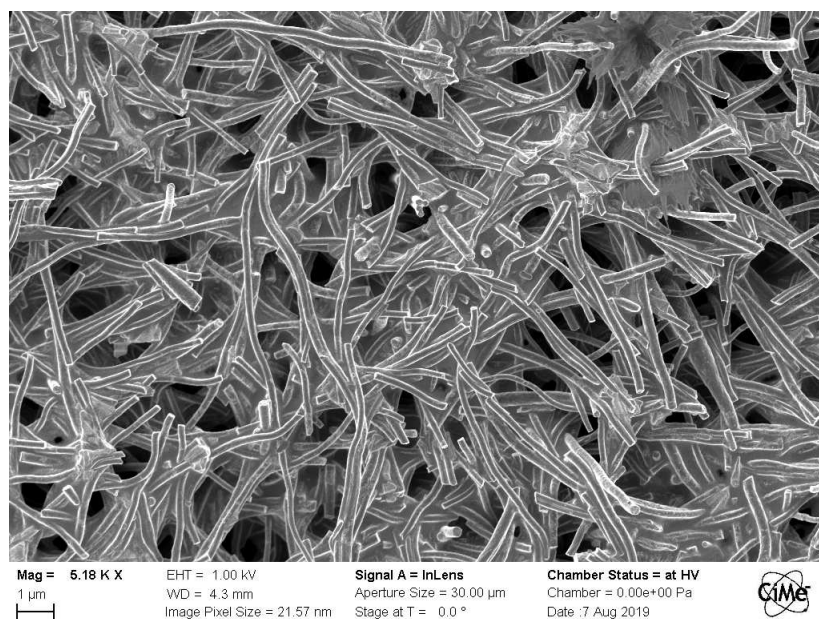


Figure 3.21: Post Mortem SEM of the CNFs. The SEI formation can be appreciate as occlusion of the pores.

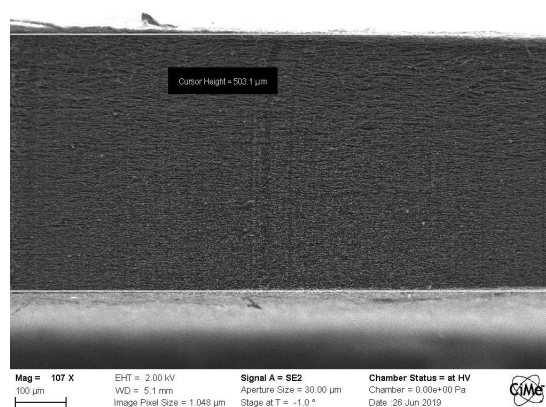


Figure 3.22: Thickness measurement of the CNFs electrode.

#### CNFs and Loading

The thickness of the mat is reduced to 50 μm as shown in figure 3.24. In the same image, produced by secondary electron with a filtering grid at 600 V, the particles of NVP are clearly visible. The active material profile has a peak at the surface, but NVP particles are present also in the bulk. The result suggests the possibility to better control the loading with respect to dip-coating: in the former case it is the filtration process which determines the profile, while in the latter is the evaporation, which is difficult to control<sup>6</sup>.

The filtration is performed on stabilized fibres, followed, after 12 hours of drying, by a carbonization step at 800 °C.

The process adopted is the one optimized for the fibres and not for the crystallization of the

<sup>6</sup>It depends on both the solution and the fibres, which implies a modification of the whole process to be modified. In Buchner filtration it may be enough to modify the loading process itself to modify the distribution.

### 3.3. ELECTROCHEMICAL CELL ASSEMBLY AND TESTING

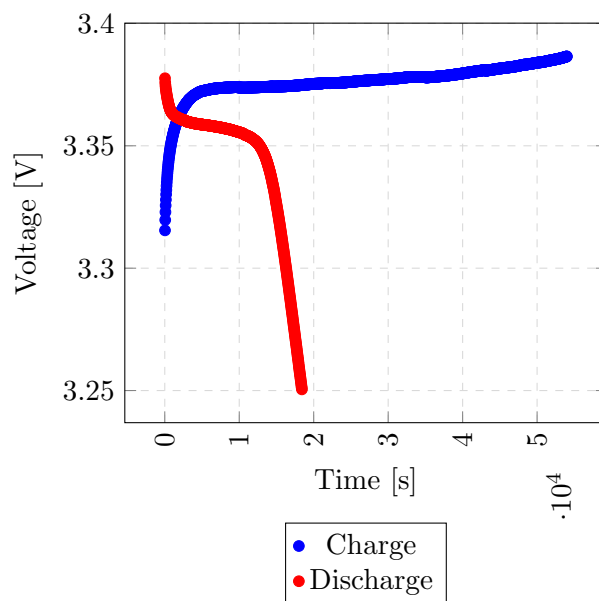


Figure 3.23: Discharge curve of the second batch.

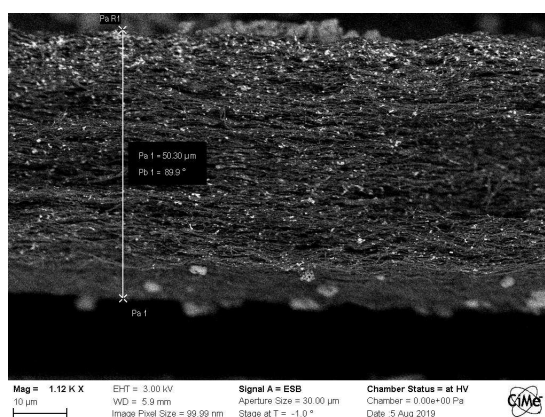


Figure 3.24: Thickness measurement of the CNFs electrode.

NVP. In particular, on the surface of the mat, big particles of NVP formed, which of course require long time to crystallize. Notwithstanding this process guarantees highly flexible fibres. After the annealing process the XRD analysis is performed on power of NVP and CNFs. No peaks linked with NVP crystal structure have been measured.

#### CV Results

While the XRD does not confirm the synthesis of active material, the mounted cell shows an open circuit voltage of 2.70 V. It suggests a partial crystallization but the CV curve shows no peaks around 3.40 V.

### 3.4. FUTURE EXPERIMENTAL PERSPECTIVE

#### EIS Results

The EIS analysis performed and reported in figure 3.25 is similar to the one of batch 1 but the process of electron transfer is weaker. Only the diffusive part at high frequency is clearly visible.

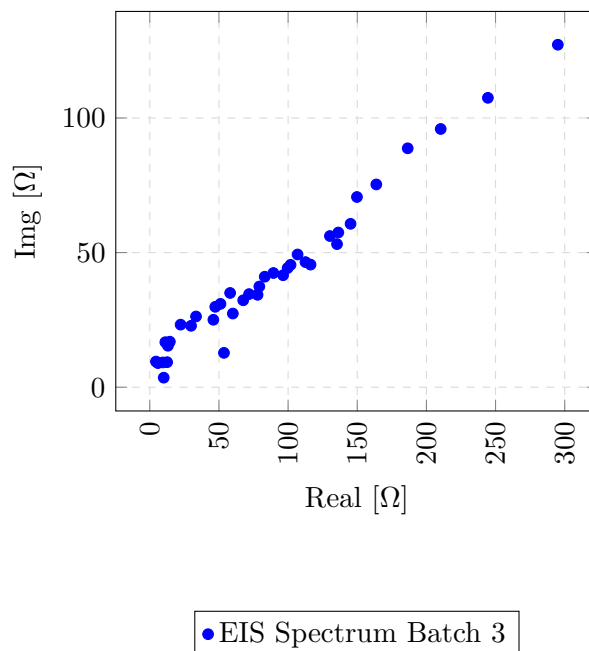


Figure 3.25: EIS spectrum of batch 3.

#### GC Results

As final step the galvanostatic cycling around 3.40 V shows a  $6 \mu\text{A h}^{-1}$  capacity. The retention is measured to be around 2 days. In figure 3.26 100 cycles are reported.

#### Conclusions

The third and final batch is promising for what concerns the loading of the active material. The poor electrochemical performances have been attributed to the short annealing process.

### 3.4 Future Experimental Perspective

As a conclusion to this chapter some interesting paths to be investigated are proposed, starting from the results of the present work.

### 3.4. FUTURE EXPERIMENTAL PERSPECTIVE

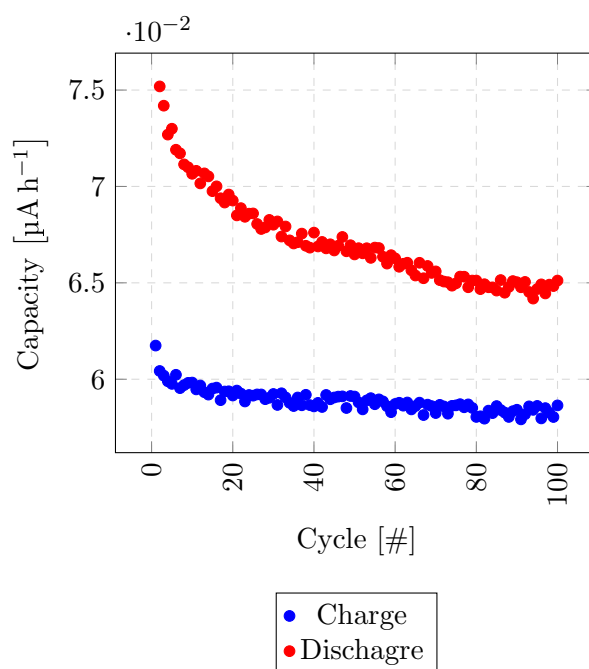


Figure 3.26: Galvanostatic cycling of batch 3.

#### 3.4.1 Study on CNFs

First of all, the optimization of the CNFs process is still to be complete. The stabilization phase has to be design taking into account a trade-off between conductivity and flexibility. [19, 14] is a good reference in term of achievable results. In order to increase the conductivity it is also possible to "dope" the CNFs with metallic atoms or carbon nanotubes[13].

#### 3.4.2 Study on Loading

A second possibility, it is the research about the loading procedure. So far the Buchner filtration is quite promising but further experiments are required to demonstrated fully controllability of the process. Up to my knowledge no works have been presented which have studied this process for sodium-ion batteries.

#### 3.4.3 Study on Cathode

As soon as the study on the process in completed, it is of paramount importance to test the structure with different materials, in order to investigated the potentialities of CNFs. It is fundamental to reach a loading comparable with the commercial ones (around 2 mA cm<sup>-2</sup>).

The manganese oxide, for example, is a promising material but the performances are reduced to one half at 25C and the actual areal capacity is rarely reported<sup>7</sup>[10, 5].

<sup>7</sup>It is highly probable that it is lower than the commercial ones, hence to increase it the power performance should estimate to lower.

## 3.5. SUMMARY

### 3.4.4 Study on Anode

In parallel with the above mentioned researches, the implementation of a full cell is necessary to get rid of the metallic sodium electrode and clearly estimate the performances. Among different possibilities, the choice of tin and tin oxide is the perfect one to test the CNFs: Tin is an highly energetic sodium anode but, due to the huge stress induced during intercalation, its cycling performances as poor. If the CNFs are actually able to accommodate the expansion of the active material, Tin anode performances should increase as reported by [22, 15].

## 3.5 Summary

The process flow starts with the production of CNFs. The electro-spinning setup used has been optimized during the all span of the work in order to obtain a reproducible and controllable process. The Relative Humidity (RH) variation has been the major problem: to obtain reproducible fibres a flux of nitrogen and a sealed box for the set up have been adopted.

After spinning, the fibres are treated with a first thermal process at about 260 °C. This is the stabilization process and it guarantees a better stability of the fibres during the carbonization process. Using FTIR characterization the process is optimized to the lowest possible temperature for the shorter possible time.

After stabilization the fibres may be directly carbonized or first loaded with the active material precursor. If the material can stand the carbonization temperature ( $\geq 800$  °C) a single high temperature process can be used to both carbonize the fibre and recover the crystalline structure of the active material, shortening the overall process time. The loading before carbonization is also more effective because the fibre is strongly hydrophilic at that stage. With the material of choice (NVP) the after-stabilization loading and after-carbonization one have both been tested. The latter requires less then half an hour while the former about 12 hours to achieve a good loading and drying.

The loading and synthesis of the NVP is done at the same time with a co-precipitation wet-chemistry process. Two paths have been explored: dip-coating and solvent evaporation; Buchner filtration with vacuum pump. The latter is both faster and more controllable.

After carbonization and crystallization of the NVP (800 °C for 8 hours), the samples are characterized and then the electrochemical cell is assembled. Two setups for electrochemical characterization have been realized: the first one consists of a Swagelok type cell, which is the main stream setup in literature but is quite bulky and permits to mount only one cell per time; A sandwich of two arrays of electrodes with a sealed chamber in the middle has also been

### 3.5. SUMMARY

prototyped. This second setup permits multiple cells to be tested in parallel (or series). The possibility to integrate the measurement system on the very same device leads to a compact, light weight and cheap setup.

The main results from characterization are summed up below:

- The stabilization process needs slow ramp and dwelling at intermediate temperature to achieve good mechanical properties of the fibres.
- Dip-coating loading is a limiting technique due to evaporation effects.
- The cell shows, in agreement with literature, good C-rate performances up to 20C.
- SEI formation is monitored and its effect on the cell resistance assessed.
- Too thick CNFs and poor loading result in a very low efficiency.
- Buchner filtration early results are promising for a more controllable loading.

Starting from those results, different paths must be followed to complete the realization of a full prototyping line: anode production; cell setup optimization; study of the electrolyte.

## References

- [1] D Andre et al. “Characterization of high-power lithium-ion batteries by electrochemical impedance spectroscopy. I. Experimental investigation”. In: *Journal of Power Sources* 196 (June 2011), pp. 5334–5341. DOI: 10.1016/j.jpowsour.2010.12.102.
- [2] Davor Balzar and Nicolae C Popa. “Analyzing microstructure by rietveld refinement”. In: 22.1 (2005), pp. 16–25.
- [3] Clement Bommier and Xiulei Ji. “Electrolytes, SEI Formation, and Binders: A Review of Nonelectrode Factors for Sodium-Ion Battery Anodes”. In: *Small* 14.16 (2018), pp. 1–20. ISSN: 16136829. DOI: 10.1002/sm11.201703576.
- [4] Vivianne I. E. Bruyère et al. “Reduction of vanadium(v) by oxalic acid in aqueous acid solutions”. In: *Journal of the Chemical Society, Dalton Transactions* 24 (2002), pp. 3593–3597. ISSN: 14727773. DOI: 10.1039/b103320b.
- [5] Mengya Feng et al. “Manganese oxide electrode with excellent electrochemical performance for sodium ion batteries by pre-intercalation of K and Na ions”. In: *Scientific Reports* 7 (May 2017). DOI: 10.1038/s41598-017-02028-0.

### 3.5. SUMMARY

- [6] W Frohs, M Heine, and E Fitzer. “Optimization of stabilization and carbonization treatment of PAN fibers and structural characterization of the resulting carbon fibers”. In: *Carbon* 24.4 (1986), pp. 387–395.
- [7] Marco Grossi and Bruno Riccò. “Electrical impedance spectroscopy (EIS) for biological analysis and food characterization: A review”. In: *Journal of Sensors and Sensor Systems* 6 (Aug. 2017), pp. 303–325. DOI: 10.5194/jsss-6-303-2017.
- [8] S. Y. Gu, J. Ren, and G. J. Vancso. “Process optimization and empirical modeling for electrospun polyacrylonitrile (PAN) nanofiber precursor of carbon nanofibers”. In: *European Polymer Journal* 41.11 (2005), pp. 2559–2568. ISSN: 00143057. DOI: 10.1016/j.eurpolymj.2005.05.008.
- [9] S. Y. Gu, J. Ren, and Q. L. Wu. “Preparation and structures of electrospun PAN nanofibers as a precursor of carbon nanofibers”. In: *Synthetic Metals* 155.1 (2005), pp. 157–161. ISSN: 03796779. DOI: 10.1016/j.synthmet.2005.07.340.
- [10] Shaohua Guo et al. “A High-Capacity, Low-Cost Layered Sodium Manganese Oxide Material as Cathode for Sodium-Ion Batteries”. In: *ChemSusChem* 7 (Aug. 2014). DOI: 10.1002/cssc.201402138.
- [11] Luke Henderson et al. “Using ionic liquids to reduce energy consumption for carbon fibre production”. In: *J. Mater. Chem. A* 4 (Oct. 2016). DOI: 10.1039/C6TA06842A.
- [12] R M Kettler, D A Palmer, and D J Wesolowski. “The dissociation quotients of oxalic acid in aqueous sodium chloride media to 175 degrees Centigrade”. In: *Organic Geochemistry. Advances and Applications in Energy and the Natural Environment. 15th EAOG Meeting 1991* 19 (1991), pp. 598–600.
- [13] Raj Ladani et al. “Improving the Toughness and Electrical Conductivity of Epoxy Nanocomposites by using Aligned Carbon Nanofibres”. In: *Composites Science and Technology* 117 (July 2015), p. 146. DOI: 10.1016/j.compscitech.2015.06.006.
- [14] Ying Liu et al. “Highly Flexible Freestanding Porous Carbon Nanofibers for Electrodes Materials of High-Performance All-Carbon Supercapacitors”. In: *ACS Applied Materials & Interfaces* 7 (Oct. 2015), pp. 23515–23520. DOI: 10.1021/acsami.5b06107.
- [15] Yongchang Liu et al. “Tin Nanodots Encapsulated in Porous Nitrogen-Doped Carbon Nanofibers as a Free-Standing Anode for Advanced Sodium-Ion Batteries”. In: *Advanced materials (Deerfield Beach, Fla.)* 27 (Sept. 2015). DOI: 10.1002/adma.201503015.

### 3.5. SUMMARY

- [16] Lorenzo Lucherini. “Production and Characterization of Electrospun CNF as Cathode Support for Sodium-Ion Cell”. MA thesis. Torino, Italy, Corso duca degli Abruzzi 24: Politecnico di Torino, 2019.
- [17] Levi Mikhael et al. “On electrochemical impedance measurements of  $\text{Li}_x\text{Co}_{0.2}\text{Ni}_{0.8}\text{O}_2$  and  $\text{Li}_x\text{NiO}_2$  intercalation electrodes”. In: *Electrochimica Acta* 45 (Feb. 2000), pp. 1781–1789. DOI: 10.1016/S0013-4686(99)00402-8.
- [18] NASA. *Battery Basics*. 2019. URL: <https://ti.arc.nasa.gov/tech/dash/groups/pcoe/battery-prognostics/battery-basics/> (visited on 08/26/2019).
- [19] Chen Renzhong et al. “Facile Fabrication of Foldable Electrospun Polyacrylonitrile-Based Carbon Nanofibers for Flexible Lithium-Ion Batteries”. In: *J. Mater. Chem. A* 5 (May 2017). DOI: 10.1039/C7TA02528A.
- [20] University of Washington. *Oxidation States of Vanadium*. 2019. URL: <http://depts.washington.edu/chem/facilserv/lecturedemo/OxidationofVanadium-UWDept.ofChemistry.html> (visited on 10/16/2019).
- [21] Bert M. Weckhuysen and Daphne E. Keller. “Chemistry, spectroscopy and the role of supported vanadium oxides in heterogeneous catalysis”. In: *Catalysis Today* 78.1-4 SPEC. (2003), pp. 25–46. ISSN: 09205861. DOI: 10.1016/S0920-5861(02)00323-1.
- [22] Jing Xia et al. “Tin disulfide embedded in N-, S-doped carbon nanofibers as anode material for sodium-ion batteries”. In: *Chemical Engineering Journal* 359 (Nov. 2018). DOI: 10.1016/j.cej.2018.11.053.
- [23] Shicheng Yu et al. “Self-standing NASICON-type electrodes with high mass loading for fast-cycling all-phosphate sodium-ion batteries”. In: *Journal of Materials Chemistry A* 6.37 (2018), pp. 18304–18317. DOI: 10.1039/c8ta07313a.
- [24] Biao Zhang et al. “Recent Advances in Electrospun Carbon Nanofibers and Their Application in Electrochemical Energy Storage”. In: *Progress in Materials Science* 76 (Oct. 2015). DOI: 10.1016/j.pmatsci.2015.08.002.

## Chapter 4

# CONCLUSIONS

As a conclusion to this thesis, a summary of the process-flow and its deliveries are presented below.

The present work begins with the production of the CNFs. Optimization of electro-spinning setup has taken a constant amount of our effort. In particular the relative humidity (RH) variation has been the major problem. In order to obtain reproducible fibres, a flux of nitrogen and a sealed box for the set up have been adopted.

After electro-spinning, the fibres are treated with a first thermal process at about 260 °C. This is the stabilization process and it guarantees a better stability of fibres during the carbonization process. Lots of time has been spent in order to optimize this step, with particular attention the the FTIR results.

The carbonization step has been marginally studied but its optimization, by means of future research, is of main interest for both fibres and active material quality.

More interesting are the results about different approaches to load the active material. Dip-coating technique has proved to be limiting from the point of view of controllability of the loading profile. On the other hand, early results about Buchner filtration are promising. A studied focused on this technique is a key element to definitely grasp the potentiality of CNFs. The production of NVP by co-precipitation has been successfully reproduced and confirmed by XRD analysis. The optimization of the crystals size and dimension of crystalline domains are the missing part to take over control of the production process.

Concerning the assembly of electrochemical cell the Swagelok setup has proven satisfactory for the testing phase. Notwithstanding the first prototype for a multi-electrodes setup would permit, in a second phase of research, to easily acquire a large amount of data, hence it is worthy to be further developed.

The electrochemical tests confirm the good cycling performances and the high c-rate capability

of the NVP-CNFs couple. More than 200 cycles have been performed on the first batch of cells, without major degradation of performances.

The testing of a tin anode and a manganese oxide cathode is the next step in order to definitely confirm the advantages derived from 3D porous nanostructures.

Present and future study for sodium-ion, to benefit from market trends, should focus on the stationary storage, pursuing good cycling, high efficiency, and capacity retention at high C-rate.

The resulting devices based on sodium-ion may be competitive or even overcome the lithium-ion technology in the long term competition.

# APPENDIX A: Additional Images

## 4.1 NVP

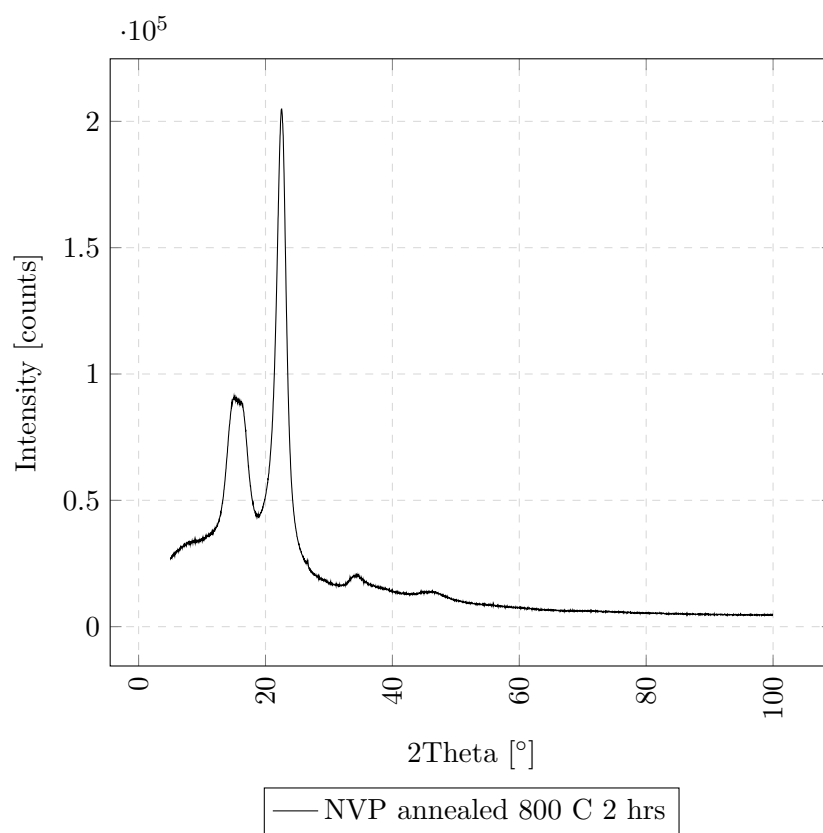


Figure 4.1: XRD data of NVP annealed for 2 h at 800 C. No peaks are visible.

#### 4.1. NVP

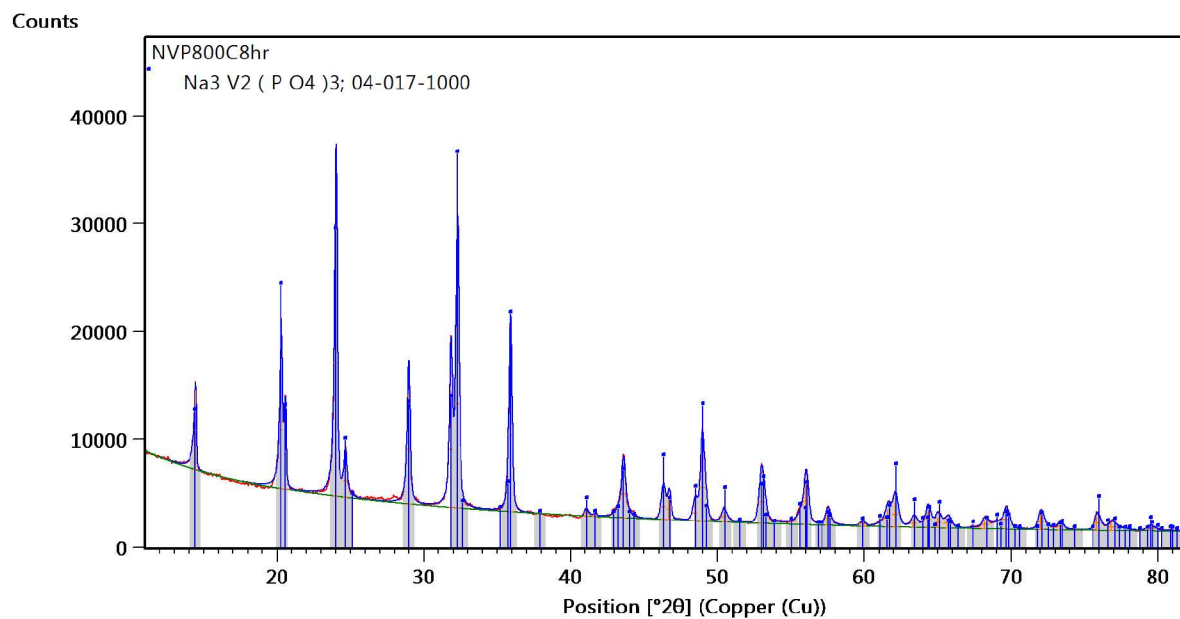


Figure 4.2: Superposition of theoretical and measured NVP XRD spectra.

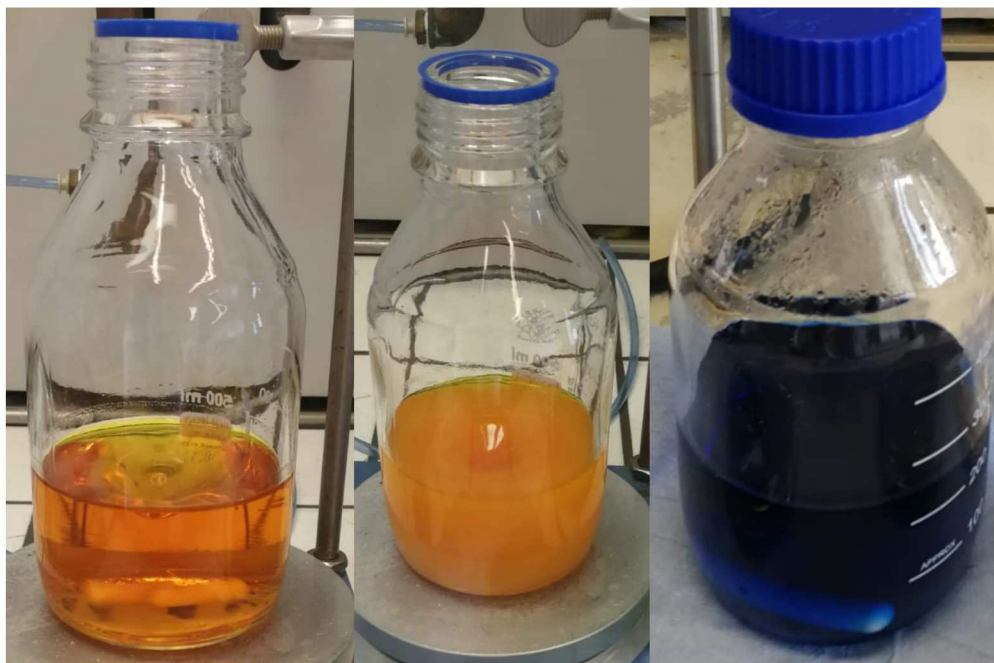


Figure 4.3: NVP precursor at different stage of preparation. The color is associated to different states of oxidation of vanadium.